NASA CONTRACTOR REPORT

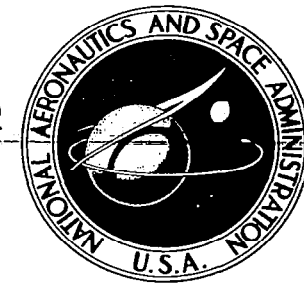

NASA CR-849

MEASUREMENT OF DYNAMIC CHARACTERISTICS OF SOILS WITH PENETROMETERS

by David P. Womack and William R. Cox

Prepared by
THE UNIVERSITY OF TEXAS
Austin, Texas
for

NATIONAL AERONAUTICS AND SPACE ADMINISTRATION • WASHINGTON, D. C. • AUGUST 1967

NASA CR-849

MEASUREMENT OF DYNAMIC CHARACTERISTICS OF SOILS WITH PENETROMETERS

By David P. Womack and William R. Cox

Prepared under Grant No. NsG-604 by
THE UNIVERSITY OF TEXAS
Austin, Texas

for

NATIONAL AERONAUTICS AND SPACE ADMINISTRATION

For sale by the Clearinghouse for Federal Scientific and Technical Information
Springfield, Virginia 22151 – CFSTI price $3.00

PREFACE

The work described herein was initiated by the National Aeronautics and Space Administration, Manned Spacecraft Center, Houston, Texas, under Contract NAS 9-3559. It was continued and completed under Grant NsG-604, with the Langley Research Center of NASA.

ABSTRACT

In this investigation the response of various soils to dynamic loads was studied by use of an impact penetrometer. A similar static penetrometer test was employed to determine any correlation between the static and dynamic cases, and to augment the evaluation of the important soil parameters affecting the impact mechanism.

Considerations for the design of the equipment and development of the test program indicated that application of the penetrometer concept would be feasible for this investigation for both the static and dynamic tests. The dynamic penetrometer was designed as a projectile instrumented with strain gages for the measurement of impact forces. The static penetrometer decided upon was the Proctor Plasticity Needle. The penetrometer parameters affecting impact were held constant in the test program by dropping the projectile vertically and from the same height each time.

Target media selected for testing were two poorly graded sands, a well graded sand, a clay, and a crushed stone. The moisture contents and densities of the sands were varied widely during testing, while the clay was tested in situ.

For the 36 tests analyzed, observations showed that the soil-projectile interaction generally agreed with existing failure theories for impacts, and that the shearing strength of the soil apparently is a principal factor. It was found that impacts in granular soil were influenced greatly by the amounts of water and air in the target materials, and that no direct correlation exists between static and dynamic tests when these constituents are varied. Remote target evaluation employing penetrometer techniques is feasible if the penetrometer is properly tested and calibrated with respect to

possible target conditions and impact velocities. Also, prediction of impact forces could be simplified through use of a dynamic penetrometer with characteristics affording the ability to extrapolate to a prototype projectile.

TABLE OF CONTENTS

LIST OF PHOTOS

LIST OF FIGURES

Page

Page

Page

LIST OF TABLES

CHAPTER I

INTRODUCTION

In the past, requirements for evaluating soil strength have been dictated almost entirely by static loading conditions. Consequently, methods devised to measure the soil strength characteristics generally have been confined to evaluation of static strengths. More recently, however, the dynamic loading conditions encountered on highways and airfields have created a need for information about the action of soils under dynamic loads. In addition, there is the current probability of terminating space probes either on land masses here on earth, or on the moon, which necessitates the evaluation of soils as target media for impacting projectiles.

For determination of soil response to impacting projectiles, a desirable test would be one which measured the strength, or hardness, of soils in situ, as well as being applicable to both static and dynamic rates of loading. Triaxial and unconfined compression tests and similar laboratory tests can be influenced by sampling disturbances and are therefore unsuitable. Static penetrometer tests, however, are easily employed on soils in situ, and application of the penetrometer technique to dynamic loading conditions is feasible.

OBJECTIVE

The primary objective of this investigation was to develop a penetrometer test to evaluate soil-projectile interaction during impact, and to compare the results of this dynamic test with those of a similar static test.

SCOPE

In this investigation, the only parameters that were allowed to vary appreciably were the soil type, density, and moisture content. Three types

of sands having different particle sizes and gradation were used. These were varied widely in density and moisture content during testing. In addition, a crushed stone, a clay, and water were used as target media.

An accurate evaluation of the soil-projectile interaction mechanism during impact seemed more easily attainable if the variations of the projectile parameters were held to a minimum. The penetrometer tests were thus designed to give repeatable conditions with little variation. Comparison of the static and dynamic types of testing was based mainly on the use of identical geometrical configurations for the contacting portions of the penetrometers.

CHAPTER II

DESIGN CONSIDERATIONS

The overall consideration for the design of test equipment was that it should be feasible in construction and operation. Also, the nature of the impact interaction effected by the dynamic test should be such that it could be correlated to other projectile-target impacts, as well as being reproducible.

FEASIBILITY

A basic consideration in the design of the dynamic test was that of instrumentation. If the instrumentation were too elaborate, the losses of portability and economy of time and money could nullify the advantages gained. However, since the information sought from the dynamic test included measurement of the impact velocity of the projectile and the acceleration-time record of the impact, it was recognized that a certain amount of electrical equipment was necessary.

It was decided to monitor the dynamic test on an oscilloscope using a strain gage circuit to measure the impact forces. It was reasoned that most people interested in reproducing this type of test could obtain and construct the necessary components easily, whereas other methods of force or acceleration measurement and the corresponding instrumentation might be unobtainable. The arrangement could be set up in the laboratory and powered by line voltage, or taken to the field and powered by a generator. The latter situation required two men and a pickup truck.

Developing a similar static testing procedure involved economic considerations, and required correlation to the dynamic test. The type of penetrometer needed was one which called for little extra equipment, little

preparation for use, and ease of handling during testing. Since so much time was to be committed to the design and construction of the dynamic test, it was decided to use, or adapt to use, one of the existing static penetration tests, rather than design a new one. After a review of the possible types of penetrometers that seemed feasible, the Proctor Plasticity Needle was chosen. This apparatus, described later in more detail, is portable and convenient to use, either in the laboratory or in the field, and requires only one person for operation.

CONTROL OF TEST CONDITIONS

As was previously mentioned, it was desired to make all impact parameters constant, except for soil type, density, and moisture content. It was found to be difficult to control dynamic parameters associated with the impact velocity due to the influence of friction and air resistance. However, geometrical parameters such as the shape of the contacting surface and the penetrometer weight were kept constant.

Velocity

The simplest way to deliver a projectile to a target is by dropping it. To minimize the possibility of varying the angle of impact of the projectile from the vertical, a guide system was needed. By employing a delivery tube for the projectile, a vertical drop for each test and a reference datum for repeatable drop heights could be ensured. The delivery tube length was selected to afford a velocity of about 15 fps. This is considered to be in the range of impact velocities of aircraft landings or parachute-controlled drops. It is assumed that accelerations caused by impact velocities that are subsonic but not static are proportional to the magnitude of the velocity.

Of the 36 tests analyzed, the average impact velocity was 15.37 fps, and the range between the maximum and minimum values was 1.71 fps. About

eighty percent of the velocities fell within ± 0.5 fps of the average, as shown on Table 4, Appendix C. The slight variations in drop height to allow for proper oscilloscope trigger time seemed to have little effect on the velocities.

Impact Mechanism

The contacting portion, or foot, of the projectile was designed as a 1.156 in. diameter (about 1.0 sq. in. area) cylindrical plate, with the flat portion as the impacting surface. This foot, described later in more detail, was designed to minimize any friction forces on its perimeter by making it only 0.32 in. thick and recessing the shank, or leg, connected to it. Experiments performed in granular media indicate that contact surface diameters of about 1.0 in. and greater give the same penetration for the same velocity and areal mass density (mass/contact area), while those diameters of less than 1.0 in. tend to give less penetration because friction is proportionately greater[2]. A contact foot with the same dimensions was also attached to the static penetrometer, giving the two types of tests geometric similarity.

CHAPTER III

APPARATUS

The equipment for this testing program was selected and designed to satisfy the considerations of the preceding chapter.

DYNAMIC PENETROMETER

Development of this part of the testing program involved designing the penetrometer and adapting it to the instrumentation.

Projectile

The impact penetrometer is shown in Figure 1. Its weight is 5.384 lb., and the foot, leg, and handle are threaded pieces. The ratio of length to diameter of the brass cylinder was selected to reduce wobbling of the projectile during delivery, and the four holes in the cylinder help reduce air resistance.

The penetration leg is annealed and heat treated beryllium copper alloy which has a modulus of elasticity of 18.5×10^6 psi and a proportional limit of 100,000 psi, making it quite suitable for the attachment of strain gages. The four strain gages were bonded symmetrically about the midpoint of the leg. The two axially oriented gages were placed diametrically opposite to each other, and the two transversely oriented gages were applied in the same manner. Waterproofing and shock protection for the strain gages and wiring were attached to the leg with tape during testing. The strain gage leads were run up through one of the holes in the cylinder and attached to the handle so they would not foul when the projectile was dropped.

Delivery Tube

The tube, shown in Figure 2, was outfitted with a fly lead hanger

FIGURE 1

DYNAMIC PENETROMETER

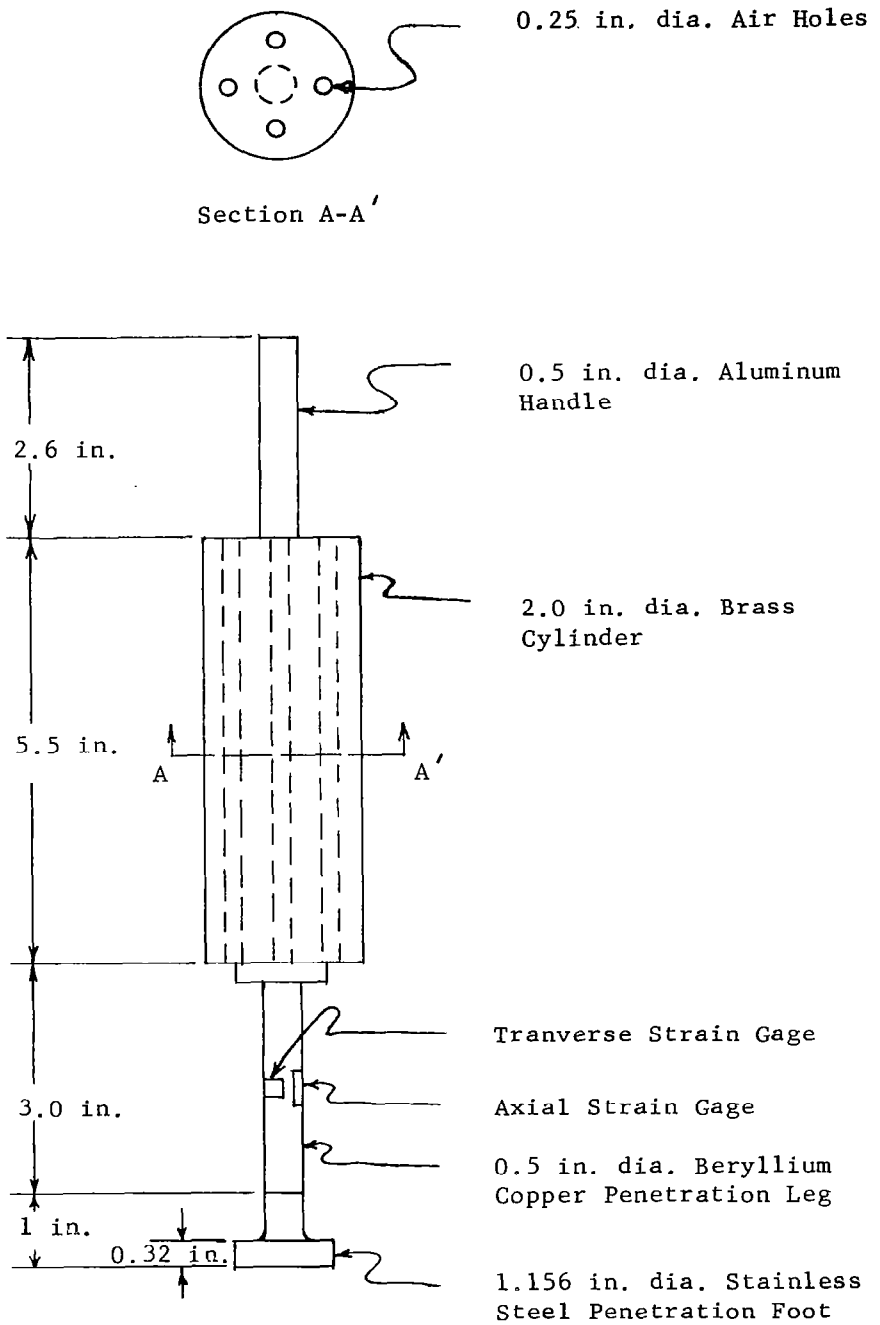

FIGURE 2
DELIVERY TUBE FOR DYNAMIC PENETROMETER

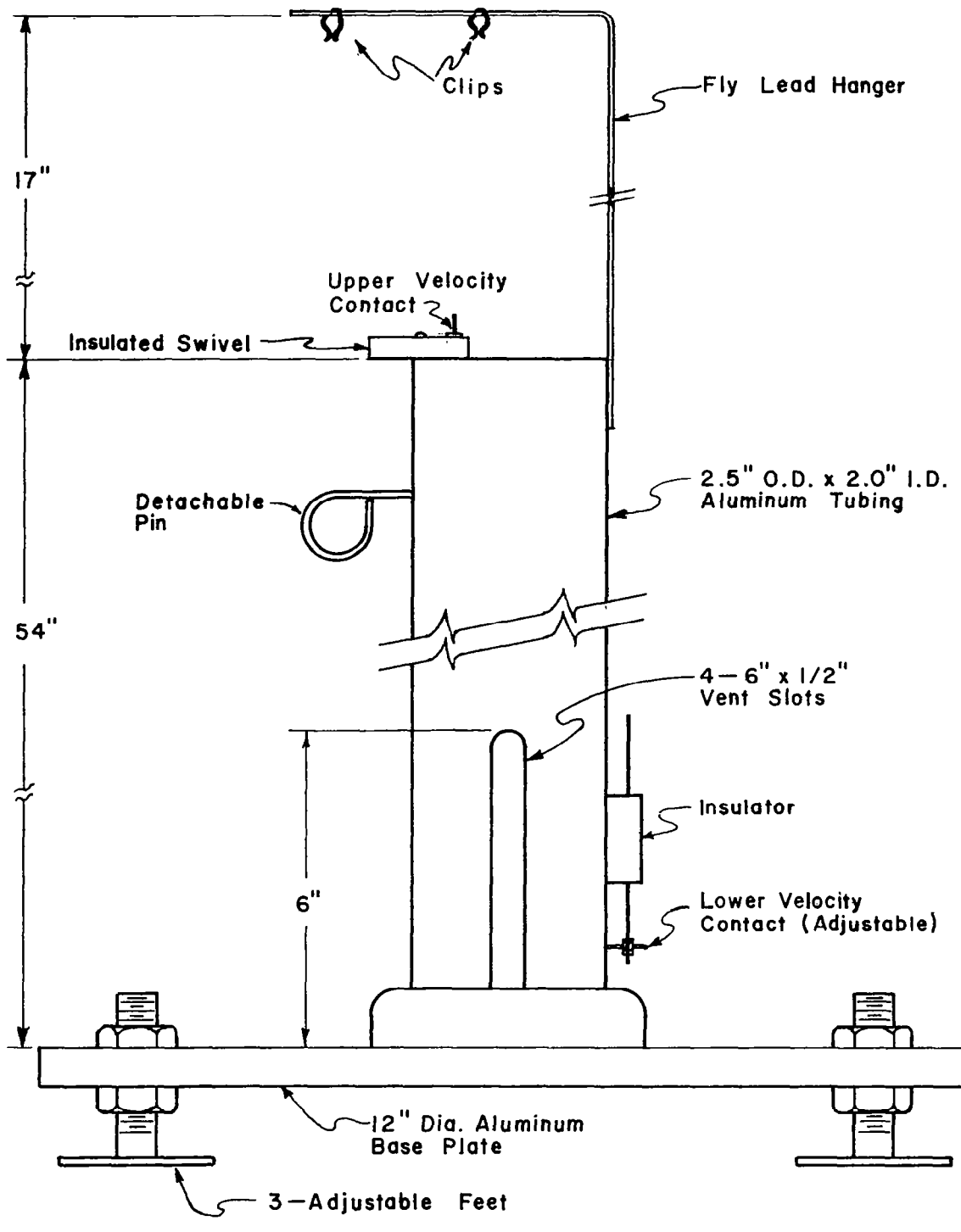

which has clips to hold the loops of the fly leads prior to a test drop. The ends of the fly leads are connected to a 4-spade plug which is detached from the socket and dropped down the tube after each test to avoid pulling the projectile back up the tube. The socket and necessary strain gage circuitry and the velocity measurement contacts were attached to the tube. The upper velocity contact is swivel-mounted in order to allow the projectile to be inserted in the top of the tube and then the contact point to be swung over to touch the top shoulder of the brass cylinder. A hole was drilled for the detachable pin 5.5 in. below the top of the tube to provide a convenient way to hold the projectile in place before a test. The lower velocity contact is a small screw attached to the end of a metal strip. The screw head sticks through a slot into the tube far enough to contact the lower shoulder of the brass cylinder of the projectile. The vent slots at the bottom of the tube help reduce air resistance to the penetrometer during a test. Clearance between the base plate on the bottom of the tube and the soil is provided for by the three adjustable feet. The bearing surfaces of these feet are 2 in. by 2 in. plates.

Electrical Instrumentation

The instrumentation for the testing procedure was employed to monitor the drop time of the projectile and the force-time trace of the impact. The components and circuits are described here while the calculations for these values are explained in Data Reduction, Chapter V.

Basic Components

The components for the dynamic test setup are shown schematically in Figure 3. The A. C. source while testing in the field was a 1.5 KVA gasoline-driven generator, while the available house power was used in the laboratory.

FIGURE 3

SCHEMATIC OF TEST SETUP

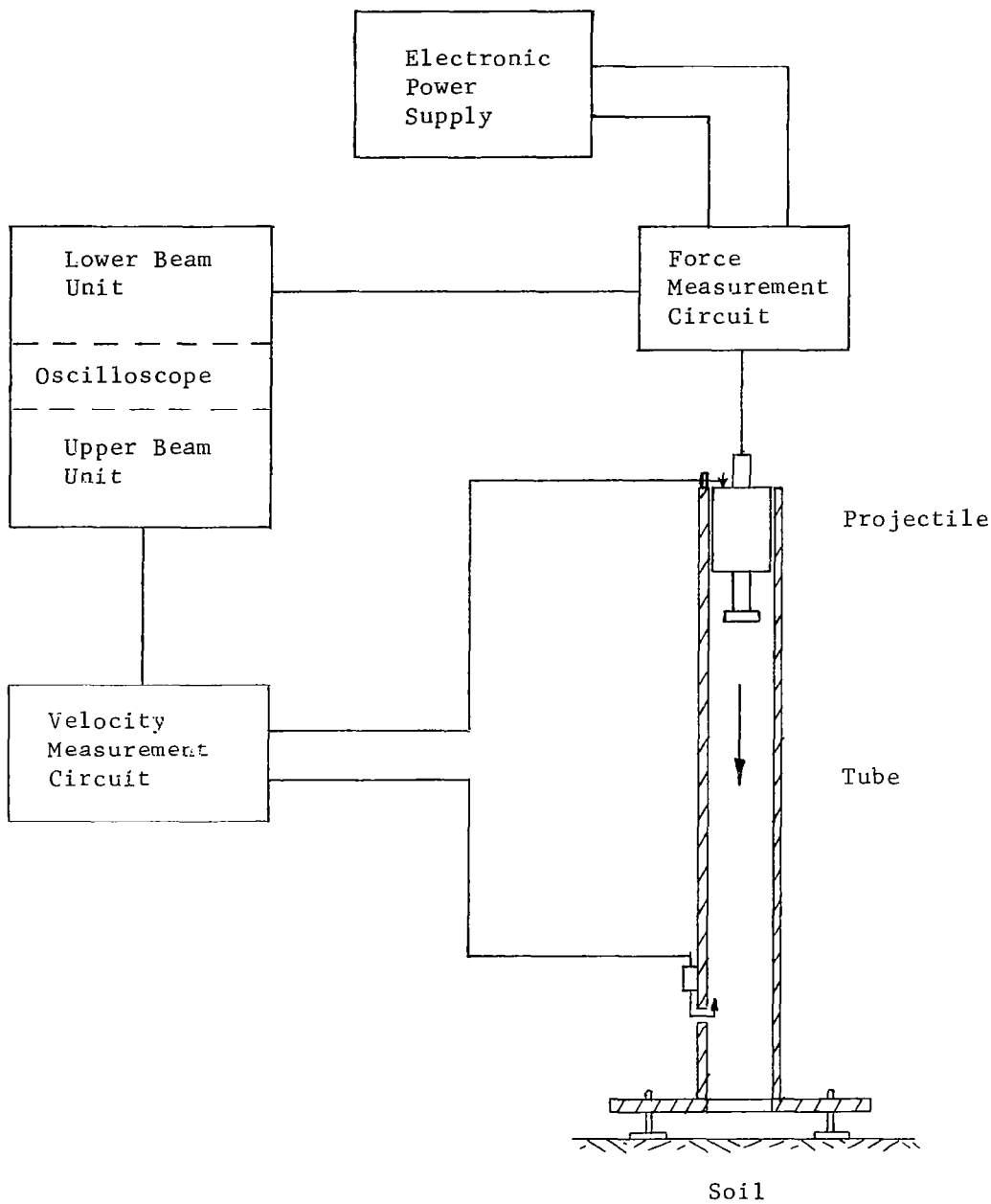

The oscilloscope used was a Type 565 dual beam Tektronix having two Type 3A3 dual-trace, differential vertical amplifiers. These plug-in units were operated in a single channel mode providing one trace each and low band width of 5 kc for high frequency noise elimination. The velocity measurement circuit output was displayed on the upper beam, and output of the force measurement, or strain gage, circuit was displayed on the lower beam. The two independent time bases provided by this oscilloscope made it possible to record simultaneously the velocity measurement trace, which lasts about 1/2 second, and the force-time pulse, lasting only hundredths of a second. All oscilloscope data was recorded by a Polaroid oscilloscope camera on 4 in. by 5 in. film. A Harrison Labs model 6204A electronically regulated and adjustable D. C. power supply provided power for the strain gages. This voltage was continuously monitored with a voltmeter during testing. The velocity measurement circuit was powered by two 1.5 V. dry cell batteries.

Velocity Measurement

Figure 4 shows that part of the circuit used to measure the drop time of the projectile. The upper and lower velocity contacts were insulated from the tube to yield zero voltage on the oscilloscope while the projectile dropped. Figure 5 explains the sequence of a typical test as recorded on Photo No. 1. At position 1 on the velocity sweep, the projectile started dropping and cleared the upper contact. The voltage dropped to zero, giving a negative slope which triggered the upper beam unit sweep. Position 2 shows the duration of the drop, and position 3 shows the point at which the shoulder of the projectile first touched the lower contact.

Force Measurement

The schematic of Figure 6 shows the penetrometer at the position

FIGURE 4

SCHEMATIC OF VELOCITY MEASUREMENT CIRCUIT

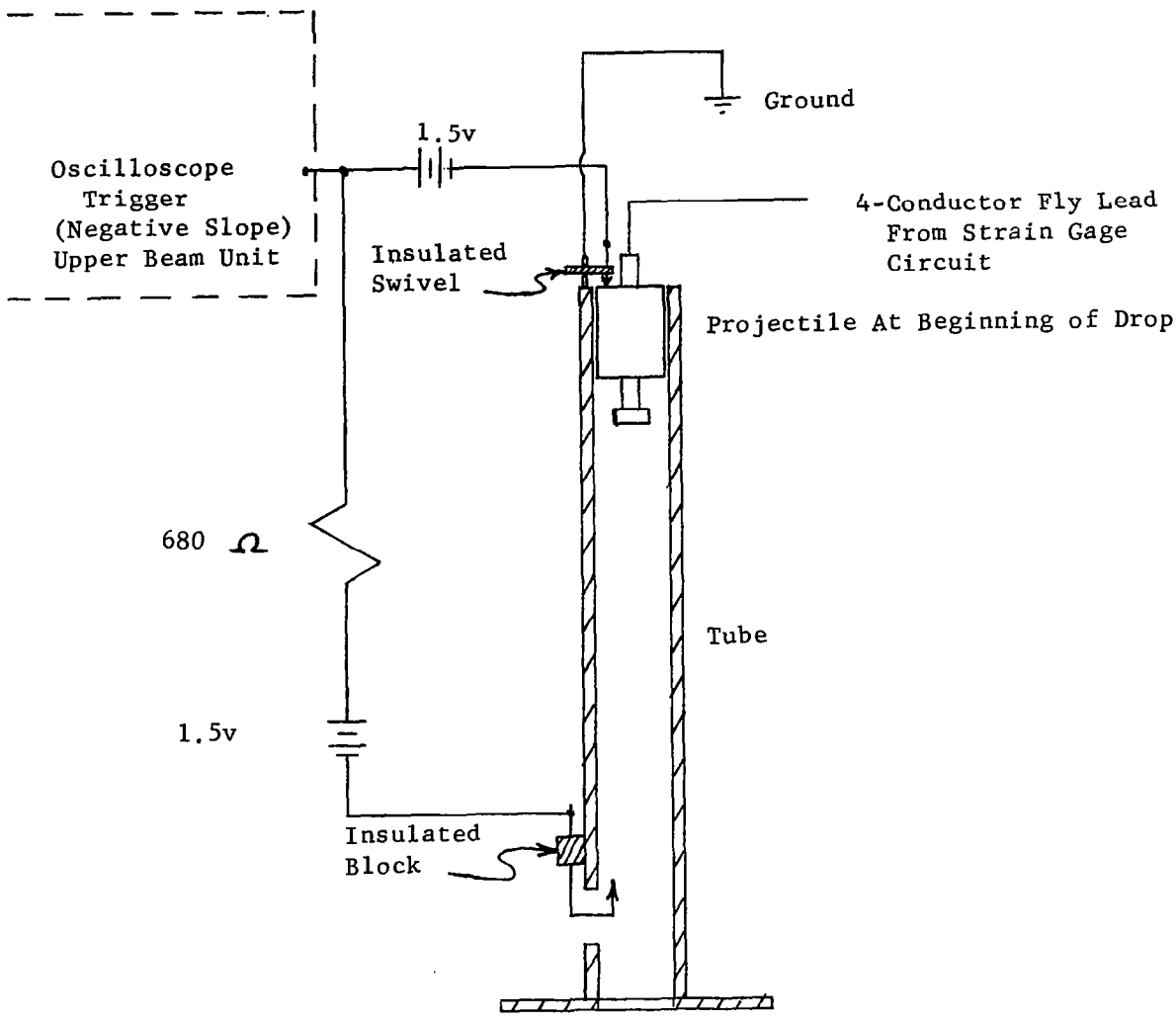

PHOTO NO. 1

TYPICAL DROP TEST RECORD

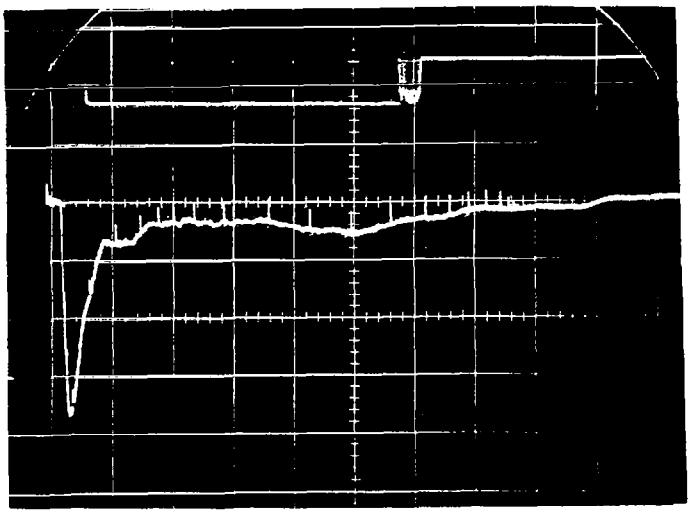

FIGURE 5

TIME SEQUENCE OF DROP TEST RECORD

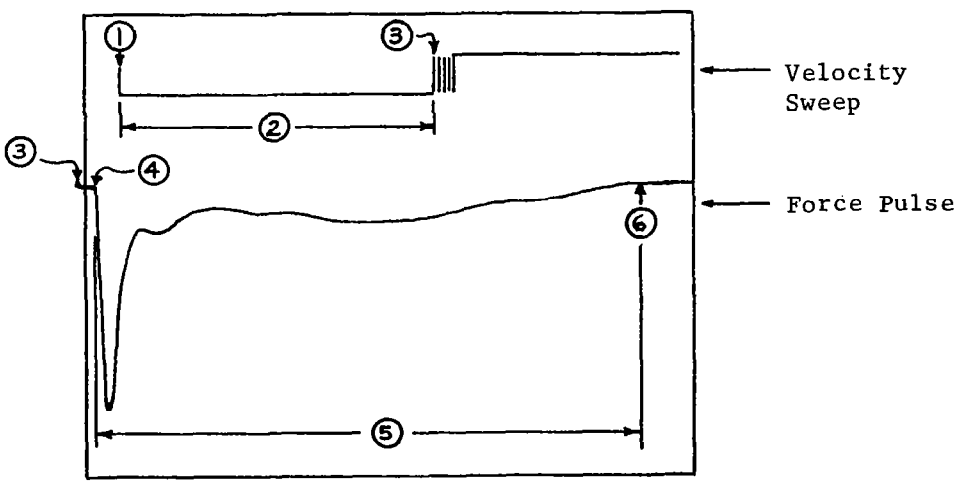

① - Start of Projectile Drop, Velocity Sweep Triggered
② - Time Measurement of Drop
③ - End of Drop, Force-Time Pulse Triggered
④ - Impact Point
⑤ - Force-Time Impact Pulse
⑥ - End of Test

FIGURE 6

SCHEMATIC OF FORCE MEASUREMENT CIRCUIT

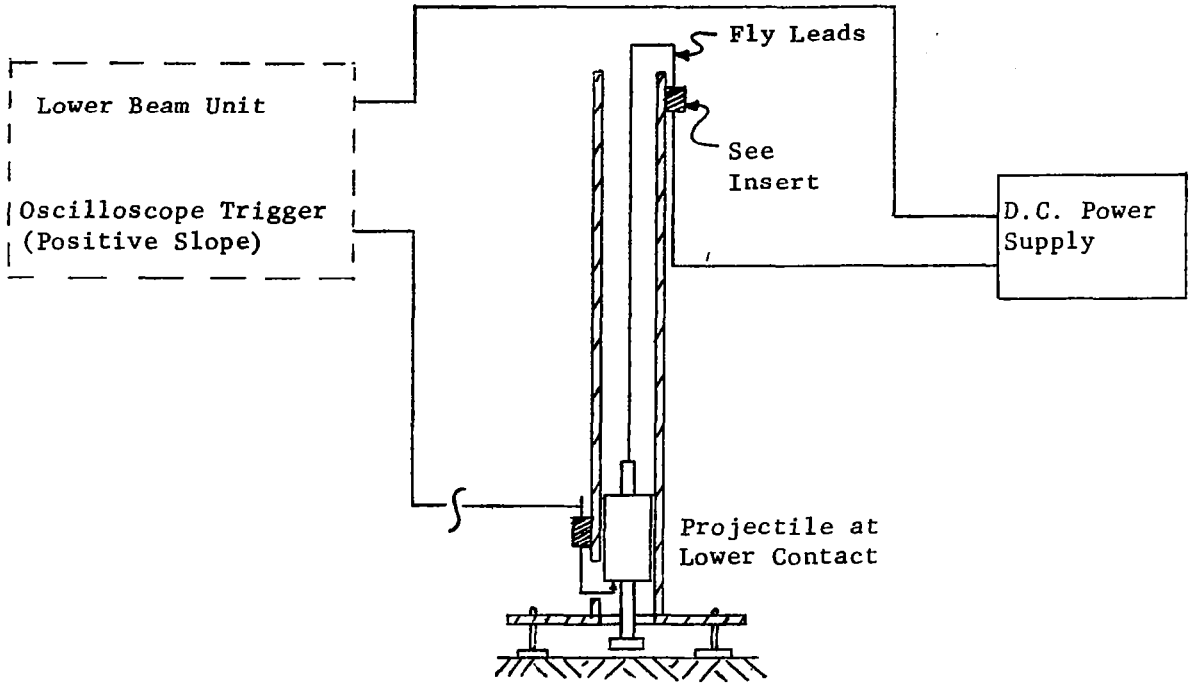

INSERT

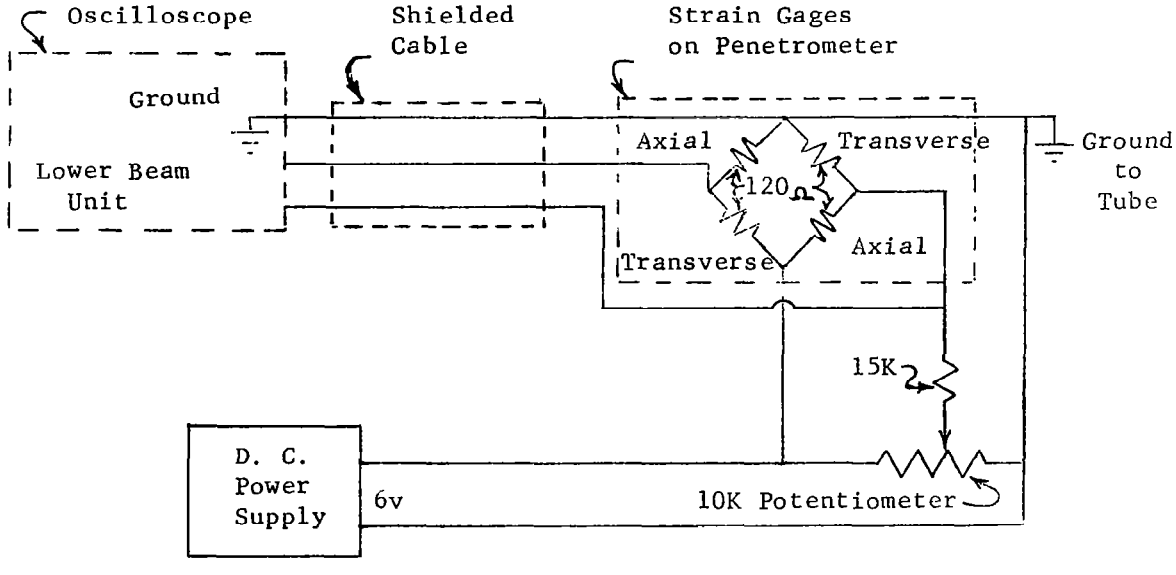

corresponding to point 3 on Figure 5. The positive voltage rise of the velocity sweep at that position triggered the sweep for the force-time pulse. The projectile impacted the target at position 4 and began the impact pulse.

The lower contact is adjustable vertically to facilitate recording of the force pulse, which only lasts 15 to 50 msec. Usually, 0.2 in. clearance was allowed between the penetrometer foot and the target when the lower contact and the penetrometer shoulder touched, which explains the time lag between points 3 and 4. The method of adjusting the lower contact to compensate for slight variations in drop height to the target was used in lieu of trying to attain the exact same drop height for each test.

The full bridge strain gage circuit, consisting of four 120 ohm Budd Metalfilm Strain Gages, is shown in the insert of Figure 6. These are type C9-141-B gages with a gage factor of 2.08. By mounting the gages in this fashion, any force component normal to the direction of impact would theoretically be cancelled out of the signal so that only axial loads would be recorded. Normal procedure was followed in balancing the circuit. Before each test series, the oscilloscope was adjusted, the voltmeter was put across the power supply, which was adjusted to 6 V., and then the gage circuit was balanced.

STATIC PENETROMETER

Figure 7 shows the plasticity needle designed by R. R. Proctor in the early 1930's to determine the condition, or plasticity, of soil undergoing compaction[5]. As previously mentioned, its portability and ease of operation made it the best static penetrometer for this testing program.

It is operated by placing the penetration foot in the desired location and then applying a vertical force to the handle. The foot should be

FIGURE 7
STATIC PENETROMETER

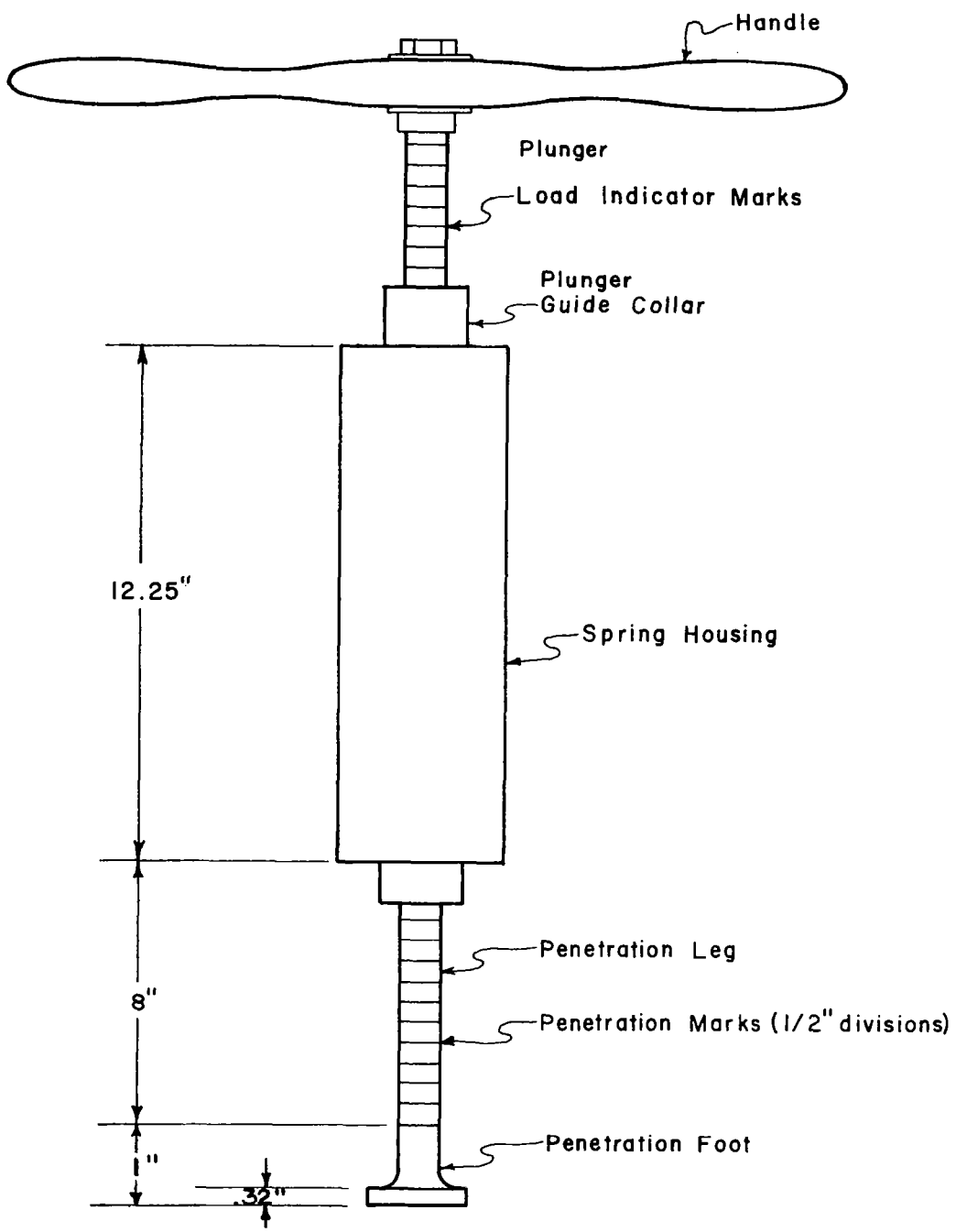

forced through the soil at 1/4 in. to 1/2 in. per second. In some materials this is not possible, and the procedure used for this program was to apply force at the rate of about 5 lbs. per second until the desired penetration or force was reached, regardless of fluctuations in the penetration rate. The penetrometer was calibrated in a compression testing machine prior to testing.

CHAPTER IV

TARGET MEDIA

The possibilities for different types of soils as targets are virtually unlimited, due to the portability of the equipment, but the target materials for the testing program included only the soils discussed in this chapter, and water. A recommended procedure was followed in describing these soil types[4]. The descriptions include the general results of the classification tests and the range of densities and moisture contents of each soil type. All the classification tests were run on the accumulated material from the moisture sample tests. Specific and detailed soil data for each drop test are listed chronologically in Appendix C.

OTTAWA SAND

This well-known type of silica sand was shipped from Ottawa, Illinois. It is referred to in this report as SP-(OS). The "SP" is the Unified Soil Classification System designation for a poorly graded sand, and the "OS" is derived from the name of the sand. It is a grayish-white colored material with mostly rounded particles.

For the samples taken, the maximum void ratio (e) was 0.729, while the minimum was 0.511. The *in situ* density, or wet density, (γ_w), varied from 104 pcf to 130 pcf. Several mechanical analyses were performed on this sand, and a representative Grain Size Accumulation Curve is shown on Figure 8. U. S. Standard Sieve Sizes 200, 150, 100, 80, 60, 40, 20, and 10 were used.

Obtaining accurate measurements of specific gravity required very close control of temperature, volume, and weights. In these measurements

MECHANICAL ANALYSIS
GRAIN SIZE ACCUMULATION CURVE

Name Ottawa Sand
Date 12-10-66

Sample No. (SP)
Sheet No. 1

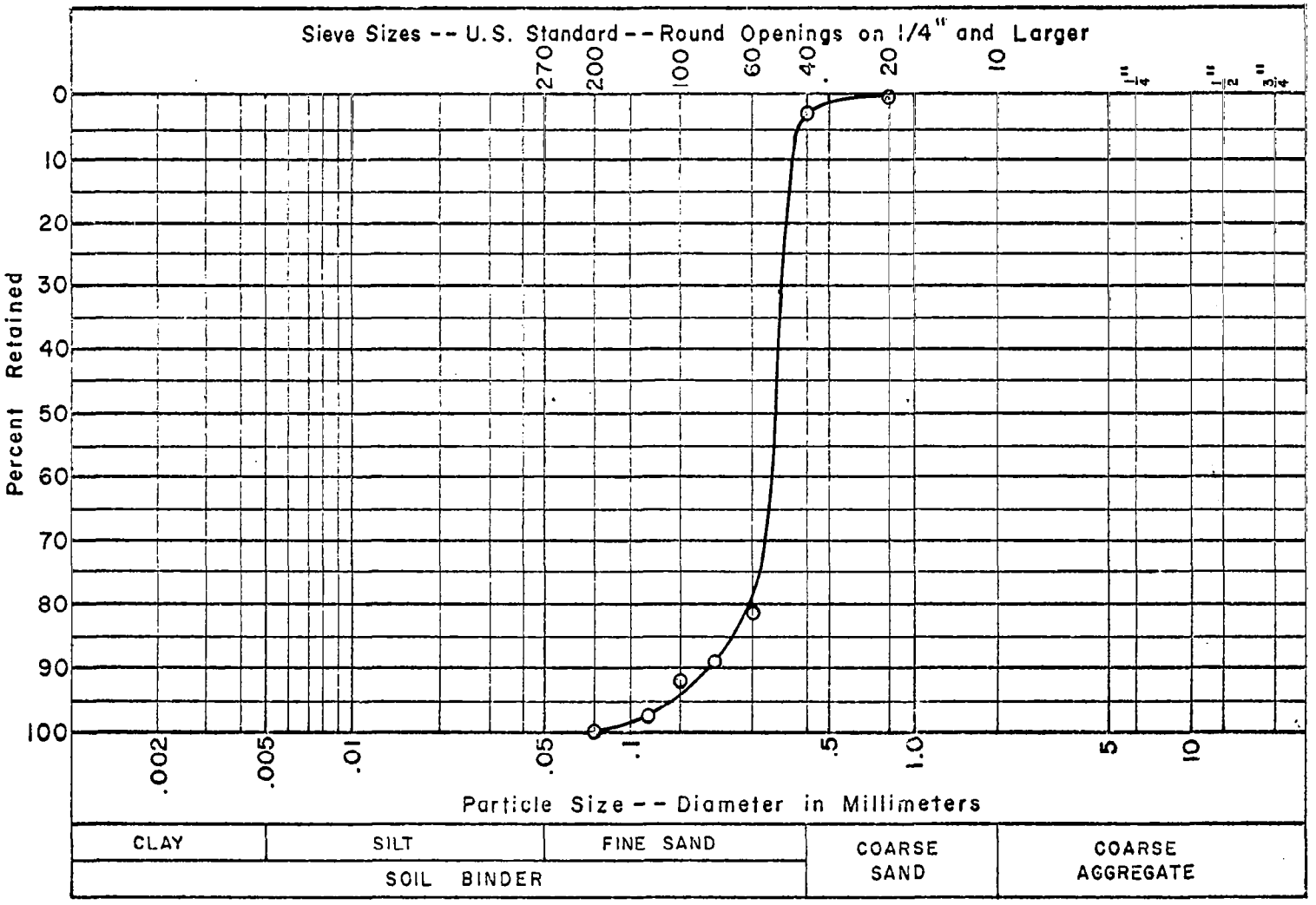

FIGURE 8

accuracy was attained by using a 100 ml. flask, calibrated at 20°C, demineralized water, temperature-controlled weighings on an electronic balance, density adjustments for temperature, and the use of heat and vacuum to drive air from the soil. The specific gravity of Ottawa Sand was found to be 2.654. Penetration tests for this material were run only in the laboratory.

COLORADO RIVER SAND

This material is referred to herein as SP-(CRS), as it has the grain size and distribution that the U.S.C.S. classification designates as "poorly graded sand". It is a clean sand, light brown in color, consisting primarily of quartz. The particles of this sand are subangular and of rough texture. It is a Colorado River deposit obtained from the Austin, Texas area. Figure 9 shows the Grain Size Accumulation Curve, for which the standard sieve sizes 200, 150, 60, 40, and 20 were used.

The density samples taken showed the maximum and minimum void ratios to be 0.884 and 0.584, respectively. Wet weight, (γ_w), of the samples varied from 95 pcf to 125 pcf. The specific gravity of Colorado River Sand was found to be 2.648. Penetration tests on this sand were run only in the laboratory.

CAPITOL AGGREGATES SAND

The field testing site for this soil was located along the Colorado River, southeast of Austin, Texas, on the property of Capitol Aggregates, Inc. The soil for laboratory testing was taken from this site. The sand is referred to in this report as SW-(CA), "SW" being the U.S.C.S. designation for a well graded sand.

Capitol Aggregates sand is a Colorado River deposit typical of the area. It is a light brown color with subangular particles comprised basically

MECHANICAL ANALYSIS
GRAIN SIZE ACCUMULATION CURVE

Name Colorado River Sand
Date 11-10-66

Sample No. (SP)
Sheet No. 1

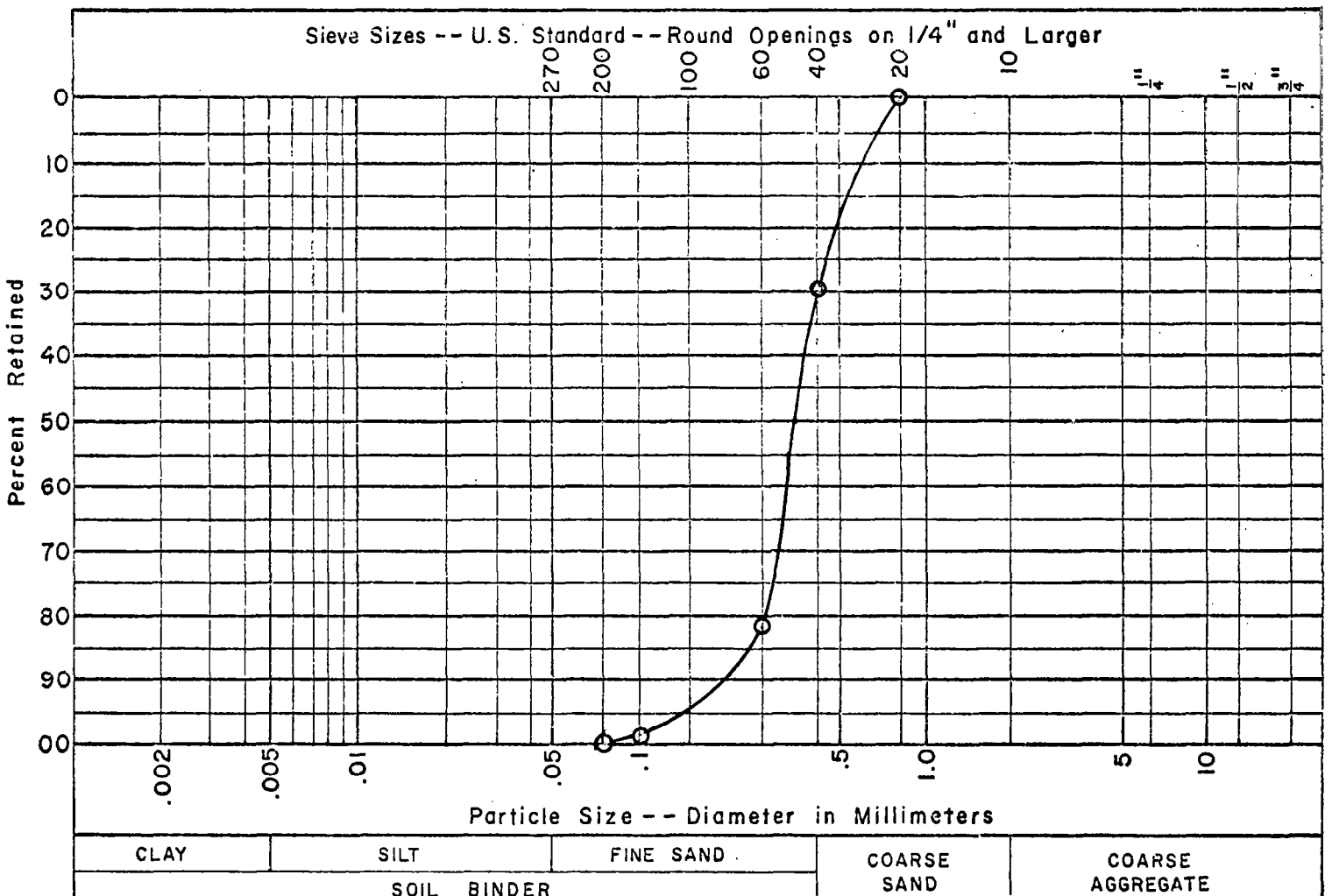

FIGURE 9

of quartz with some limestone and feldspar. The rock fragments are fresh to slightly weathered. The maximum void ratio, (e), of the tested material was 0.705, while the minimum was 0.429. The wet weight, (γ_w), varied from 99 pcf to 132 pcf. This sand tended to form a crust or cementation at low moisture contents in the field. Penetrometer tests (Nos. 10-10-2, 10-10-3, and 10-10-7) clearly show these effects and are discussed later.

U. S. Standard Sieve Sizes 200, 100, 40, 20, and 1/4 in. were used in the mechanical analysis of this sand. The representative curve, Figure 10, gives an accurate picture of the particle size distribution. Of all the mechanical analyses run for this sand, individual curve deviations vary less than 10%. The specific gravity of this sand was found to be 2.644.

DEL RIO CLAY

The test site for this clay was at The University of Texas Balcones Research Center in Austin. It is a typical Central Texas clay, and is indexed in this work as CH-(BS). "CH" is the U.S.C.S. classification for inorganic clays of high plasticity, while "BS" stands for "Black Soil".

Tests were run and samples taken over an area of about 30 by 10 ft in which the soil varied in color from dark brown to black. It is a preconsolidated clay, and contains some calcareous nodules up to 1/4 in. in size, as well as tiny grass roots and very slight traces of sand. When the specimen is broken, the surface of the fracture appears dull and crumbly. Its dry strength is high, being hard to crush with the fingers, and it has high plasticity.

From four borings run in the immediate area, the average liquid limit, plastic limit, and plasticity index for the clay were found to be 59%, 34%, and 25%, respectively. The void ratio, (e), varied from 0.968 to 0.870, while the wet weight, (γ_w), varied from 112 pcf to 118 pcf. The

MECHANICAL ANALYSIS
GRAIN SIZE ACCUMULATION CURVE

Name Capitol Aggregates Sand
Date 12-10-66

Sample No. (SW)
Sheet No. 1

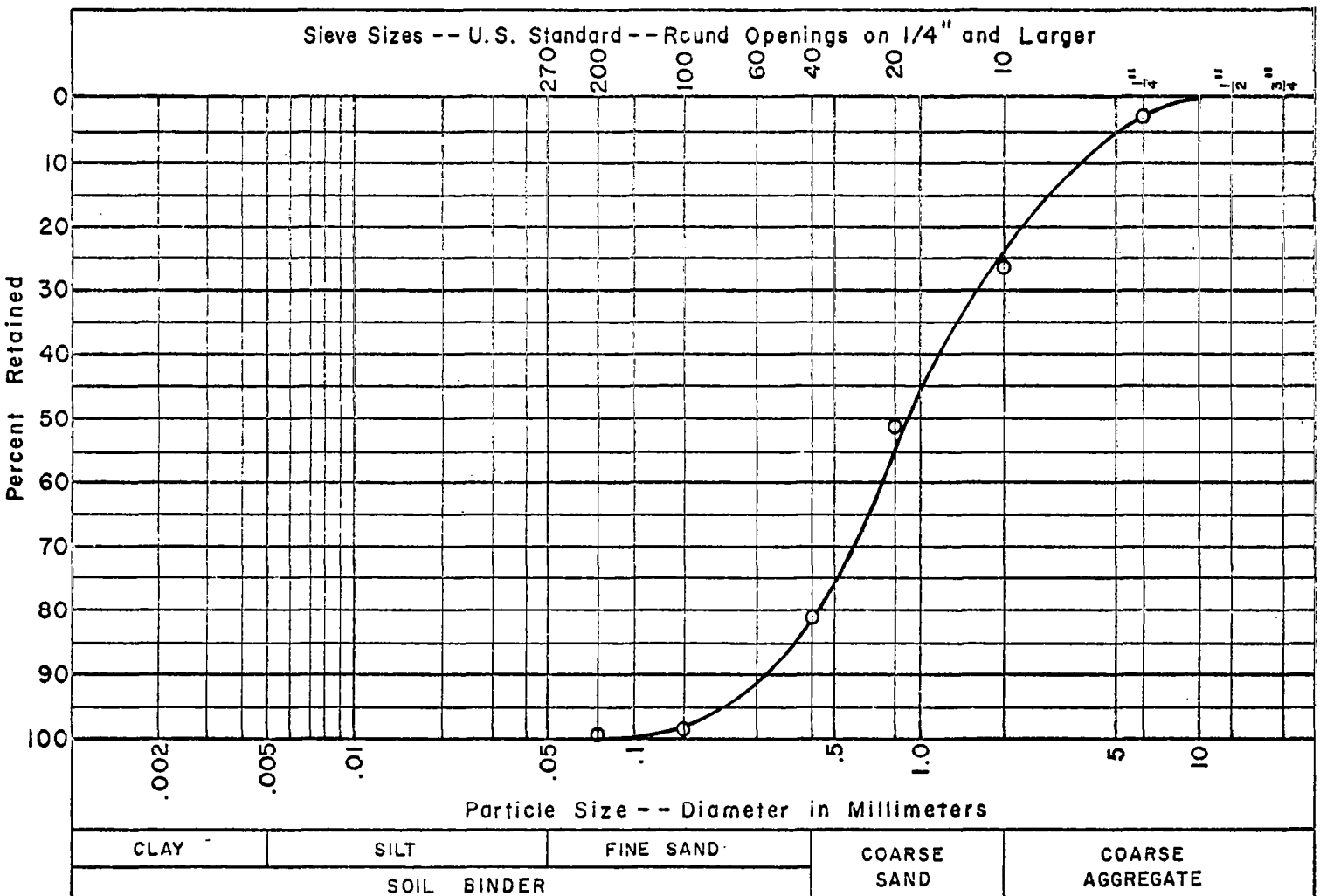

FIGURE 10

average unconfined compressive strength was determined as 0.75 tsf. Standard "Quick" triaxial compression tests run on the borings yielded an average angle of internal friction, (ϕ), of the clay of 4^{o}, while an average value for the cohesion, (c), was found to be 5 psi.

A specific gravity analysis of this soil showed that value to be 2.678. Tests on the clay were run only in the field.

TEXAS CRUSHED STONE

This material was obtained from the Central Texas area. It is designated as SP-(TCS), has been washed and screened, and is composed mostly of crushed limestone with small quantities of quartz. The particles are fresh, angular and rough textured. It is a poorly graded coarse sand, almost gravel-sized. The mechanical analysis is shown in Figure 11, for which sieve sizes 50, 40, 30, 20, 10, and 4 were used.

The void ratio, (e), for this test was about 0.9, while the wet density, (γ_w), was 87 pcf. The specific gravity of Texas Crushed Stone was found to be 2.691. Tests were run on this material only in the laboratory.

MECHANICAL ANALYSIS
GRAIN SIZE ACCUMULATION CURVE

Name Texas Crushed Stone
Date 11-28-66

Sample No. (SP)
Sheet No. 1

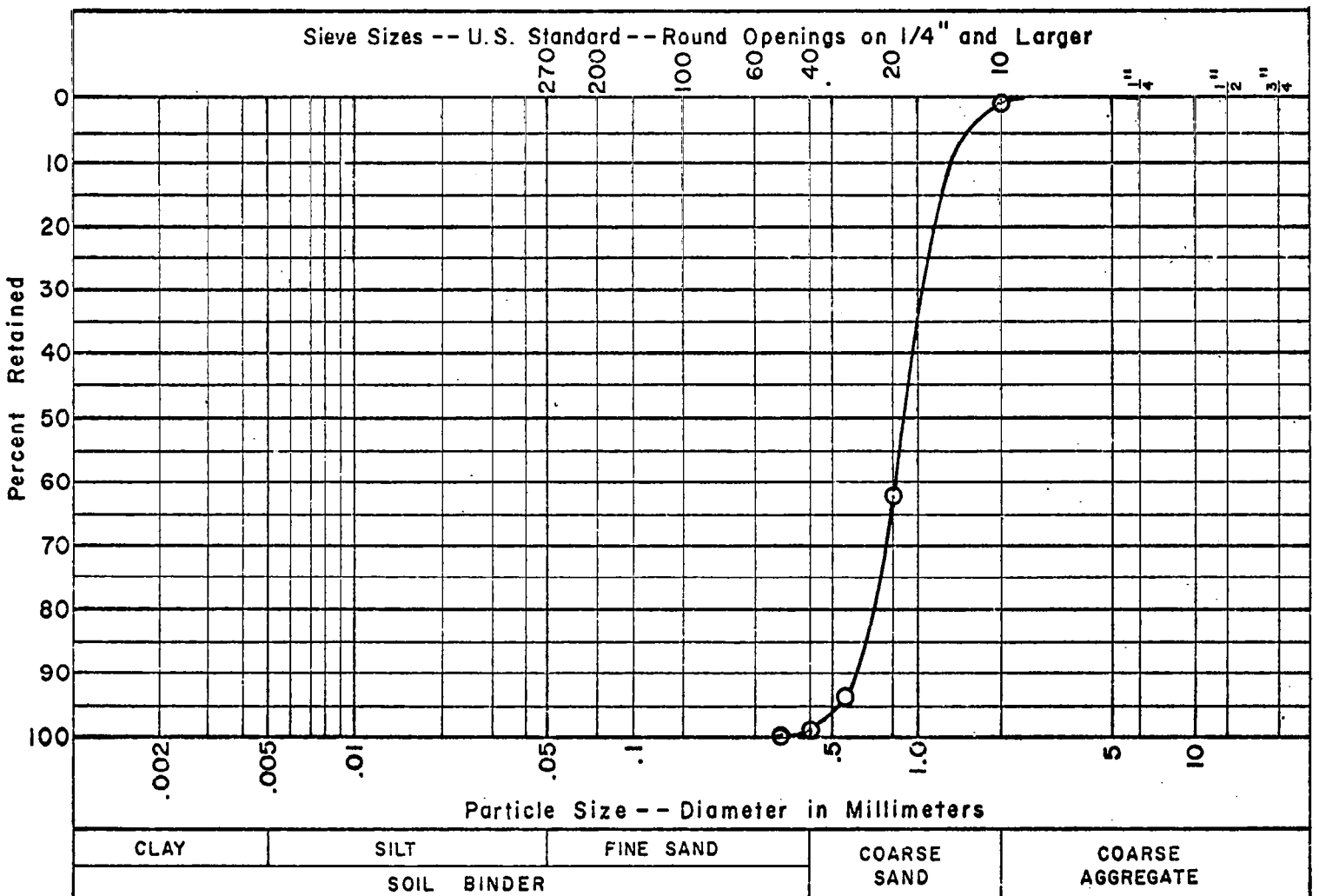

FIGURE 11

CHAPTER V

EXPERIMENTAL PROCEDURES

The procedures for this investigation are described in two main categories: data collection and data reduction.

DATA COLLECTION

The investigation procedure was the same for all targets, with the exception of the slight variations between laboratory and field testing. The arrangement for field testing is shown in Photo No. 2.

Target Preparation

Preparation of targets for in situ testing generally required removing grass and other non-soil materials, and leveling the impact surface. This was done by hand, or, as in the case of the clay, with a shovel.

Laboratory tests, including most of the tests in this program, were run on sand placed in a waterproof 32-gallon can, 20 in. in diameter. Enough material was placed in the can to fill half of it. The sand was vibrated to the desired density when it was dry or saturated, but when moist it had to be hand-packed, layer by layer.

Several tests were run on each soil condition to minimize the possibility of a poor test being used in data analysis. For these multiple tests on the same soil condition, the sand underwent the same preparation process each time. The chronological soil data listing, Table 3 in Appendix C, shows this control of the soil density and moisture.

Equipment Preparation

After the target area was prepared, the tube was set in place and leveled. The height of the base above the soil was then measured by sticking

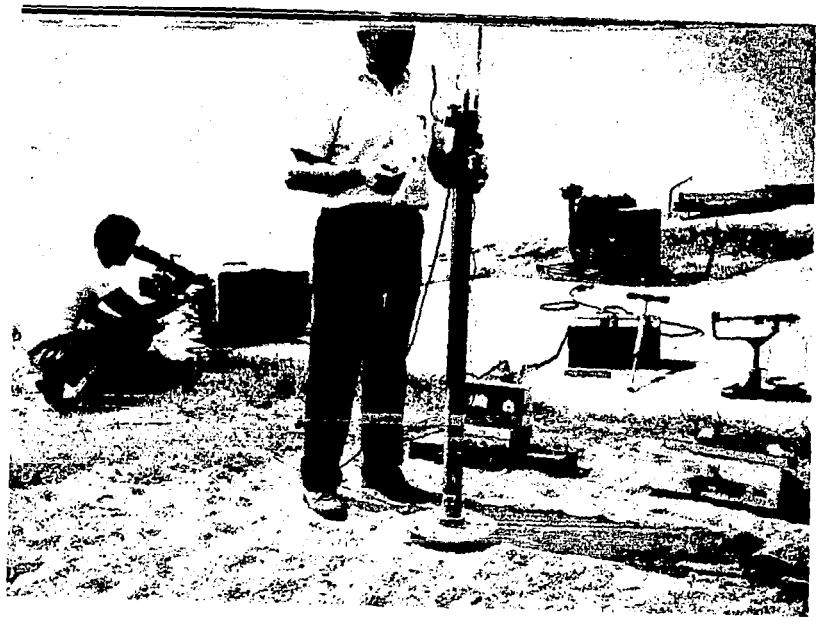

PHOTO NO. 2
Field Testing Arrangement

a graduated dowel through holes in the base around the impact area, and the lower velocity contact was set in the desired position. The oscilloscope was set, the information recorded, and the input voltages checked. A final check on the position of the trace was usually made, after which the Polaroid camera shutter was opened and the equipment was ready for a drop.

Testing

After the pin was pulled, the projectile was held firmly against the upper contact and released. After the drop, the fly leads could be detached, the tube removed, and the penetration of the projectile measured. The static penetration tests were then performed, usually two or three around the impact point. The method followed was to penetrate to the same depth as the projectile, read that force level, then penetrate until the force level reached 100 lbs., thereby obtaining an approximate static force-penetration curve. The average of the static tests was used. This procedure is shown in Photo No. 3.

A sample was then taken from a nearby but undisturbed portion of the impact area, as in Photo No. 4, and weighed immediately. Samples were oven-dried, usually for 24 hours, thus completing the necessary data collection procedures.

DATA REDUCTION

Reduction of the test data included processing the dynamic penetration information for computer analysis, and doing the necessary computations and plotting of the soil data and static tests.

Process

The photograph records of the velocity and force-time traces were reproduced in the form of positive image transparencies through the use of a

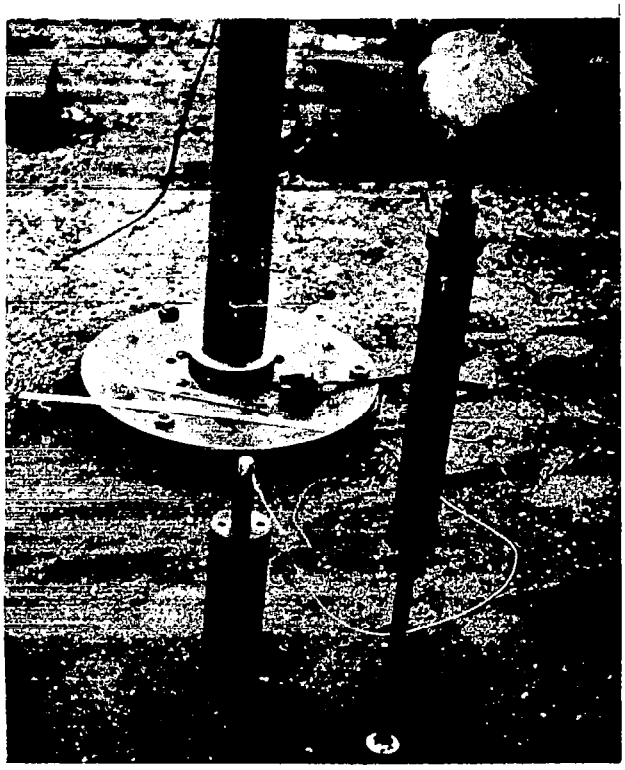

PHOTO NO. 3
Method of taking static penetrometer test.

PHOTO NO. 4
Soil sampling method.

3-M Co. Model 70 dry photo copier. An overhead projector was employed to project enlarged records on 11 in. by 17 in. graph paper, which were then traced onto the paper for analysis. The force-time trace was then divided into equal time increments, and the ordinate of the curve at each increment was recorded and punched on computer cards. The length of the velocity trace between voltage changes, the oscilloscope settings, the clearance between the tube base and soil, the lower velocity contact setting, and the necessary constants were also punched for computer operation.

Computations

The Principle of the Conservation of Momentum states that for an impacting body having a lumped mass:

$$F(dt) = m(dv) \tag{1}$$

where; F = instantaneous force

t = time

m = mass of the body

v = penetrating velocity.

The left side of the equation is the area under the force-time pulse, the integration of which yields the change in penetrating velocity:

$$\frac{1}{m} \int_0^t F(dt) = V_i - v = u \tag{2}$$

where; V_i = impact velocity

u = change in penetrating velocity.

If the instantaneous velocity, (v), during penetration equals the impact velocity, (V_i), minus the change in penetrating velocity, (u), it

follows that:

$$\int_0^t v(dt) = y \qquad (3)$$

where; y = penetration depth.

A computer program was written to manipulate the data in this manner after applying the necessary computation constants. Obtaining the correct impact velocity, (V_i), obviously was quite important, and calculating it with the known drop time between contacts was done as follows.

The equation of the motion of the mass is:

$$h = \frac{1}{2} g t^2 \qquad (4)$$

where; h = drop height

g = acceleration due to gravity

t = corresponding drop time.

If the effective acceleration were reduced somewhat due to air resistance and friction to a value (g'), then:

$$h_1 = \frac{1}{2} g' t_1^2 \qquad (5)$$

where; h_1 = drop height of the projectile between velocity contacts

t_1 = drop time between velocity contacts (measured on oscilloscope).

If (h_2) were the total drop height of the projectile to the target, and if (V_i) were the impacting velocity, then:

$$V_i = \sqrt{2g'h_2} \quad . \qquad (6)$$

Substituting: $$g' = \frac{2h_1}{t_1^2} \quad (7)$$

yields: $$V_i = \frac{2}{t_1}\sqrt{h_1 h_2} \quad . \quad (8)$$

Checks were made on this method of obtaining impact velocity by inserting supplemental velocity contact positions, and the results were in good agreement with the chosen mode of calculation.

Appendix B contains a discussion, input instructions, a listing, and representative output from the FORTRAN program used. It calculates the instantaneous forces, velocities, and penetrations for the time increments chosen. Also available is the option to have it plot out the force-time and force-penetration curves of each test, which are included in this text.

The reduction of the static penetrometer data consisted of drawing the force-penetration curves and tabulating forces. The soil data calculations included determinations of the unit weights, and the volumetric amounts of the components - air, water, and solids.

CHAPTER VI

RESULTS

The results of this investigation generally are in agreement with existing impact theories. Information has also been developed on other aspects of dynamic interaction, such as the influence of the volume constituents on impact response. Recommendations are made for an improved penetrometer testing program.

ANALYSIS OF DATA

An analysis of representative test data, presented here in several forms, yields significant information about impact behavior under the conditions of this testing program.

Characteristics of Impacts

In general, there are three types of impacts - elastic, plastic, and penetration. Perfectly elastic impacts never occur, but can be closely approximated by impact between solid steel objects, or even between steel and concrete. Figure 12, (a), shows the characteristic deformation and force-time pulse, respectively, for elastic impact[3]. These same characteristics are shown for plastic impact in Figure 12, (b), wherein a non-deforming penetrator enters a softer material for a distance usually less than the diameter of the penetrator. Penetration impact, represented in Figure 12, (c), is the most complex of the three types. For a given input energy (the same mass and velocity of the penetrator), the maximum force of the elastic impact will be larger than that of the plastic impact, which is larger than that of the penetration impact. The maximum time for the elastic impact will be shorter than that of the plastic impact, which is shorter than the penetration

FIGURE 12

DEFORMATIONS AND FORCE-TIME CHARACTERISTICS OF

IMPACT TYPES

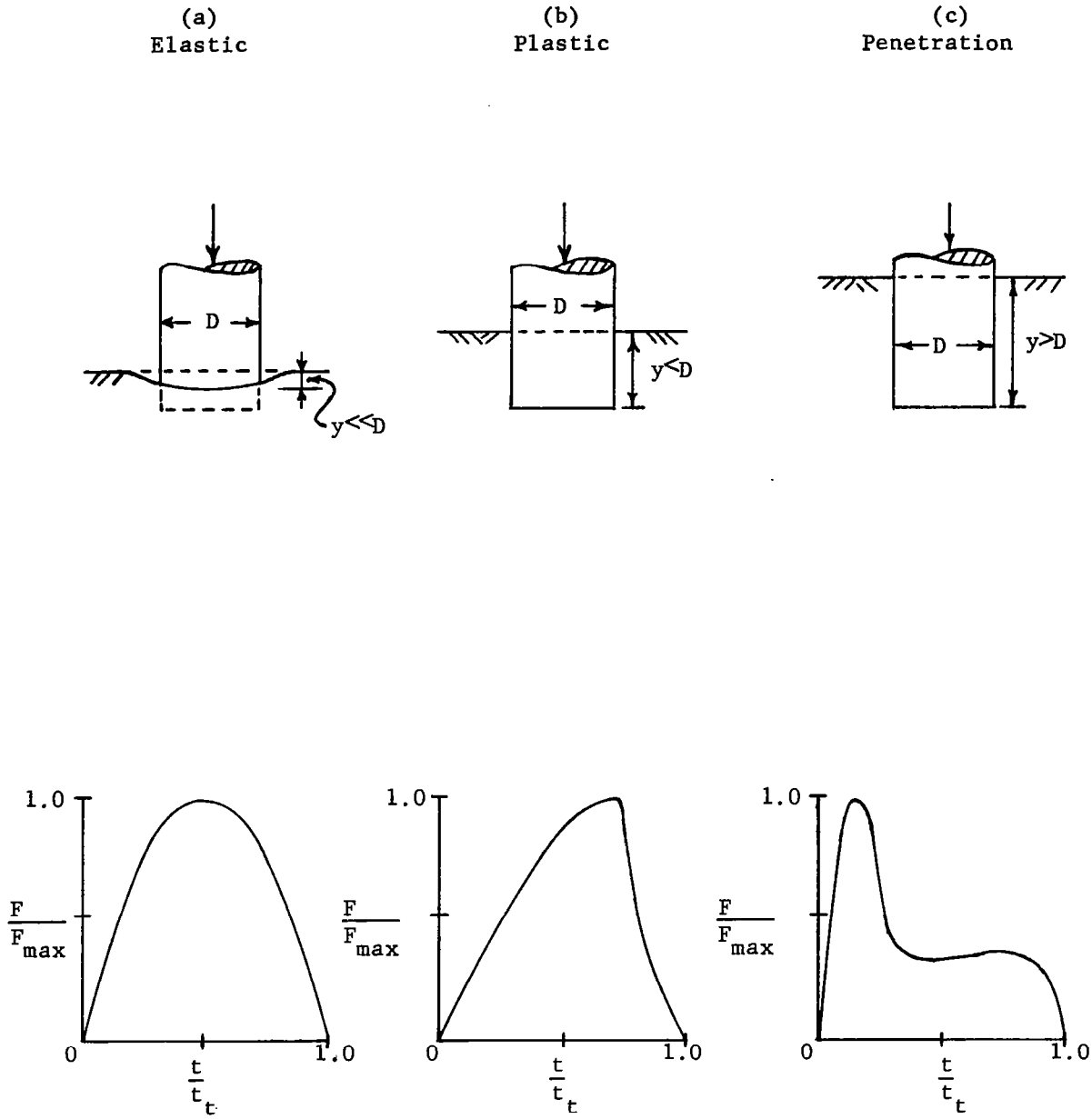

impact time. Most projectile-soil impacts are of the penetration or plastic type of impact or a combination thereof.

In an attempt to describe the impact mechanism between a blunt-ended cylinder and a non-compressible soil target, several references are made to the Prandtl-Terzaghi system for plastic equilibrium after failure beneath a continuous footing[9]. In this analysis, shown in Figure 13, the most notable simplifying assumptions made are: (1) the base of the footing is rough, (2) its depth below the surface is less than its width, (3) the footing exerts a constant, uniform, vertical pressure on the soil, and (4) that the soil is a homogeneous, isotropic, continuum which fails in general shear. Zone I of the failure mechanism is a wedge zone of active pressure in which the soil is in elastic equilibrium and acts as part of the footing. At the instant of failure it is resisted by the passive earth pressure, (P_p), acting at an angle (ϕ) with the surface, and by the cohesion force, (C_a), acting tangentially to the wedge surface. The Zones II are zones of radial shear whose failure planes are the logarithmic spirals shown. The zones of passive pressure, Zones III, have the tangential failure planes. The cohesion force, (C_a), is due to the cohesion of the soil, (c), while (ϕ) is the angle of internal friction of the soil.

It is emphasized that this system is, at best, an oversimplification for a complex static condition. Therefore, correlation to the dynamic case, which is an unstable case including viscous and inertial factors, is quite difficult to effect. However, investigations have shown that some correlation exists between the Prandtl-Terzaghi bearing capacity formula and experimental values for a one-inch wide penetrator in a simulated cohesionless soil[1]. Also, analyses of projectile penetrations in soil-like cohesive media[7], and into cohesionless sand and slightly cohesive soils[10] suggest the

FIGURE 13

PLASTIC EQUILIBRIUM AFTER A SOIL FAILURE
BENEATH A FOOTING

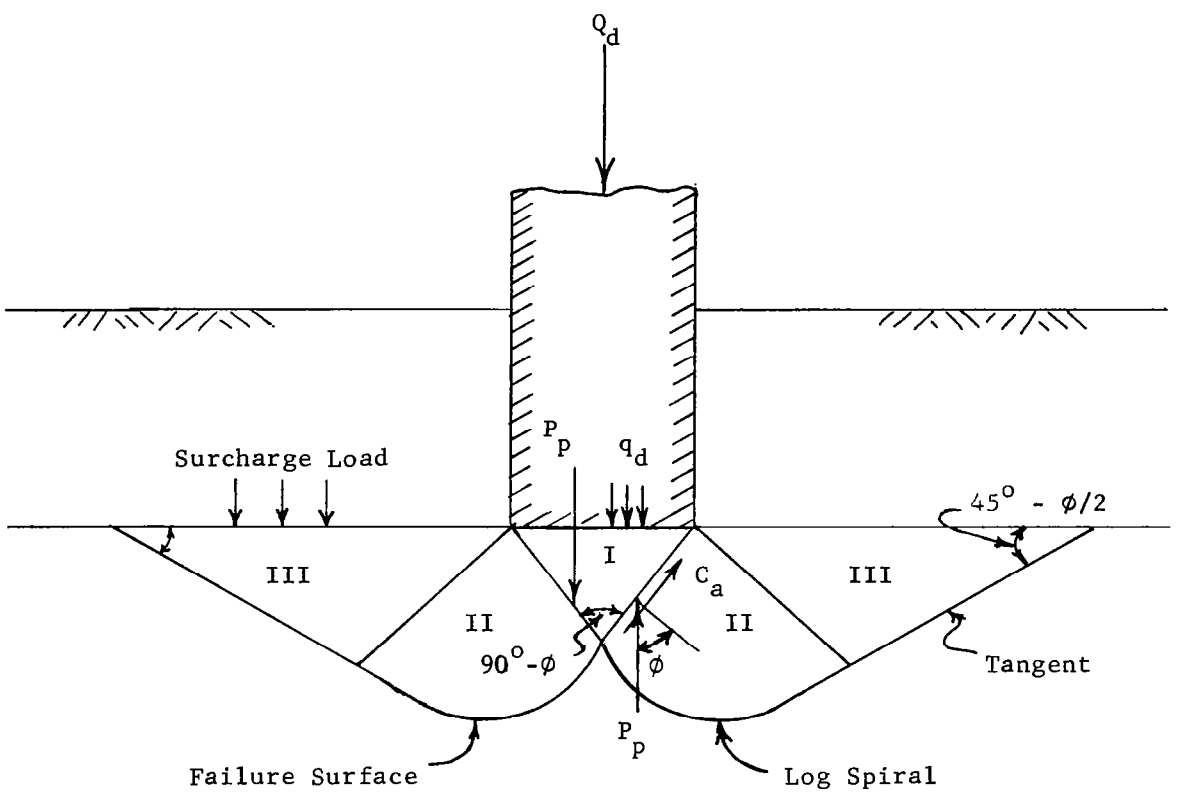

occurrence of a penetration mechanism similar to the Prandtl-Terzaghi system. Figure 14 shows just such a type of assumed mechanism and the direction of soil flow. High speed photographs of projectiles penetrating both two-dimensional granular target media (small steel cylinders), and dry Ottawa sand, clearly show the formation of a soil wedge, shear fronts, and soil ejection.

Soil Characteristics Regarding Impacts

Soils may be classified into four different general types with regard to impact behavior[11]. By assuming that soil impacts undergo some form of the above mechanism, explanation of impact-related phenomena for certain conditions is simplified.

The first type is saturated dense sand and silt and saturated over-consolidated clays, and is included in this investigation, except for silt. Statically, these soils have a higher undrained strength than drained strength, and shearing causes a volume increase. Under dynamic loads, the drainage does not take place and the material is essentially incompressible. Observations show that soils with sufficient cohesive strength (clays) allow the penetration hole to stay open after an impact. The volume of the original hole, or volume of displaced soil, is about equal to the volume of the soil rising above the original surface and closing in on the hole. Saturated sands tend to flow around the penetrator foot and fill the hole shortly after the impact process is ended, even though the characteristic raised surface for incompressible materials is evident.

The second type includes dense, dry-to-moist sands, silts, and clays. Experimental data for this investigation include the sands, but not silts and clays. The effects of penetration impacts on these sands vary because of varying moisture content. The dry sands eject much of the displaced

FIGURE 14

ASSUMED CONTINUOUS PENETRATION MECHANISM

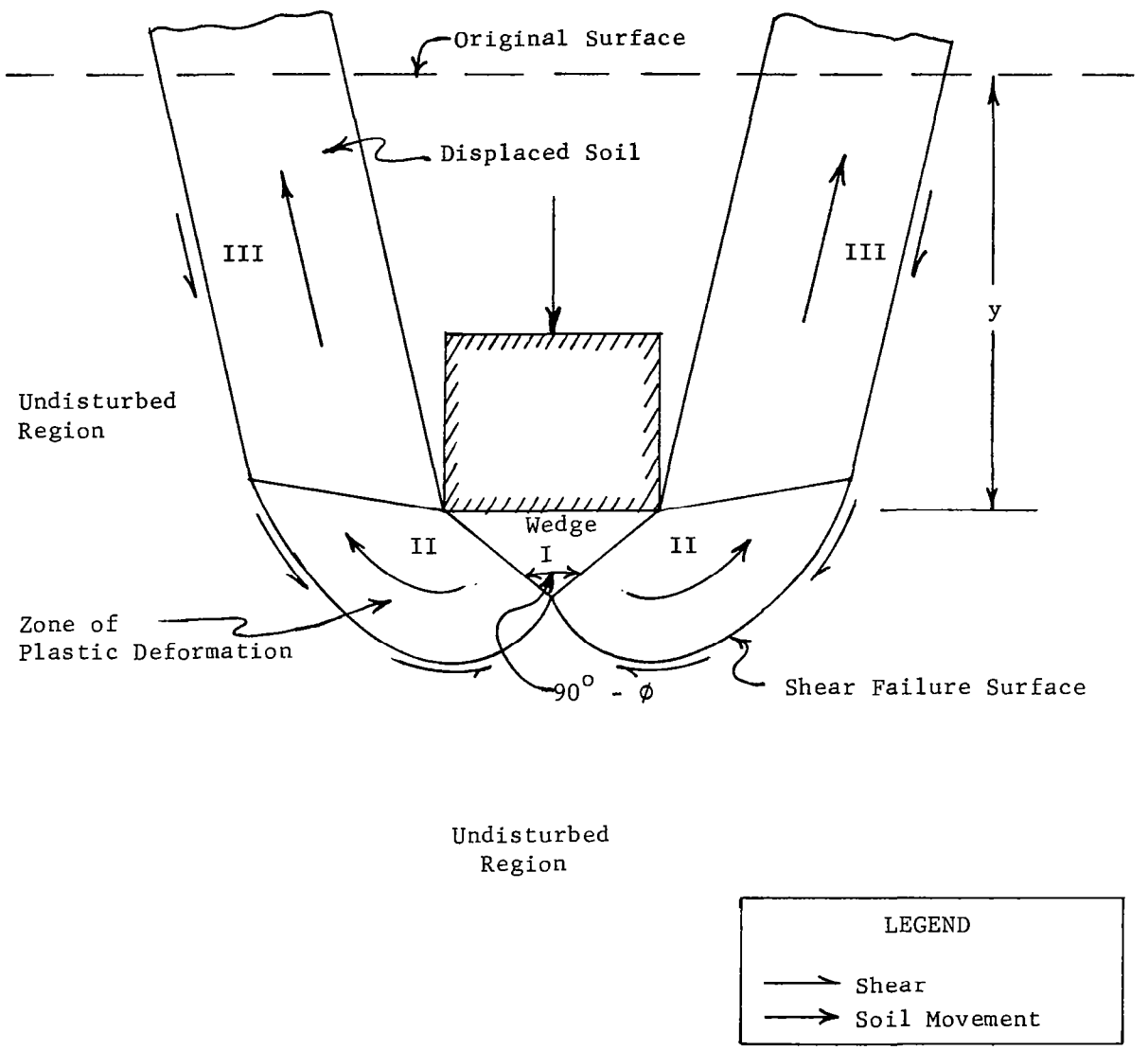

material, while the moist sands tend to show the characteristic raised surface with radial tension cracks around the open hole. Their frictional strength consists of resistance to particle sliding and slipping, and resistance to volume change. At the low velocities and confining pressures of this test program, these effects were not pronounced, even though there was some evidence of crushing behavior. Dessicated clays should behave much like a brittle solid until slippage occurs, then as a plastic solid.

Saturated loose sand and silts and saturated normally consolidated clays constitute the third general soil type. Statically, these materials have a drained strength higher than the undrained strength, and tend to decrease in volume when sheared. No drainage occurs during an impact, causing the material to be essentially incompressible and at constant volume with high pore pressures. This in turn reduces the total pressure between particles and causes the effective pressure to be small. If, in noncohesive material, this effective pressure approaches zero, the material behaves as a viscous fluid, in a process called liquefaction. Approximately the same is true for clays.

The fourth general type of soil includes loose, dry-to-moist sands and silts. Some loose sands were tested in this investigation. The materials decrease in volume when sheared and act as compressible media. Shock waves should decrease the friction of the sand and collapse the structure of silt. Resistance to compression after this collapse would be the only important characteristic of this soil to resist penetration until shearing resistance took effect at the critical density. The displacement of the soil above the original surface during this type of impact is scarcely noticeable as the process is accompanied by considerable crushing and densification.

Representative Test Data

An attempt was made to include in both this chapter and Appendix C all usable data, because in the case of research such as this which includes many parameters and measurements, there may be no present knowledge of the possible analyses which could be applied to these data.

The force-time pulses, or "signatures", of tests on the soils described in Chapter IV and Appendix C were reduced for calculation by the computer program described in Appendix B. Since multiple tests were run on most of the soil conditions, only the representative information from each condition is included in this chapter.

Table No. 1 shows static and dynamic force-penetration data, and the pertinent soil data: wet weight, (γ_w), and volumetric percentages of solids, (s_v), water, (w_v), and air, (a_v). Figures 15 through 22 show the dynamic force-time and force-penetration curves for these representative soil tests as plotted by the computer. The static force-penetration curves as well as the measured penetration depths have been added to these curves.

Discussion of Data

Because of the complex nature of the impact mechanism, some characteristics of these data were observed to be affected by various conditions. It was desired to define or explain these conditions when possible, in addition to discussing and analyzing data.

Impact Tests

As previously discussed, the types of projectile-soil impacts are the continuous penetration type, the plastic type, or a combination of the two. An examination of the force-time signatures will reveal that the provisions for essentially plastic impact are met by test 10-10-9 in the clay,

TABLE NO. 1

REPRESENTATIVE TEST DATA

TEST NO.	SOIL DATA					DYNAMIC				STATIC	
	TYPE					MAX. FORCE		PENETRATION		FORCE	PENETRATION
		γ_w	s_v	a_v	w_v	F_c	F_s	Calculated	Measured	P	Measured
		(pcf)	(%)	(%)	(%)	(lbs)	(lbs)	(in)	(in)	(lbs)	(in)
11-22-1	Water	62.4	0.0	0.0	100.0	5.0	5.7	3.21	3.5	--	--
11-22-7	SP-(TCS)	86.9	52.6	47.4	0.0	474.2	44.3	2.64	2.7	115*	2.7
11-15-3	SP-(OS)	108.0	65.4	34.6	0.0	262.2	64.5	3.55	3.5	66	3.5
11-9-3	SP-(OS)	107.0	57.8	24.7	17.5	284.0	94.7	3.22	3.0	69	3.0
11-10-1	SP-(OS)	118.8	60.4	10.2	29.4	116.8	121.6	2.35	2.6	58	2.6
11-11-4	SP-(OS)	130.0	66.2	2.7	31.1	176.8	140.8	1.84	1.7	15	1.7
11-16-2	SP-(CRS)	100.4	60.7	39.3	0.0	407.7	61.5	2.81	2.8	69	2.8
11-16-5	SP-(CRS)	99.8	55.8	31.7	12.5	257.7	82.8	3.35	3.4	72	3.4
11-18-2	SP-(CRS)	111.6	56.1	13.7	30.2	208.0	173.1	1.73	1.7	72	1.7
11-18-4	SP-(CRS)	121.0	60.6	6.4	33.0	116.4	197.8	1.83	1.9	81	1.9
12-2-3	SW-(CA)	111.0	67.2	32.8	0.0	357.5	68.0	3.41	3.5	100	3.5
10-10-7	SW-(CA)	101.2	59.6	36.0	4.4	484.9	111.5	1.71	1.9	110*	1.9
12-2-5	SW-(CA)	101.3	58.6	33.8	7.6	192.1	96.0	2.55	3.0	77	3.0
12-2-8	SW-(CA)	131.5	70.0	4.2	25.8	431.1	213.6	1.16	1.3	10	1.3
10-10-9	CH-(BS)	112.0	50.8	5.8	43.4	--	310.7	0.96	0.8	200*	0.8

* Extrapolated values

FIGURE 15

FORCE-TIME AND FORCE-PENETRATION CURVES FROM TESTS IN WATER AND TEXAS CRUSHED STONE, SP-(TCS)

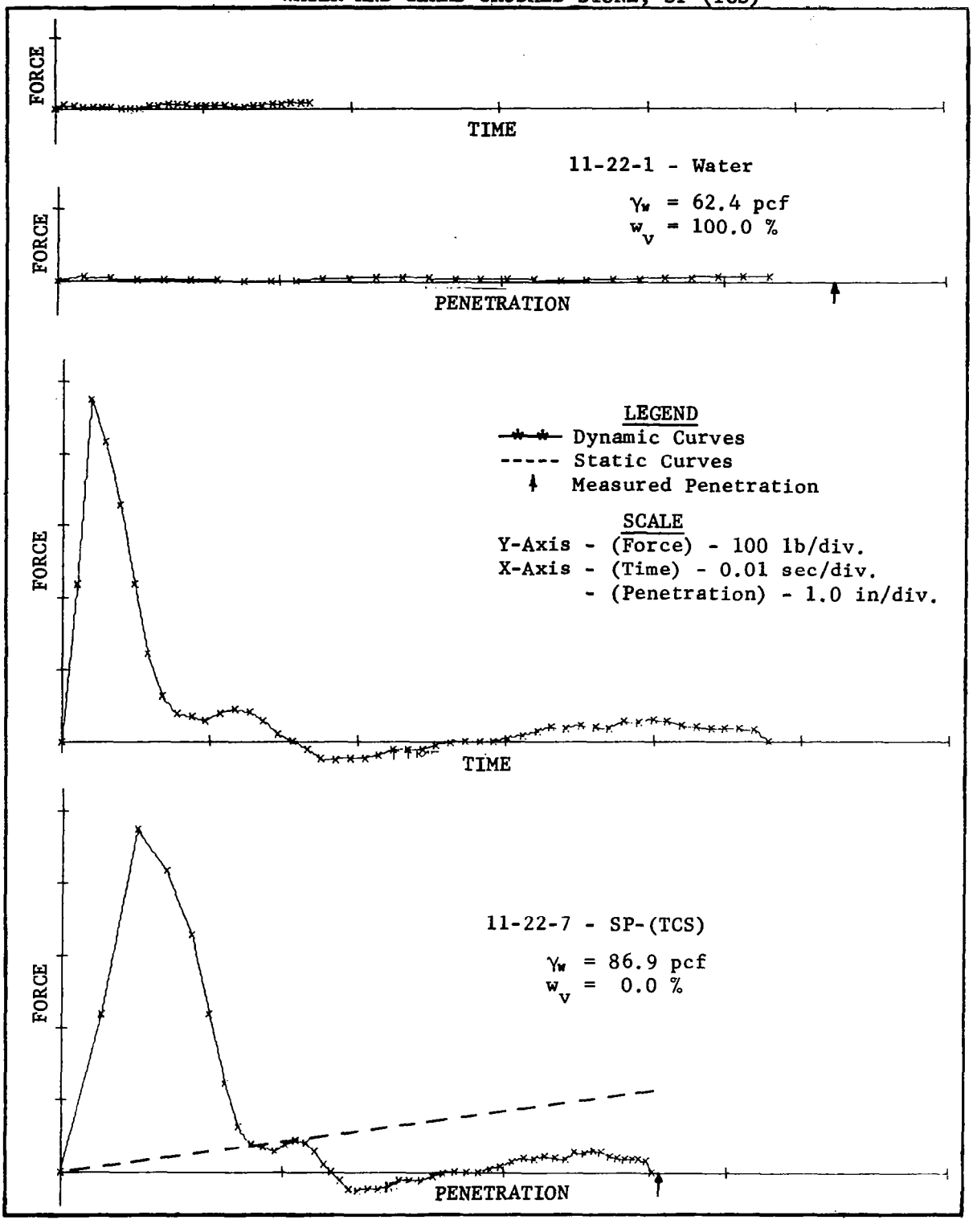

FIGURE 16

FORCE-TIME AND FORCE-PENETRATION CURVES FROM TESTS IN OTTAWA SAND, SP-(OS)

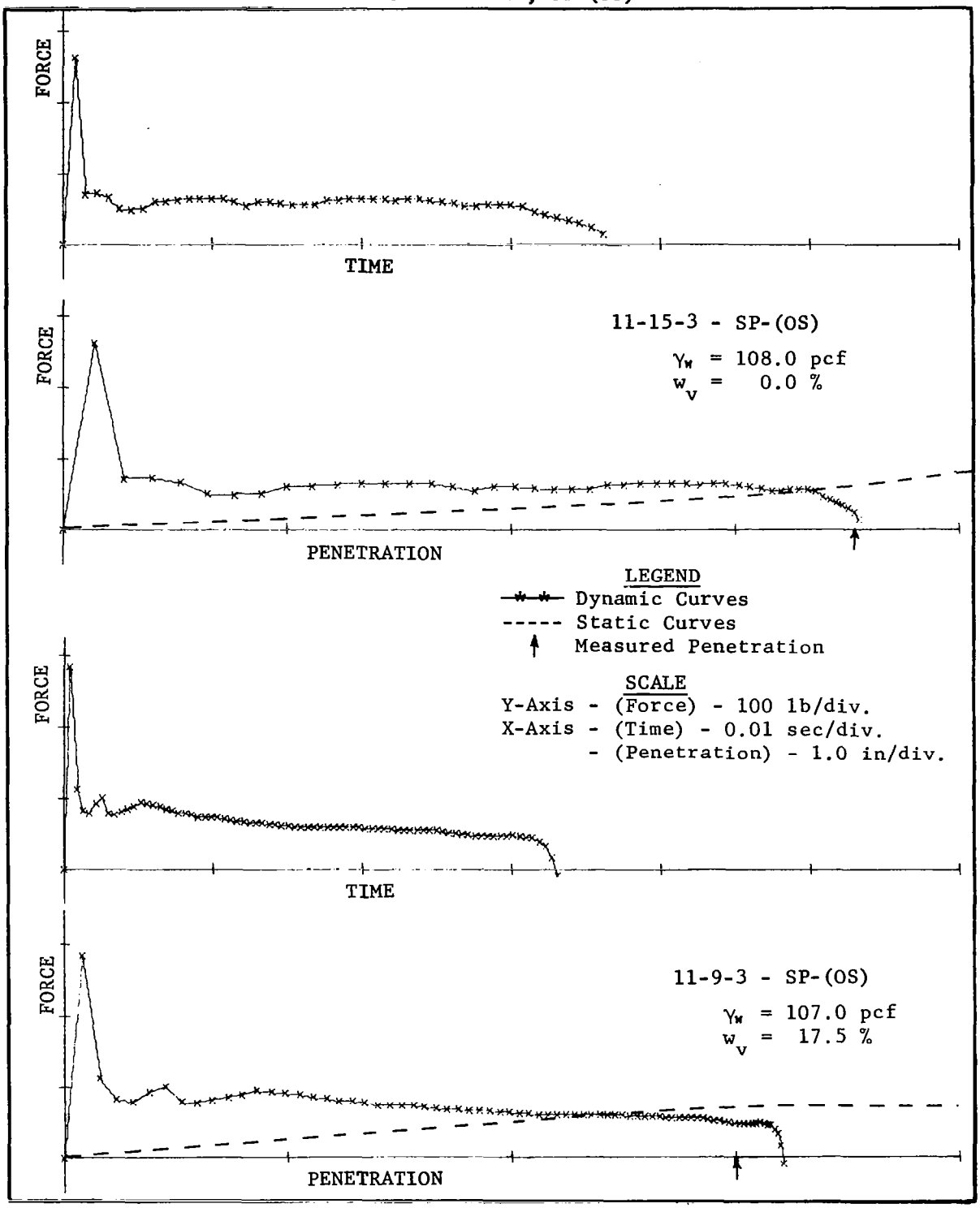

FIGURE 17

FORCE-TIME AND FORCE-PENETRATION CURVES FROM TESTS IN OTTAWA SAND, SP-(OS)

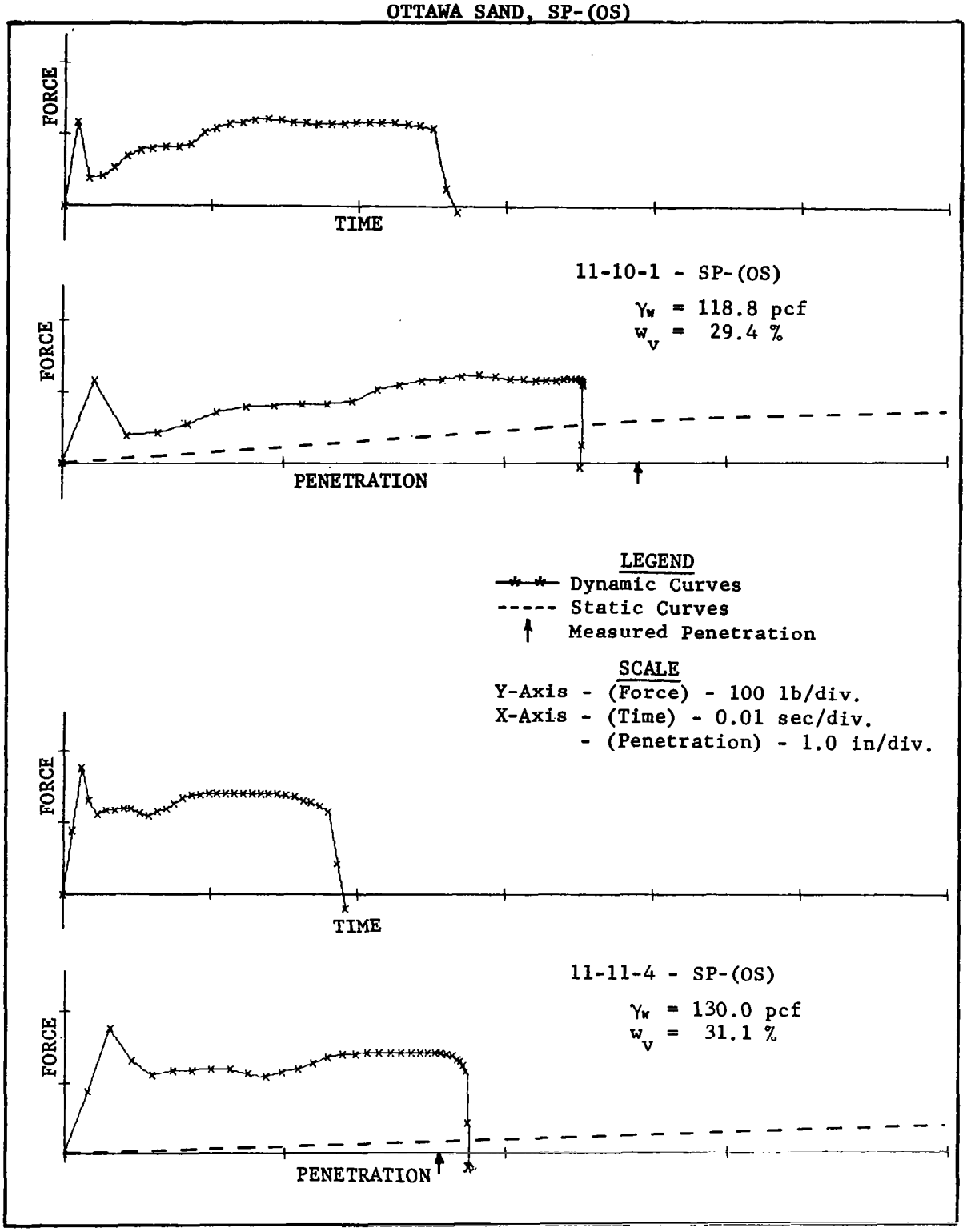

FIGURE 18

FORCE-TIME AND FORCE-PENETRATION CURVES FROM TESTS IN COLORADO RIVER SAND, SP-(CRS)

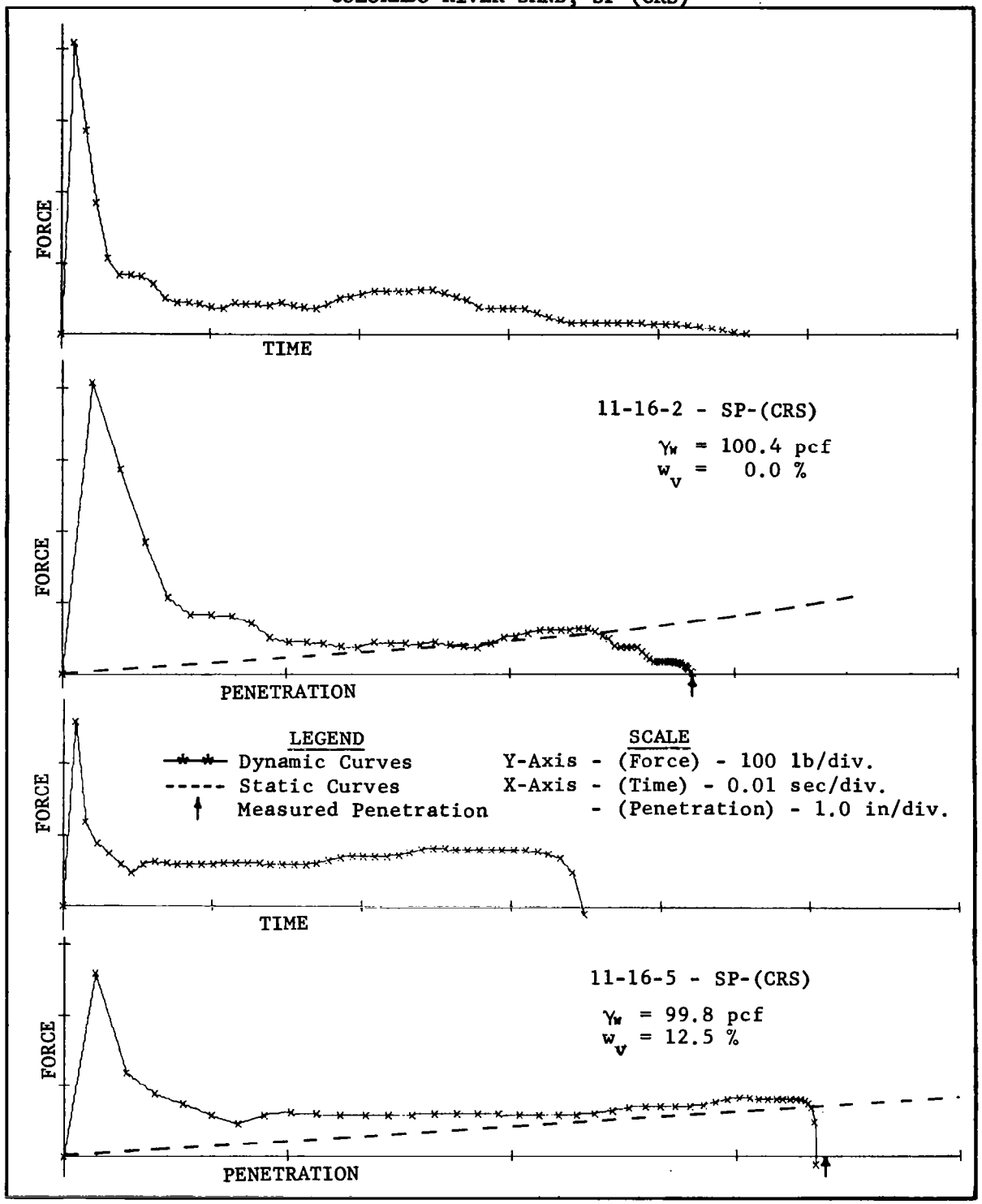

FIGURE 19

FORCE-TIME AND FORCE-PENETRATION CURVES FROM TESTS IN COLORADO RIVER SAND, SP-(CRS)

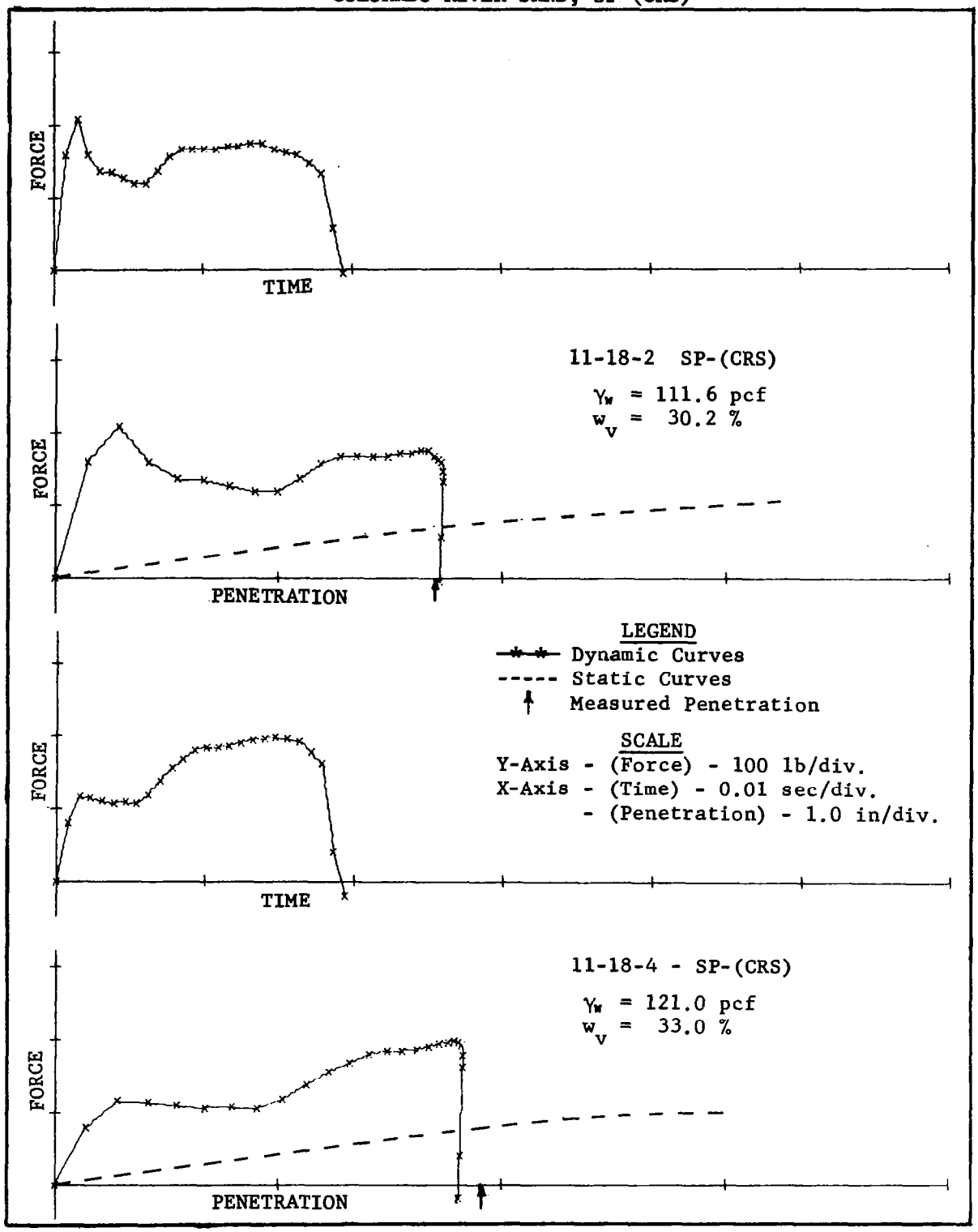

FIGURE 20

FORCE-TIME AND FORCE-PENETRATION CURVES FROM TESTS IN CAPITOL AGGREGATES SAND, SW-(CA)

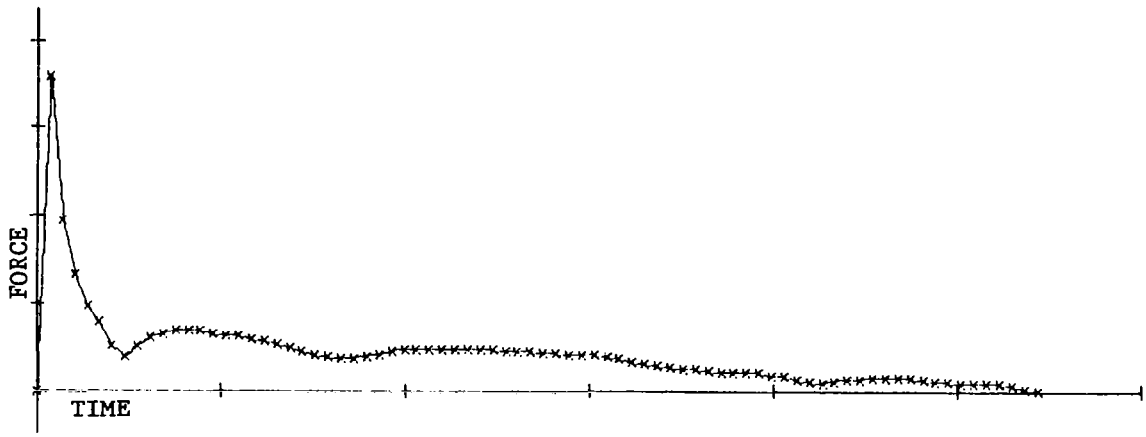

12-2-3 - SW-(CA)

γ_w = 111.0 pcf

w_v = 0.0 %

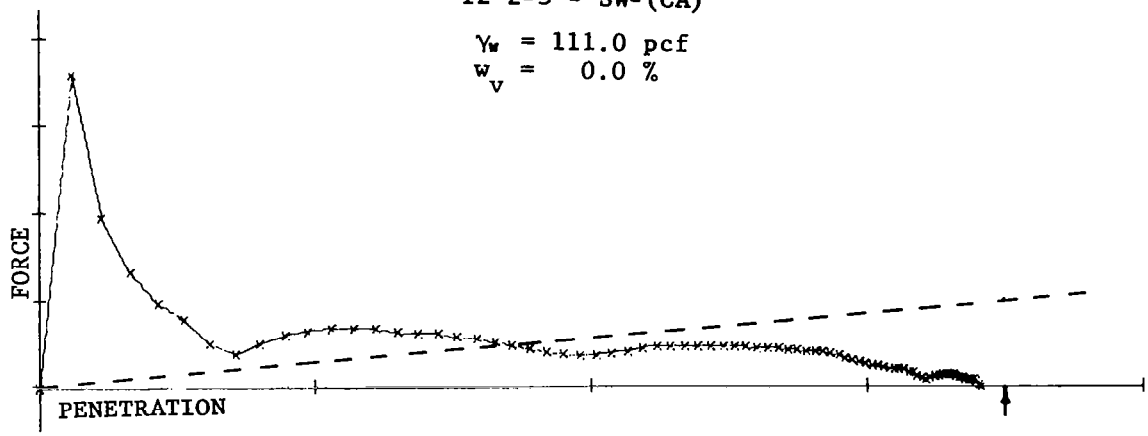

LEGEND

Dynamic Curves

Static Curves

Measured Penetration

SCALE

Y-Axis - (Force) - 100 lb/div.

X-Axis - (Time) - 0.01 sec/div.

- (Penetration) - 1.0 in/div.

FIGURE 21

FORCE-TIME AND FORCE-PENETRATION CURVES FROM TESTS IN CAPITOL AGGREGATES SAND, SW-(CA)

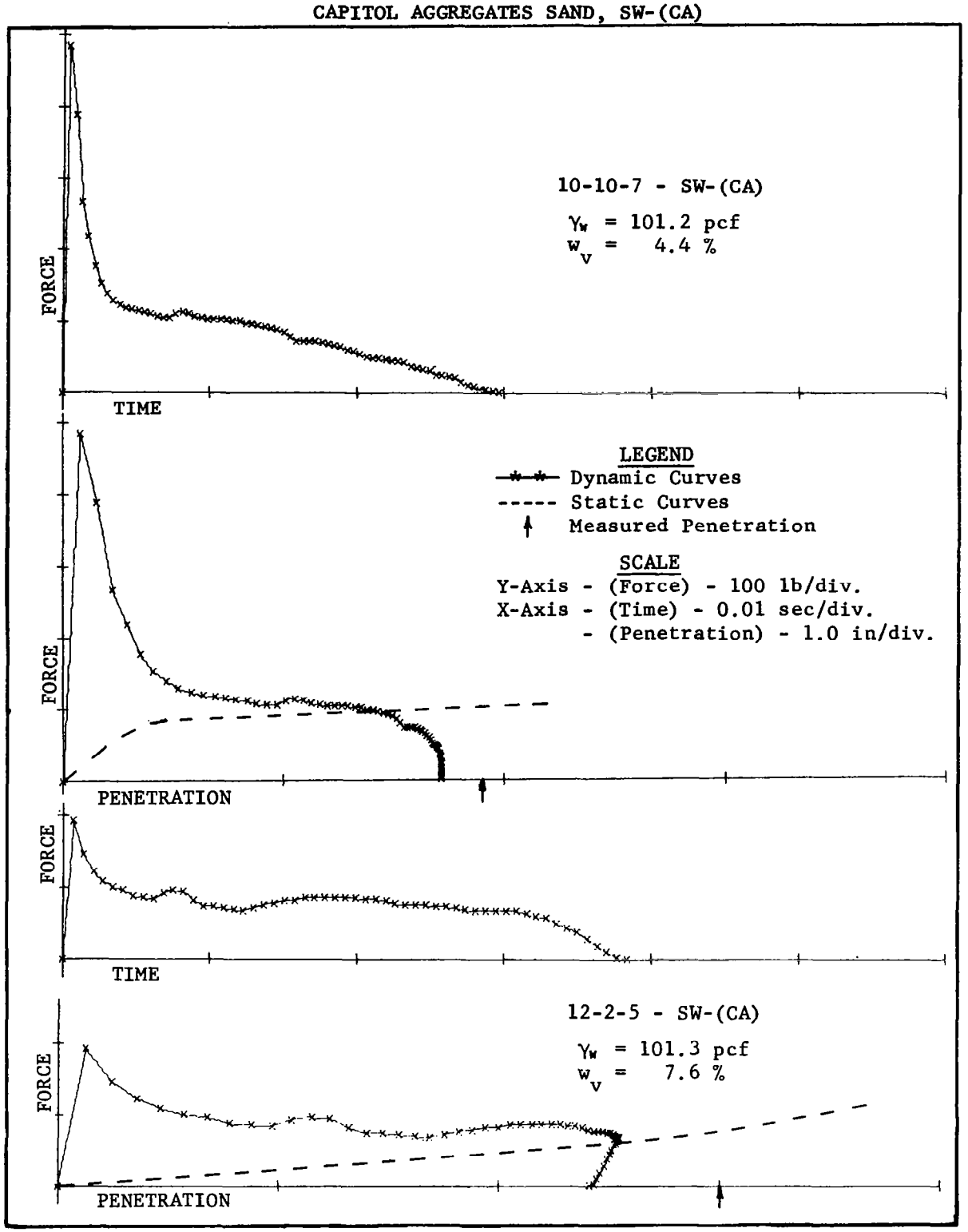

FIGURE 22

FORCE-TIME AND FORCE-PENETRATION CURVES FROM TESTS IN CAPITOL AGGREGATES SAND, SW-(CA), AND DEL RIO CLAY, CH-(BS)

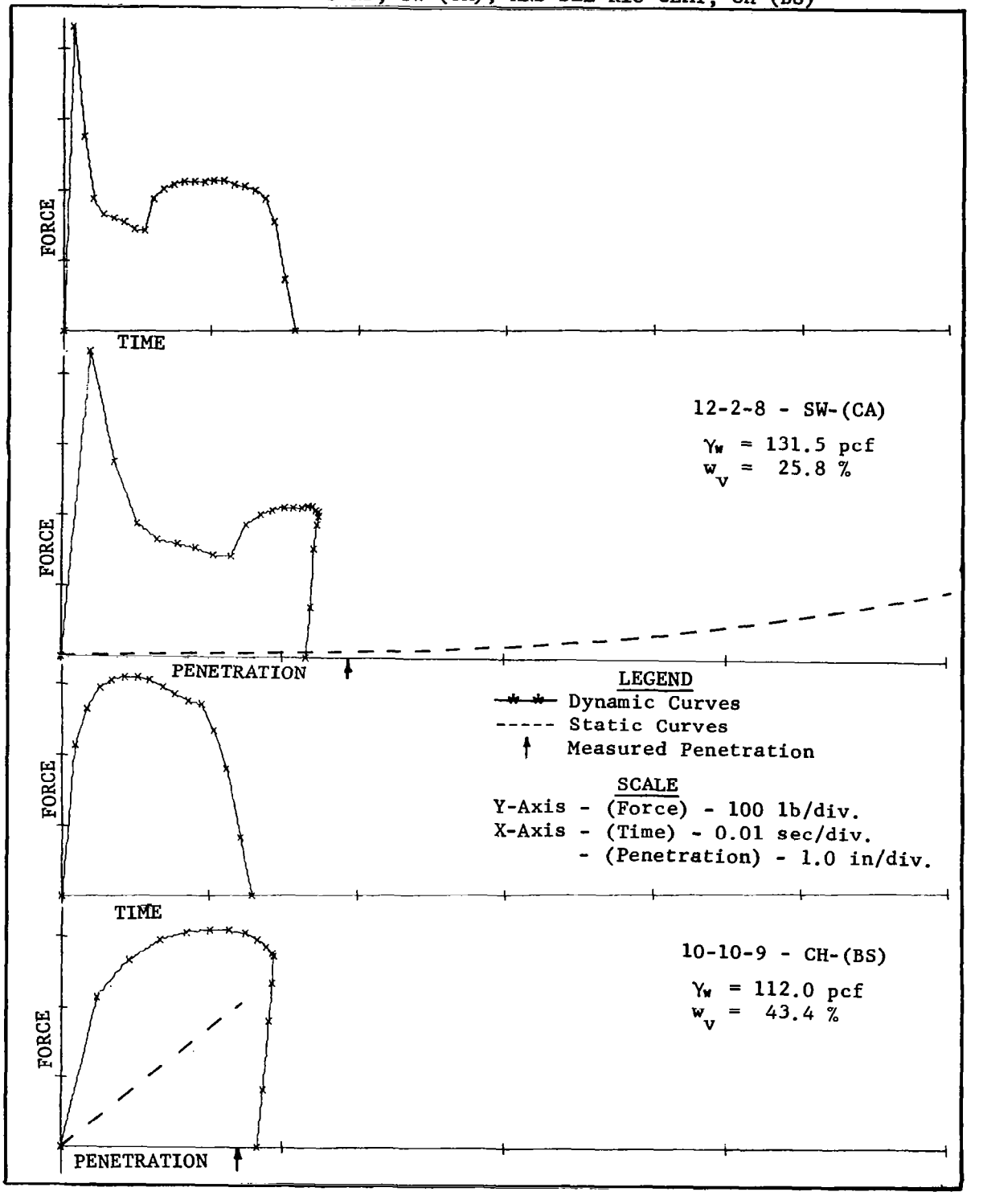

Figure 22. The combination type of impact is generally seen in tests on the saturated or nearly saturated sands, and the continuous penetration type of impact is seen in the impacts on sands with low water content.

On virtually all of the penetration type of impact tests in sands there is an initial force peak, or spike, which also has been encountered in many other investigations of impacts in granular media. This force is listed as the initial contact force, (F_c), in Table No. 1. A secondary force peak, listed as (F_s), usually occurs some time later in the test.

An attempt to analyze the force, (F_c), leads to several theories. The process of liquefaction, previously described as the densification of a loose soil after being impacted, and behavior of the soil as a viscous fluid in the process, could certainly be attributed to some of the cases. Of course, for most of the tests, the density of the sand exceeded, or was close to, the critical density, and liquefaction probably did not occur. Comparison of the test signature of 11-22-7-SP-(TCS), Figure 15, with any of the signatures from the fine grain sands at zero moisture shows a significant difference. This is apparently due to the impact of the penetrometer foot with a relatively smaller number of grains, each having a much larger mass than the fine grain sands, causing them to blast out a crater which was almost 2 in. deep. The tests in the finer sands show a slight trend in this direction as the average grain size increases from (OS) to (CA). From observations, it would also appear that the size of the spike varied from one time to the next when the only soil condition that varied was the surface condition. Smoothing the soil surface by hand after vibration tended to decrease the size of the spike, while impacting on a vibrated, but manually undisturbed, surface yielded a high (F_c). The possibility of some influence by shock waves cannot be discounted.

In any event, for a cylindrical plate contacting surface, the value of (F_c) can be quite high and short in duration, making it extremely difficult to record with precision. As a result, the measured values of (F_c) appear to be random and have no relationship with any other important parameter. In this analysis, the contact force, (F_c), is not significant, recognizing, however, that in a few cases it is large enough to obscure the value of (F_s). A different contact geometry is recommended for future tests if this is to be avoided completely.

For impacts in cohesive soil (10-10-9 in Figure 22), there is no contact force, (F_c), and the peak force for these tests is listed as (F_s). This secondary force tends to exhibit values for cohesive and noncohesive targets alike, which are influenced by various parameters. Figures 23, 24, and 25 show dynamic impact relationships between (F_s), (y), and the total pulse time, (t_t), of an impact, for this investigation. The shape of the curves is due to the nature of the system, which has a constant energy input. However, the relative arrangement of the points suggests that some principal factor, probably shearing strength, influences most soil impacts.

Coulomb's equation for shear is as follows:

$$s = c + p \tan \phi \qquad (9)$$

where;

s = shearing resistance

c = cohesion

p = component of effective stress normal to the surface of sliding

ϕ = angle of internal friction.

The principal source of shear for cohesive soils is the cohesion, (c), while it is internal friction, (ϕ), for noncohesive material. The correlation

FIGURE 23

SECONDARY MAXIMUM FORCE VERSUS MAXIMUM PENETRATION

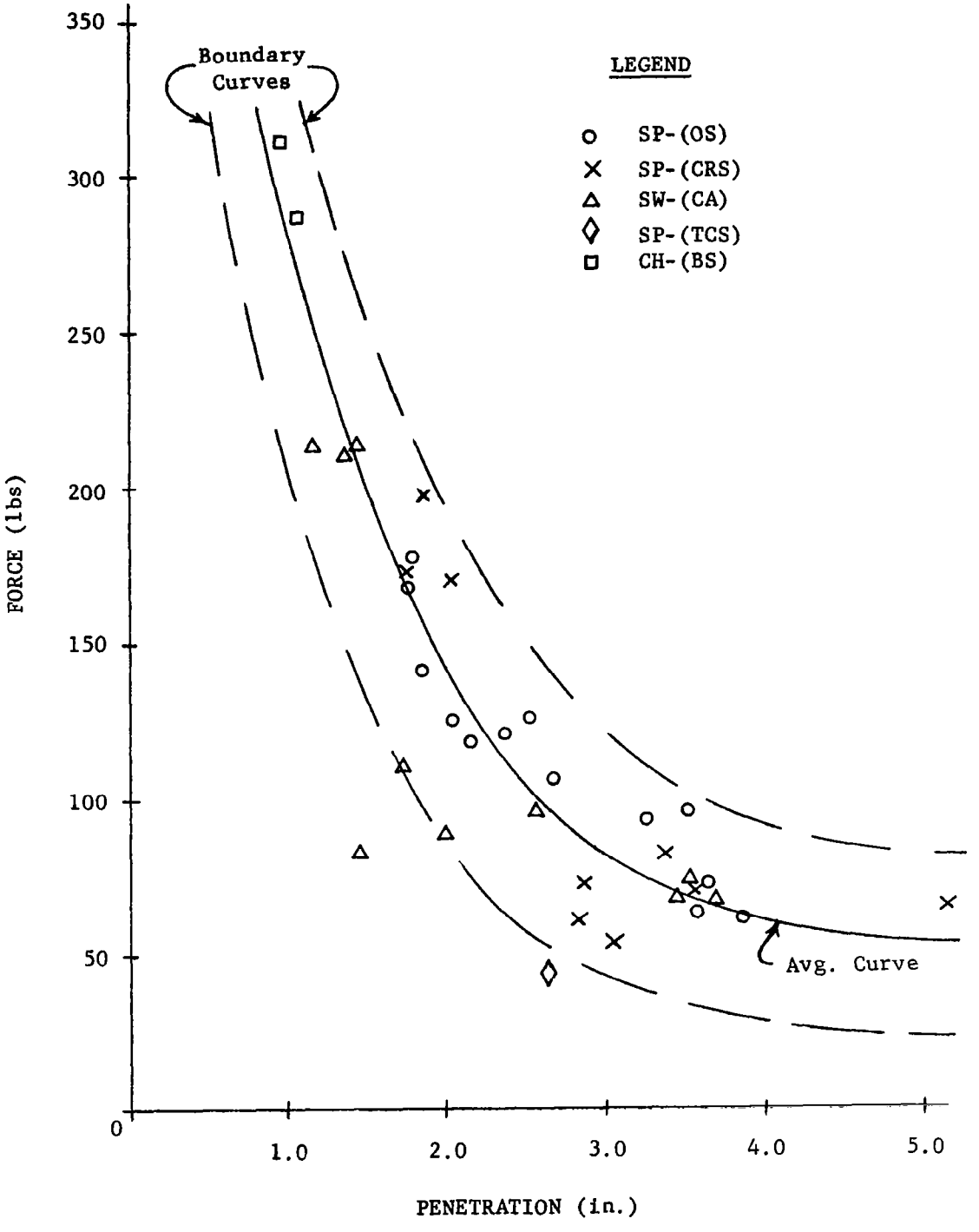

FIGURE 24

MAXIMUM PENETRATION VERSUS TOTAL PULSE TIME

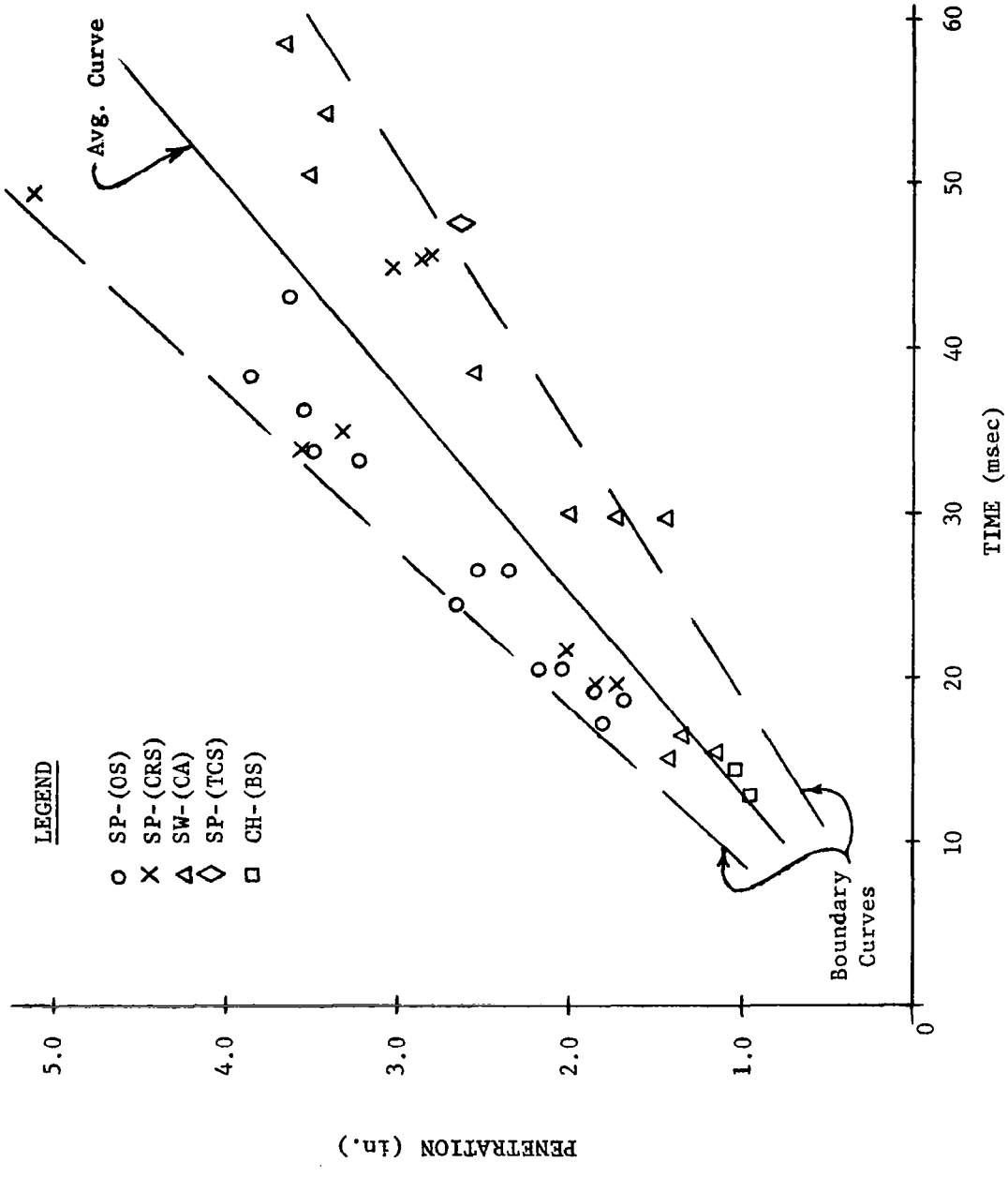

FIGURE 25

SECONDARY MAXIMUM FORCE VERSUS TOTAL PULSE TIME

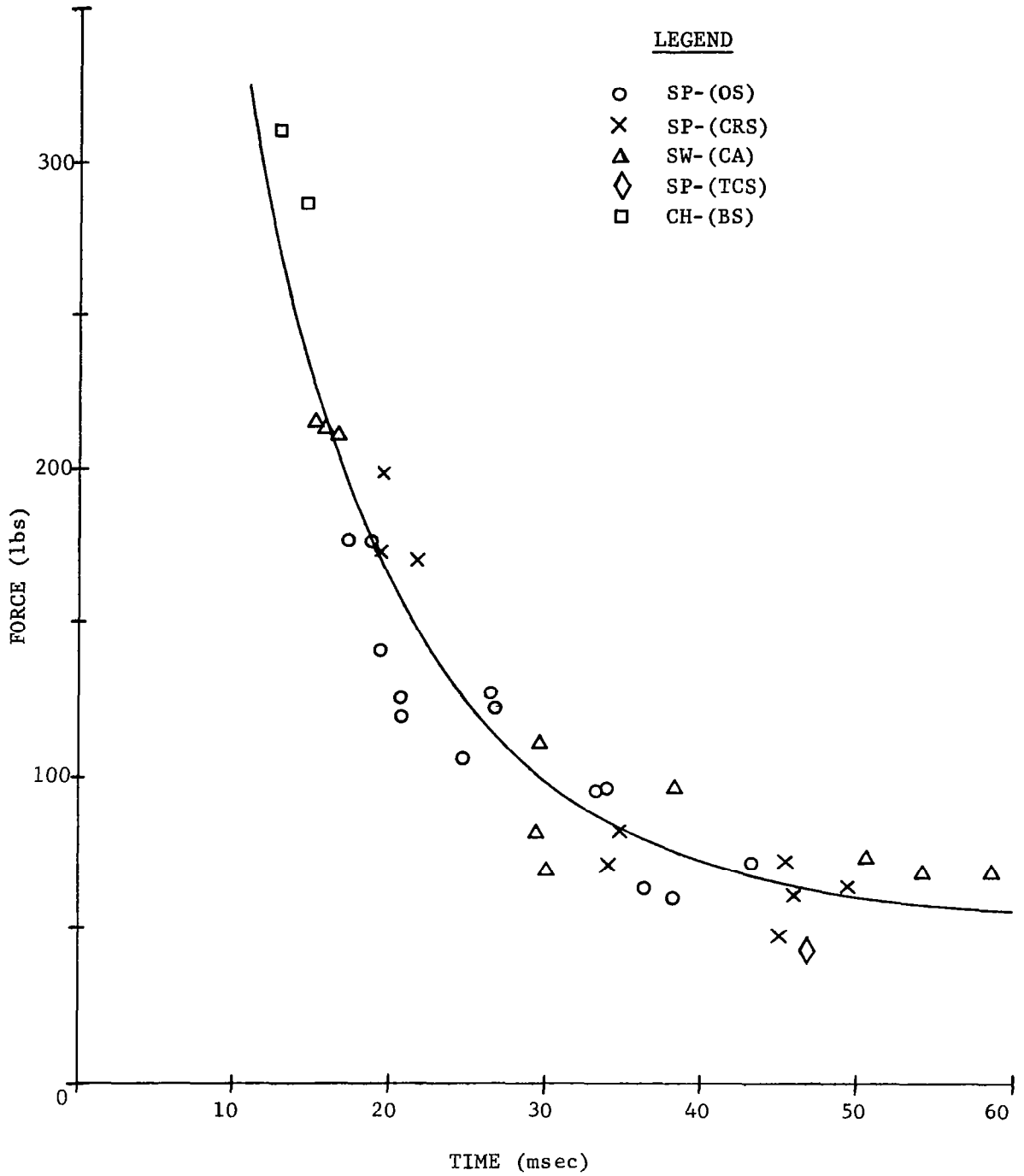

of (F_s) for both soil types on the curves of Figures 23 and 25 tends to point out that shearing resistance is the main influencing factor. It is recognized that density and possibly other parameters have decided influence on impact relationships, but this investigation did not reveal significant information to that effect.

Remote Target Evaluation

The problem of remote target evaluation for impact is of interest for the possibility of landings on earth, but it is extremely critical in the case of extraterrestial landings. The penetrometer concept is quite a valuable tool for this type of target evaluation, as it is feasible to send an instrumented probe, or penetrometer, virtually anywhere landings are anticipated. It should be pointed out that great care must be exercised in the use and interpretation of penetrometer tests, remote or otherwise.

Figure 23 shows the secondary peak force, (F_s), versus penetration depth, (y), for the tests of this investigation. The average curve and the boundary curves show the variable nature of penetration-force relationships. Analysis of this relationship for dynamic tests shows that: (1) penetration varies with different energy input (area under force-time curve); (2) it varies when the energy input is constant and the total pulse time, (t_t), of the test is varied, as in Figure 26, (a); (3) if the energy input, time of pulse, and maximum force levels are held constant, but the centroid of the area of the curve is shifted with respect to time, the penetration will vary accordingly, as shown in Figure 26 (b)[6].

Figure 24 shows the average and boundary curves for the penetration versus total pulse time, further illustrating the above discussion. In Figure 25, however, it is seen that the relationship of (F_s) to the total pulse time is without the variations which accompany penetration. The trends

FIGURE 26

MAXIMUM PENETRATION-IMPACT PULSE RELATIONSHIPS

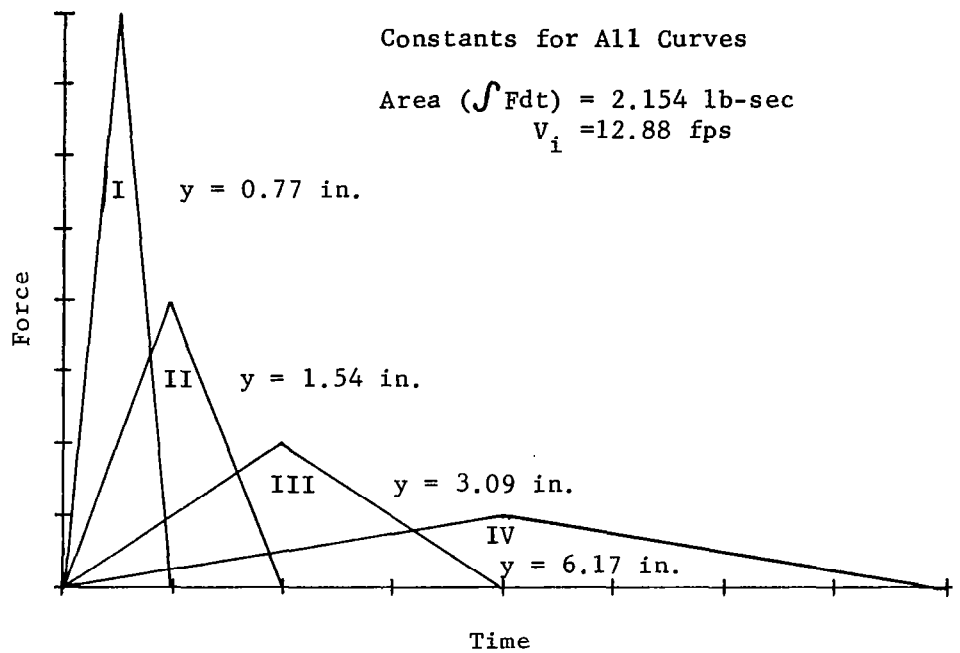

(a) Constant Energy Input, Varying Pulse Time

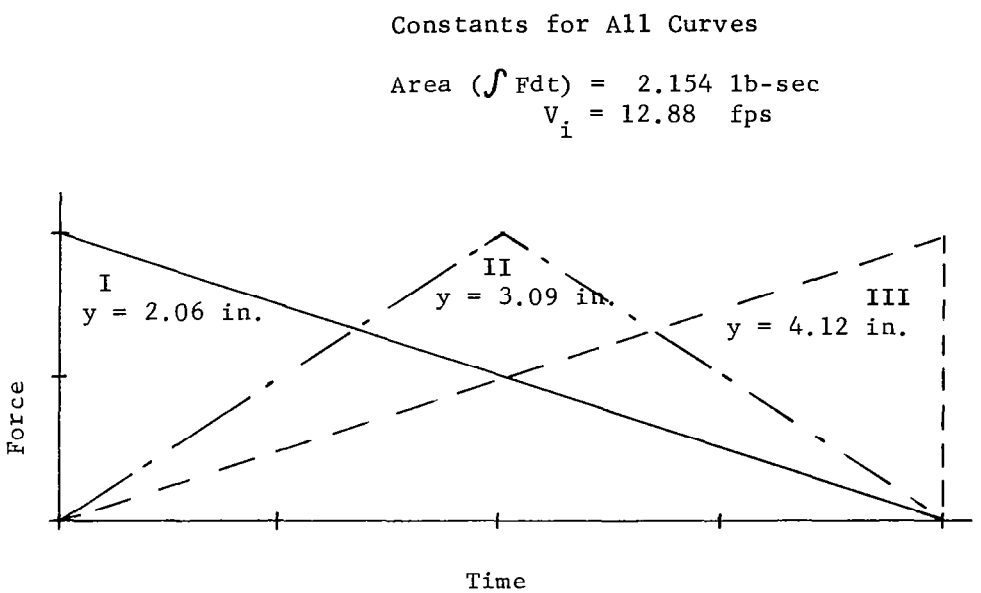

(b) Constant Energy Input and Pulse Time, Shifting Area Centroid

observed in these curves indicate that it is feasible to evaluate a remote target.

In order to use a penetrometer system for remote target evaluation, a complete investigation would have to be run on the characteristics of impact response to the system by a comprehensive range of target media. This investigation, or calibration, of the penetrometer-target impact parameters would necessarily include all the expected input energy levels, as well as all contact shapes, diameters and other geometric parameters which might be varied. Then for a given set of parameters, such as those included in this investigation, curves similar to Figures 23, 24, and 25 would tell enough about the material to evaluate it fairly well from such scant information as length of pulse (t_t).

For example, if a remote penetrometer transmitted the information that (t_t) was 30 msec, use of a curve as in Figure 25 would reveal that the expected force level, (F_s), was 95 lb. Use of both Figures 23 and 24 would show the expected penetration to be between 2 and 3 inches.

Of course, if the complete signature or other additional data were obtained from the remote penetrometer, identification of the target impact characteristics would be simplified that much more.

Effects of Soil Constituents on Impact

Figure 27 is a triangular phase diagram for earth materials. The axes are determined by the volume percentage of the three constituents, solids, air, and water[6]. The normal regimes for rock and *in situ* soils are shown. It is recognized that some *in situ* soils, usually clays, fall outside this soil regime. The soil phase conditions for the impact tests of this program are shown on the diagram. Analysis of test data in relation to the phase condition of the target media seemed a logical step in the process

FIGURE 27

EARTH MATERIALS PHASE DIAGRAM

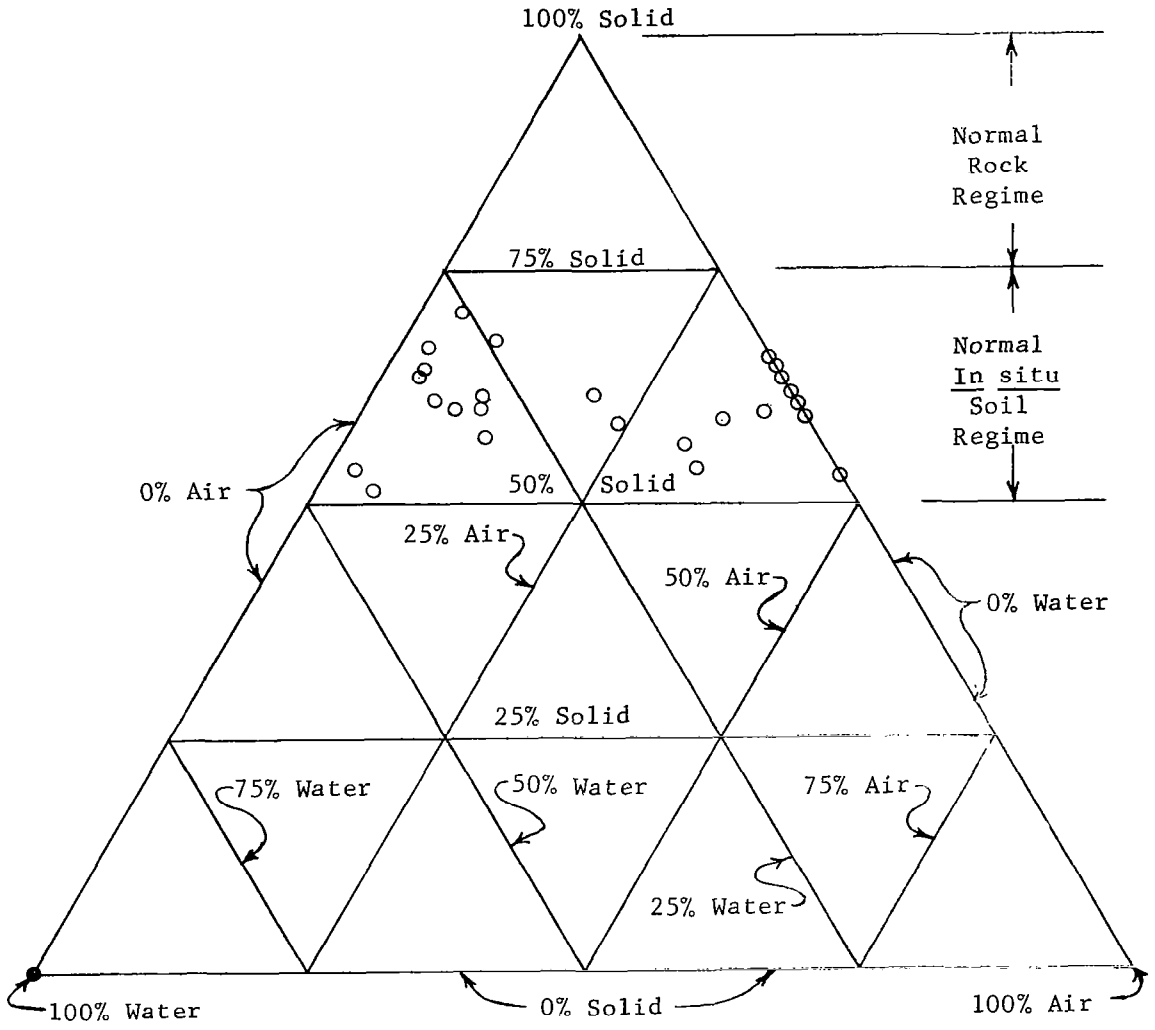

LEGEND

○ Soil Phase Condition on Impact
● Water Phase Condition on Impact

Constituent percentages are expressed in terms of volume.

of determining to what extent these constituents influence such impact-penetration parameters as shearing resistance, soil flow, viscosity, edge effects, wave effects, and pore pressures.

The groups of curves for Ottawa Sand on Figures 16 and 17 show the force-time signature gradually increasing from the continuous penetration type of impact to the plastic-penetration type. It can be seen that the wet weight of the soil, (γ_w), and the volume percentage of water (w_v), increase during this trend. A more complete picture of this trend is obtained by observing the force-penetration curve under each force-time signature for the tests. Most notable in these curves is the fact that (F_s), the secondary force peak, or plateau, as the case may be, gains in magnitude, and that the ends of the force-penetration curves show an increasing trend to shorten, peak out, and drop abruptly, as the density and moisture content increase. Inspection of the curves for CRS and CA, Figures 18 through 22, shows the same trends. A good comparison of these to a purely plastic impact is made on Test No. 10-10-9, Figure 22. The saturated, dense cases (Tests Nos. 11-11-4, Figure 17, 11-18-4, Figure 19, and 12-2-8, Figure 22) show the slight rebound effect on the force-penetration curves. Test No. 10-10-7, Figure 21, was run in material with a heavy crust, which influenced the signature as shown.

In an attempt to develop the relationships of the soil constituents to the impact parameters, curves of (F_s) versus (s_v), (a_v), (w_v), and (γ_w) were plotted for the non-cohesive materials. The most marked relationships were those of (F_s) versus (w_v), Figure 28, and (F_s) versus (a_v), Figure 29. The first of these shows that the dry tests tend to group while the saturated tests form a level. Individual curves could have been drawn for each sand type, but a lack of complete data precluded this, and the average curve was applied. The same effects are visible on the (F_s) versus (a_v) plot, and an

FIGURE 28

SECONDARY MAXIMUM FORCE VERSUS VOLUME PERCENTAGE OF WATER FOR NONCOHESIVE MATERIAL

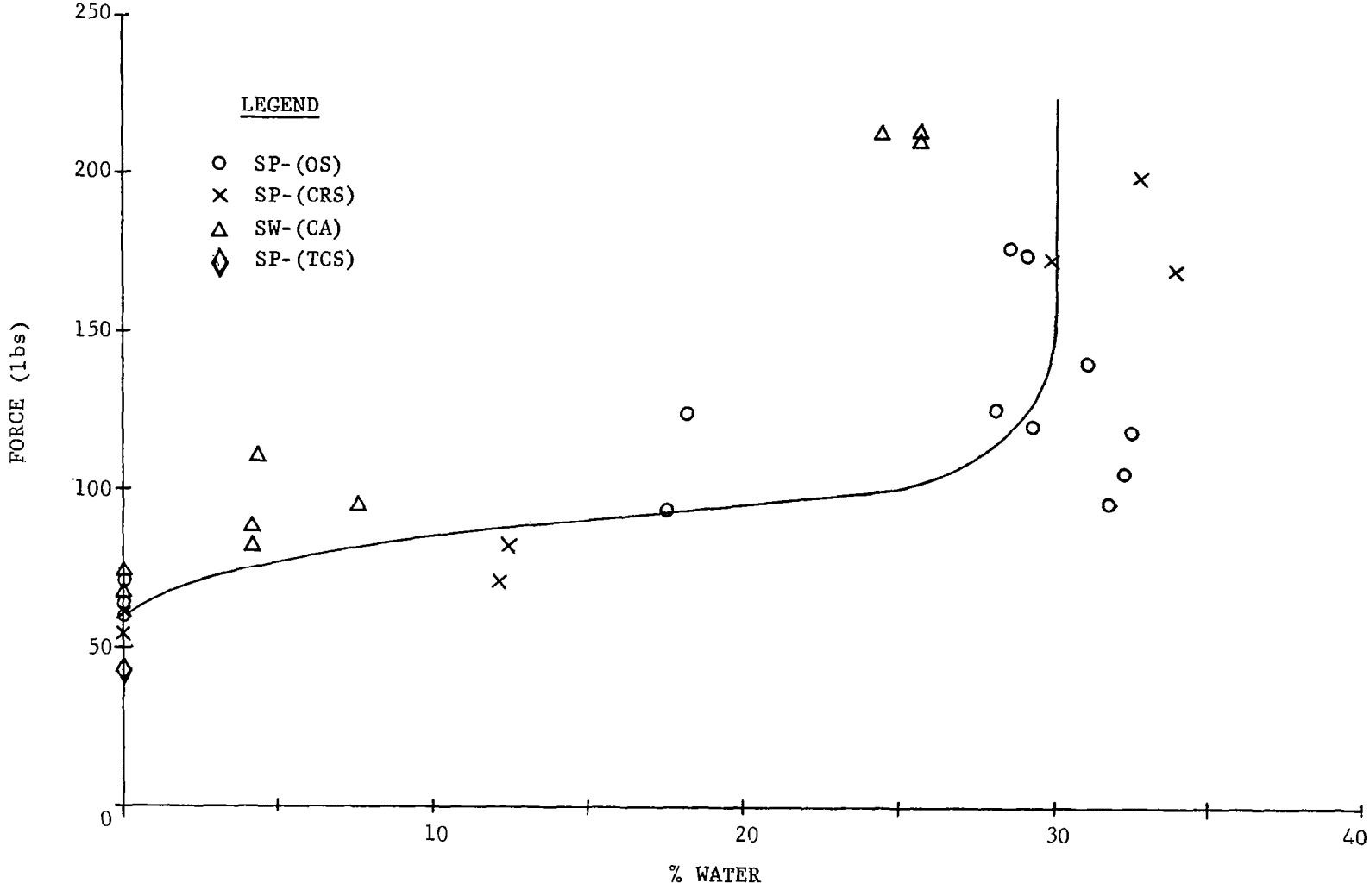

FIGURE 29

SECONDARY MAXIMUM FORCE VERSUS VOLUME PERCENTAGE OF AIR
FOR NONCOHESIVE MATERIAL

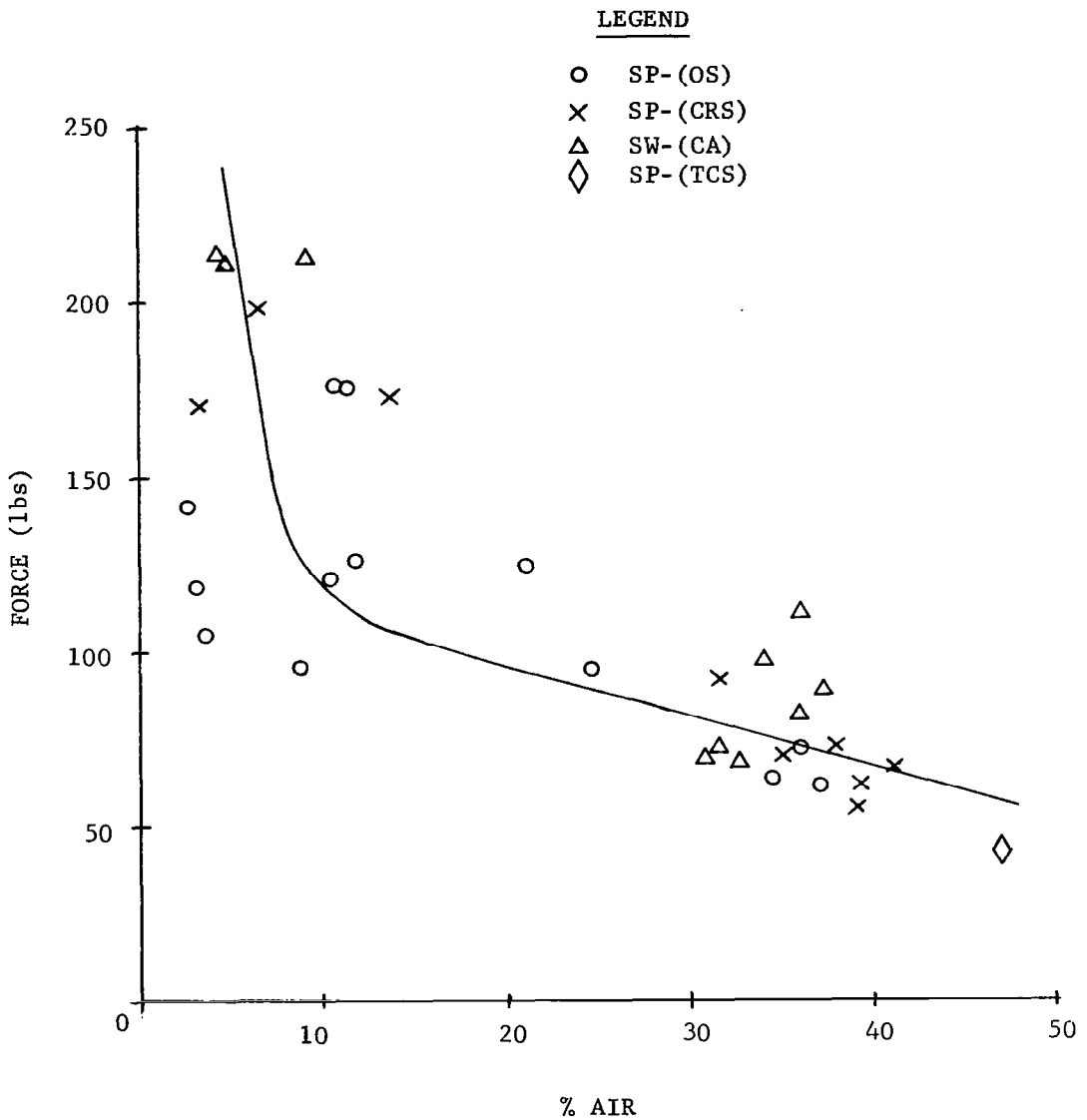

average curve was also employed. It must be remembered that the shearing resistance of each sand influences the force level encountered, and that the angle of internal friction, (ϕ) upon which this resistance depends principally, varies between the sand types and between the moisture contents for each sand type. No attempt was made to analyze this varying friction angle.

It is evident that the density of a material can vary while one of its constituents is held constant. It was therefore decided to use a triangular phase diagram to show the trends in the force levels.

Figure 30 is a partial triangular phase diagram for the noncohesive target media of this investigation. The areas outlined by the dotted lines include the average force levels, (F_s), which were encountered for impacts on soils made up of those constituents. It is emphasized that the method used here is incomplete in that it contained only tests on four materials, but that expanded use of just this type of diagram for the four previously mentioned basic types of materials could help define the impact characteristics of a target by only identifying it and determining its moisture content.

An improved penetrometer system designed with the capability of extrapolating impact characteristics to other penetrating bodies could prove to be doubly useful in target evaluation for impact. By applying phase diagram-force level information coupled with extrapolation to prototype for other important parameters, the impact of a projectile could be well defined.

Correlation of Static and Dynamic Test Data

The static tests yielded the average force-penetration curves plotted on Figures 15 to 22. They vary widely with the dynamic force levels as the soil condition changes. In an attempt to define and understand this variation, several relationships were investigated. Once again the percentages

FIGURE 30

IMPACT FORCE LEVELS FOR NONCOHESIVE TARGET MATERIALS

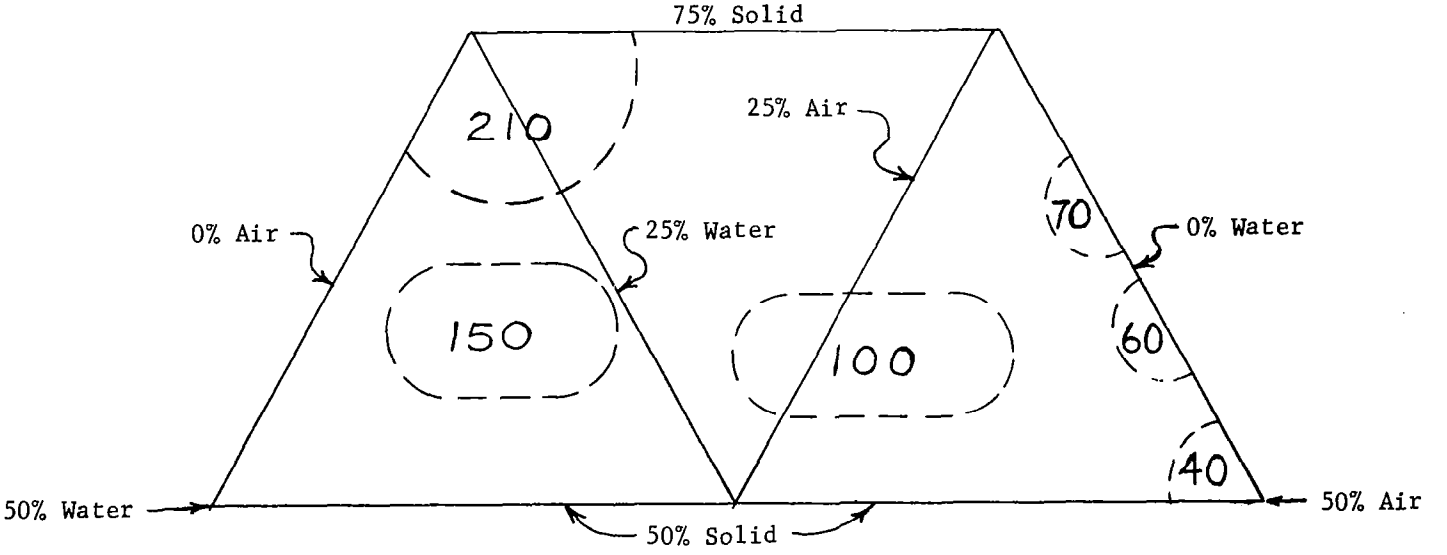

Note: Impact forces are expressed in pounds.

of air and water in the target material were found to be the most influential factors.

Figure 31 is a plot of the ratio of (F_s) to (P) versus (w_v) for noncohesive material. (P) is the static force required to penetrate to the depth of the dynamic test. The plot of (F_s)/(P) versus (a_v) is shown in Figure 32. The grouping of data around (F_s)/(P) = 1.0 on both plots tends to support the conclusion that (F_s) is influenced by the shearing resistance of the soil as in static tests. The number of points in this region for which (F_s)/(P) is less than one can be attributed to the influence of air blast during impact. The tube used in this test tended to add to this effect. It seems that just before impact on dry, granular material, the air blast permeates the target and adds to the breakdown of the soil. This effect has been recorded on high speed film in an investigation involving larger models[6].

The trend of the average curve drawn on both figures indicates that the correlation between the static and dynamic penetration tests on noncohesive materials deteriorates in meaning as the water content of the target is increased. The influence of high pore pressures under dynamic loads accounts for this phenomenon. Once the sand has water, the pore pressures develop and the air blast is decreased. By the time the soil is saturated, the static penetration test is meaningless. The clay data on these curves do not follow the trend of the noncohesive media because they do not drain under static or dynamic conditions.

It seems evident that a static penetration test is not useful in evaluating target media for impact except under certain restricted conditions, but that it may be used in conjunction with dynamic tests to aid in evaluation of the target.

FIGURE 31

DYNAMIC-STATIC FORCE RATIO VERSUS VOLUME PERCENTAGE OF WATER

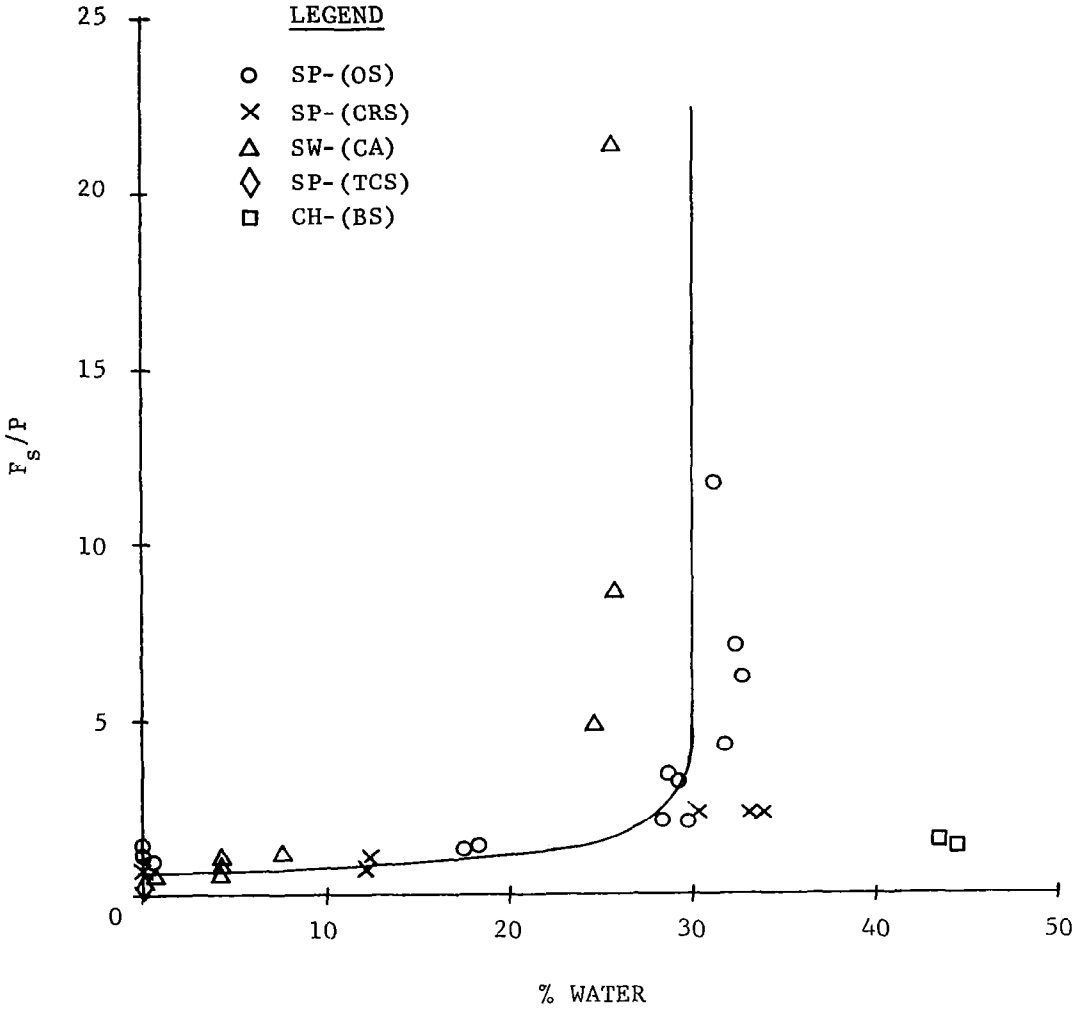

FIGURE 32

DYNAMIC-STATIC FORCE RATIO VERSUS VOLUME PERCENTAGE OF AIR

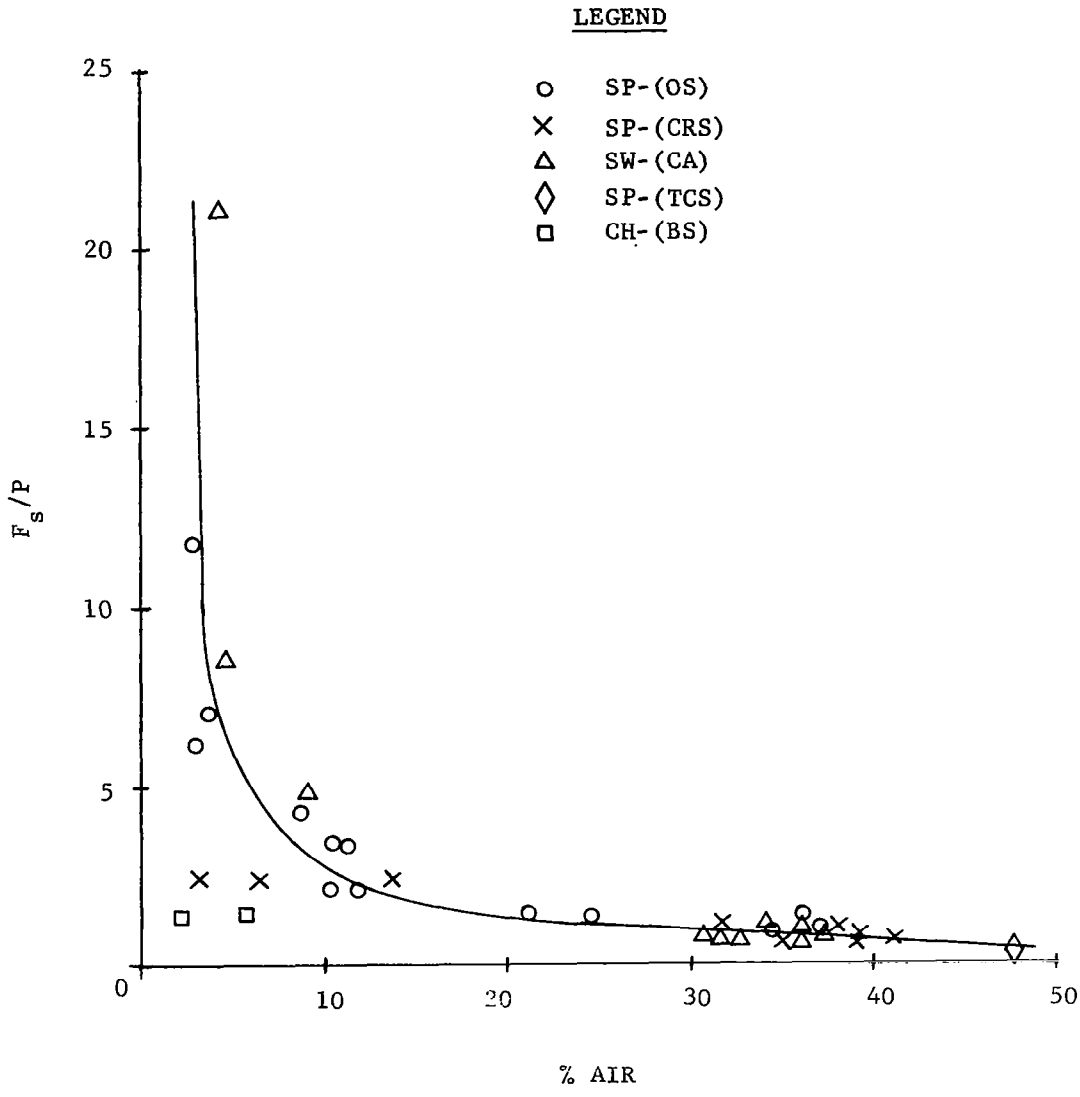

SUMMARY OF CONCLUSIONS

The results of this investigation generally support the assumptions about failure conditions and mechanisms based principally on the Prandtl-Terzaghi system. Observations of tests revealed the soil volume displacement at the surface during impact and other evidence supporting this conclusion. For the types of soils tested, which included parts of three of the four basic types of soils (classified with respect to impact response), the results in the form of signatures and force-penetration curves showed that most soils do yield impact responses of the continuous penetration type, plastic type, or a combination of the two. Soils with cohesion, such as clays, yield typical plastic types of impact response, while dense granular soils with high water contents yield the combination type, and drier cohesionless materials yield the continuous penetration type of response.

For the circular plate contact surface used in this investigation, the initial force peak, (F_c), appears to have no relation to any important parameter. It is recognized that closer monitoring of this portion of the test under different conditions could prove this wrong. The secondary force peak, or plateau, (F_s), appears to be large dependent upon the shearing strength of the soil. Some other factors, primarily density, also showed some influence on the impact response of the target media.

Using a penetrometer system for remote target evaluation is quite feasible. Proper calibration of this system with regard to target conditions and expected input energies could yield much information about the impact parameters. Effective definition of the expected target impact response could be possible with only scant data from the remote penetrometer. Additional data, in the form of a force-time signature, could aid in obtaining a very complete picture of the target qualities.

Analysis of the effects of the different soil constituents on impact response shows that for dense, cohesionless materials the relative amounts of water and air involved are quite important. The dry sands showed possible evidence of air blast by the projectile, while sands with moisture clearly showed the high force levels effected by the high pore pressures encountered. Cohesive soil targets tested did not show significant variations of force caused by particular volume constituents.

Use of a soil constituents triangular diagram to help relate impact force levels with target constitution could prove to be very useful in target evaluation. A properly calibrated, or tested, penetrometer system used in conjunction with a volumetric phase-force diagram and proper scaling to prototype methods could predict quite closely a soil-projectile impact interaction.

Data taken for this investigation show that the use of a similar static penetration test for analysis of the impact response of sand is quite limited. For dry sands, the correlation between static and dynamic tests is good, but addition of water tends to cause the dynamic forces to be much greater than the static forces for equal penetrations. Insufficient data were collected for cohesive soils, but indications are that the difference between the two types of forces would not be so pronounced, or dependent on water content, because clays will not drain appreciably, even under static loads.

It is emphasized that the tests for this program were too few and limited in scope for it to be comprehensive. In addition, test conditions such as penetrometer size and weight may have induced certain unforeseen influence upon the results of the analysis which are not fully understood.

RECOMMENDATIONS

Expanded research in several areas of this type of investigation could add considerably to the usefulness of penetrometer testing. A comprehensive program including dynamic and static testing in many more soil types and conditions could yield much information. Detailed observation of the contact force, (F_c), and possible influencing factors is recommended.

It appears that much research on the nature of impact mechanisms for soils is needed. Investigation of the parameters influencing impacts, such as shearing strength of soils, could be an area of fruitful research.

The problems encountered in this investigation related to instrumentation point out several possibilities for improvement. Proper shielding of all wiring, including the fly leads, is important. Use of accelerometers to record the signatures appears to be less troublesome than use of a strain cell, in light of some of the difficulties of this program.

Several improvements are recommended for the design of a projectile. The over-all geometry should be such that deep penetration does not affect the signature. In this program the shoulders of the brass cylinder influenced most tests which penetrated more than four inches. A configuration such as an artillery shell, with the instrumentation packaged inside, would eliminate these problems. Use of a conical or hemispherical contact surface is recommended in lieu of a plate to avoid an excessively large contact force spike. Preliminary tests on the various designs available could help determine the optimum configuration. The size, weight, and diameter of the projectile should be designed with extrapolation to a prototype in mind, if necessary.

APPENDIX A

EQUIPMENT CALIBRATION

For the strain gage circuit as shown in Figure 6, the theoretical strain sensitivity, or output, is expressed as:

$$dE = \frac{NVF}{4} \Delta\epsilon \qquad (10)$$

where;

dE = output voltage

N = number of active gages

V = voltage across the bridge

F = gage factor

$\Delta\epsilon$ = input strain in in./in.

The number of active gages, based on a Poisson's Ratio of the beryllium copper of 0.30, is 2.60, the voltage used was 6.0, the gage factor is 2.08, and the input strain per 100 lb. is 2.75×10^{-6} in./in., (100 lb/.1964 sq. in. x 18.5 x 10^6 psi). This gave 449 lb/mv as the theoretical calibration value.

The penetrometer was then calibrated by loading it statically in a compression testing machine, and a value of 440 lb/mv was obtained. However, use of this value in analyzing test data gave results which could not satisfy the conservation of momentum principle, Eq. (1), and it gave calculated values of penetration which were completely unrealistic when compared to the measured penetration values. Although the theoretical output seemed to agree with the static calibration value, it should be pointed out that the theoretical calibration could be influenced by slight changes in Poisson's ratio of beryllium copper, by changes or non-uniformity in cross-sectional area of the cell, or by misalignment of the gages.

The oscilloscope was checked for amplitude and sweep-time errors using a Tektronix Time Base Generator. Then the procedure for arriving at the impact velocity was thoroughly examined, and no significant amount of error was detected in any case. Moreover, a survey of literature showed that this discrepancy between a strain gage circuit output for dynamic loads and one for static loads has been encountered previously and in approximately the same ratio[8]. It was assumed that the difference lay in uneven stress distribution under dynamic loads.

To arrive at the final strain gage output of 562.5 lb/mv, a range of several outputs was used in the integration process. This value gave results for calculated penetration which agreed quite closely with the measured values. In regard to the comparison of computed and measured penetrations, it is recognized that the measured penetration cannot be an exact measure of the absolute maximum penetration occurring during a test due to projectile rebound and measurement errors.

In any event, a check of the results by the energy balance method using the output value of 562.5 lb/mv satisfied the conservation of momentum requirement. In this method of calibration, the area of the force-penetration curve represents the total potential energy of the system (in the case of significant rebound, this energy is represented by the area of the curve bounded by the curve up to the point of maximum penetration, the x-axis, and a vertical ordinate through the point of maximum penetration). A comparison of this area with the total energy of the system showed differences between them averaging less than 3%.

The investigation of the discrepancy between the two calibrations was not pursued further, it being assumed that the stress fields present during the two loading conditions are different. The validity of the results

and conclusions presented in this thesis still hold in principle, even allowing for the possibility of the calibration being wrong. In that case, the magnitude of the parameters involved would differ from those shown here, but their values relative to one another would not change.

In addition, the method used in this investigation for integration of the force-time curve was to analyze that part of the signal up to the point where the force initially returned to zero. It was found that substantial error crept into the unused part of the signature due to poor resolution of the smaller signal and cumulative errors encountered in the integration process.

APPENDIX B

COMPUTER PROGRAM FOR DATA REDUCTION

FORTRAN program DYPEN was written for use on a Control Data Corporation 6600 computer to integrate force-time data taken from oscilloscope records of this investigation. The numerical integration is performed by addition of trapezoidal increments of area bounded by the curve and the time axis.

LISTING FOR FORTRAN PROGRAM DYPEN

The following listing included program DYPEN, with instructions and definitions, and two subroutines for plotting the force-time and force-penetration curves of this investigation. These subroutines, GRAPH1 and GRAPH2, are for use on the plotting facilities of The University of Texas Computation Center, however, and probably have limited use elsewhere.

```
      PROGRAM DYPEN (INPUT,OUTPUT, PLOT, TAPE 34 = PLOT)
C
C                              PROGRAM INSTRUCTIONS
C
C              THIS FORTRAN PROGRAM, WRITTEN FOR USE ON THE CDC 6600
C     COMPUTER, WILL CALCULATE THE INSTANTANEOUS TIMES, FORCES, VELO-
C     CITIES, AND PENETRATIONS FOR IMPACT BY THE DYNAMIC PENETROMETER ON
C     THE TARGET MEDIUM. THIS IS DONE BY DOUBLE INTEGRATION OF THE FORCE
C     -TIME RECORD. THE PROGRAM ALSO AFFORDS THE OPTION OF PLOTTING
C     FORCE-TIME AND FORCE-PENETRATION CURVES FOR EACH DATA SET.  THE
C     NECESSARY INPUT DATA ARE EXPLAINED BELOW.
C
C                                 INPUT DEFINITIONS
C IDENT = TEST IDENTIFICATION
C N     = NUMBER OF DATA POINTS--MUST BE BETWEEN 4 AND 100, INCLUSIVE
C IGRAF = PLOT ROUTINE CONTROL--0=NO PLOT, 1=PLOT
C XMULT = NUMBER OF GRAPH DIVISIONS PER INCREMENT (INCREMENT = AREA BETWEEN 2
C                                                              DATA POINTS)
C YFRAT = VERTICAL O-SCOPE SCREEN CM. PER GRAPH DIVISION (FOR FORCE-TIME CURVE)
C XFRAT = HORIZONTAL O-SCOPE SCREEN CM. PER GRAPH DIVISION (FORCE-TIME CURVE)
C YFSET = O-SCOPE SENSITIVITY SETTING FOR FORCE TRACE, MV/CM
C XFSET = O-SCOPE SWEEP SETTING FOR FORCE TRACE, SEC/CM
C VINC1 = VELOCITY GAGE HEIGHT INCREMENT, INCHES
C VINC2 = VELOCITY CLEARANCE HEIGHT INCREMENT, INCHES
C VSET  = O-SCOPE SWEEP SETTING FOR TIME TRACE, SEC/CM
C VTIM  = LENGTH OF VELOCITY RECORD, GRAPH DIVISIONS
C DATA  = FORCE CURVE DATA POINTS, GRAPH DIVISIONS
C
C        SUCCESSIVE SETS OF DATA MAY BE RUN BY ADDING TO END OF LAST DATA SET.
C
C        TO END CALCULATIONS, ADD 2 BLANK CARDS TO END OF LAST DATA SET.
C
C     DIMENSIONING VARIABLES
      DIMENSION DATA(100),FORS(100),OVEL(100),VEL(100),PEN(100),
     1          TIME(100),IDENT(5)
C     SKIPPING PAGE
  100    PRINT 1
    1    FORMAT (1H1)
C     READING IDENTIFICATION CARD
```

```
      READ 2,(IDENT(I),I=1,5)
    2 FORMAT (5A10)
C   READING IN VALUES FOR CALCULATION AND CONTROL
      READ 3, N,IGRAF,XMULT,YFRAT,XFRAT,YFSET,XFSET
    3 FORMAT (I3,5X,I2,5X,F4.2,4(3X,E10.3))
C   CHECKING FOR PROGRAM CONTINUATION
      IF (N) 4,1000,4
C   READING ADDITIONAL VALUES
    4 READ 5, VINC1,VINC2,VSET,VTIM
    5 FORMAT(E10.3,3(5X,E10.3))
C   READING DATA
      READ 6, (DATA(J),J=1,N)
    6 FORMAT (10F8.3)
C   PRINTING OUT IDENTIFICATION
      PRINT 2,(IDENT(I),I=1,5)
C   PRINTING DATA
      PRINT 50,N,XMULT,YFRAT,XFRAT,YFSET,XFSET,VINC1,VINC2,VSET,VTIM
   50 FORMAT (///,15X,20HINPUT CONTROL VALUES,//,5X,3HN =,I3,4H PTS,
     112X,8HXMULT = ,F3.1,8H DIV/INC,/,8H YFRAT =,E9.3,7H CM/DIV,3X,7HXF
     2RAT =,E9.3,7H CM/DIV,/,8H YFSET =,E9.3,6H MV/CM,4X,7HXFSET =,E9.3,
     37H SEC/CM,/,8H VINC1 =,E9.3,4H IN.,6X,7HVINC2 =,E9.3,4H IN.,/,8H
     4VSET =,E9.3,7H SEC/CM,4X,6HVTIM =,E9.3,4H DIV)
      PRINT 60
   60 FORMAT (///,17X,17HINPUT DATA POINTS,/)
      PRINT 61, (DATA(J),J=1,N)
   61 FORMAT (5F10.2)
      PRINT 1
C   CHECKING FOR INVALID INPUT
      IF (N-4) 7,9,9
    7 PRINT 8
    8 FORMAT (69H INVALID VALUE OF N INPUTTED, N MUST BE BETWEEN 4 AN
     1D 100, INCLUSIVE.)
      GO TO 100
C   DEFINING COMPUTATION CONSTANT
    9 FCONS = 562.5*YFSET*YFRAT
C   CALCULATING FORCE VALUES
      DO 10 J=1,N
   10 FORS(J) = DATA(J)*FCONS
C   DEFINING COMPUTATION CONSTANT
```

```
      TCONS = XMULT*XFRAT*XFSET
C     CALCULATING TIME INCREMENTS
      TIME(1) = 0.0
         DO 11 J=2,N
      L = J-1
   11 TIME(J) = TCONS + TIME(L)
      IF (IGRAF) 110,120,110
  110 CALL GRAPH1 (TIME,FORS,IDENT,N)
  120    CONTINUE
C     CALCULATING VELOCITY CHANGE VALUES
      OVEL(1) = 0.0
         DO 12 J=2,N
      L = J-1
   12 OVEL(J) = (FORS(L) + FORS(J))*(TCONS*16.08)/5.384 + OVEL(L)
C     CALCULATING IMPACT VELOCITY
   13 HG = 45.90 + VINC1
      HT = HG + VINC2
      PROD = HG*HT
      GTIM = VTIM*VSET*XFRAT
      VI = (SQRTF(PROD))/(6.0*GTIM)
C     CALCULATING INCREMENTAL VELOCITIES
         DO 14 J=1,N
   14 VEL(J) = VI-OVEL(J)
C     CALCULATING THE INCREMENTAL PENETRATIONS
      PEN(1) = 0.0
         DO 15 J=2,N
      K = J-1
   15 PEN(J) = (VEL(K)+VEL(J))*(TCONS* 6.0)+PEN(K)
C     PRINTING OUT COMPUTATIONS
   16    PRINT 17,HT,VI
   17    FORMAT (///,5X,14HDROP HEIGHT = ,E11.5,3X,6HINCHES,/,19H IMPACT
     1 VELOCITY = ,E11.5,3X,3HFPS,///)
C     PRINTING OUT TABULATIONS
         PRINT 18
   18    FORMAT (4X,4HTIME,12X,5HFORCE,10X,8HVELOCITY, 7X,11HPENETRATION
     1,/,5X,3HSEC,13X,3HLBS,13X,3HFPS,12X,6HINCHES,/)
         DO 20 J=1,N
         PRINT 19, TIME(J),FORS(J),VEL(J),PEN(J)
   19    FORMAT (/,1X,E10.3,5X,E12.5,5X,E11.4,5X,E11.4)
```

```
   20    CONTINUE
C      CHECKING FOR PLOT ROUTINE
      IF (IGRAF) 21, 100, 21
   21 CALL GRAPH2 (PEN,FORS,IDENT,N)
   22    CONTINUE
         GO TO 100
 1000 CALL AXTERM (0)
      PRINT 1
         PRINT 1001
 1001    FORMAT (24H CALCULATIONS TERMINATED)
      END
C
C      BEGINNING PLOT ROUTINE FOR FORCE-TIME CURVE
      SUBROUTINE GRAPH1 (TIME,FORS,IDENT,N)
      DIMENSION TIME(100),FORS(100),IDENT(5),KIP(2)
      CALL AXES (0.060,6.0,0.0,1.5,550.0,2.75,0.25,0.01,100.0,0,50)
      CALL PLOT (TIME,FORS,N,-2)
      CALL PLO TITL (IDENT,40,0,2,2.1,1.25)
      KIP(1) = 10HTIME  SEC/
      KIP(2) = 3H100
      CALL PLO TITL (KIP,13,0,2,2.2,-0.2)
      KIP(1) = 10HFORCE  LBS
      CALL PLO TITL (KIP,10,1,2,-0.3,2.0)
      CALL AX  TERM (1)
         RETURN
      END
C
C      BEGINNING PLOT ROUTINE FOR FORCE-PENETRATION CURVE
      SUBROUTINE GRAPH2 (PEN,FORS,IDENT,N)
      DIMENSION PEN(100),FORS(100),IDENT(5),KIP(2)
      CALL AXES (4.0,6.0,0.0,1.5,550.0,2.75,0.25,1.0,100.0,0,50)
      CALL PLOT (PEN,FORS,N,-2)
      CALL PLO TITL (IDENT,40,0,2,2.1,1.25)
      KIP(1) = 10HPENETRATIO
      KIP(2) = 6HN  IN.
      CALL PLO TITL (KIP,16,0,2,2.2,-0.2)
      KIP(1) = 10HFORCE  LBS
      CALL PLO TITL (KIP,10,1,2,-0.3,2.0)
      CALL AX  TERM (1)
```

DATA INPUT

A listing of the input required for a computer run, including plots, of two data sets is as follows:

```
11-18-2-SP-(CRS)                                    7.77 E-02    7.78 E-02    2.    E-01    5.    E-03
26          1         2.0                                  1.0  E-01          6.30 E+01
8.0  E-01              2.0  E-01
  0.00    18.00    23.80    18.00    15.50    15.40    14.50    13.50    13.50    15.50
 17.80    18.90    19.00    19.00    19.10    19.50    19.50    19.80    19.80    19.00
 18.60    18.00    16.60    15.10     6.50    -1.00    -3.10    -4.10    -4.60    -4.60
11-18-3-SP-(CRS)                                    7.75 E-02    7.78 E-02    2.    E-01    5.    E-03
29          1         2.0                                  1.0  E-01          6.40 E+01
6.7  E-01              2.0  E-01
  0.00    11.00     8.25     9.30    10.60    12.50    13.60    13.50    13.75    14.50
 15.90    17.90    18.60    19.50    19.00    19.40    19.25    19.10    18.90    19.00
 18.60    18.25    18.00    17.25    16.60    15.75    12.50     3.00    -1.10    -2.90
```

PROGRAM OUTPUT

Printed output for the computations of the two previously listed data sets follows on the next six pages. The plotted curves are found on Figure 19, page 46, and Figure 40, page 96.

11-18-2-SP-(CRS)

INPUT CONTROL VALUES

N = 26 PTS		XMULT = 2.0 DIV/INC	
YFRAT	=7.770E-02 CM/DIV	XFRAT	=7.780E-02 CM/DIV
YFSET	=2.000E-01 MV/CM	XFSET	=5.000E-03 SEC/CM
VINC1	=8.000E-01 IN.	VINC2	=2.000E-01 IN.
VSET	=1.000E-01 SEC/CM	VTIM	=6.300E+01 DIV

INPUT DATA POINTS

0.	18.00	23.80	18.00	15.50
15.40	14.50	13.50	13.50	15.50
17.80	18.90	19.00	19.00	19.10
19.50	19.50	19.80	19.80	19.00
18.60	18.00	16.60	15.10	6.50
-1.00				

DROP HEIGHT = 4.69000E+01 INCHES
IMPACT VELOCITY = 1.59138E+01 FPS

TIME SEC	FORCE LBS	VELOCITY FPS	PENETRATION INCHES
0.	0.	1.5914E+01	0.
7.780E-04	1.57342E+02	1.5548E+01	1.4686E-01
1.556E-03	2.08042E+02	1.4699E+01	2.8806E-01
2.334E-03	1.57342E+02	1.3850E+01	4.2133E-01
3.112E-03	1.35489E+02	1.3170E+01	5.4746E-01
3.890E-03	1.34615E+02	1.2542E+01	6.6748E-01
4.668E-03	1.26748E+02	1.1935E+01	7.8174E-01
5.446E-03	1.18007E+02	1.1366E+01	8.9051E-01
6.224E-03	1.18007E+02	1.0818E+01	9.9406E-01
7.002E-03	1.35489E+02	1.0229E+01	1.0923E+00
7.780E-03	1.55594E+02	9.5523E+00	1.1846E+00
8.558E-03	1.65210E+02	8.8069E+00	1.2703E+00
9.336E-03	1.66084E+02	8.0371E+00	1.3490E+00
1.011E-02	1.66084E+02	7.2653E+00	1.4204E+00
1.089E-02	1.66958E+02	6.4915E+00	1.4846E+00
1.167E-02	1.70454E+02	5.7074E+00	1.5416E+00
1.245E-02	1.70454E+02	4.9153E+00	1.5912E+00
1.323E-02	1.73077E+02	4.1171E+00	1.6333E+00
1.400E-02	1.73077E+02	3.3128E+00	1.6680E+00
1.478E-02	1.66084E+02	2.5247E+00	1.6952E+00
1.556E-02	1.62587E+02	1.7610E+00	1.7153E+00
1.634E-02	1.57342E+02	1.0176E+00	1.7282E+00
1.712E-02	1.45105E+02	3.1483E-01	1.7344E+00

1.789E-02	1.31993E+02	-3.2903E-01	1.7344E+00
1.867E-02	5.68181E+01	-7.6775E-01	1.7293E+00
1.945E-02	-8.74125E+00	-8.7946E-01	1.7216E+00

11-18-3-SP-(CRS)

INPUT CONTROL VALUES

N = 29 PTS		XMULT = 2.0 DIV/INC	
YFRAT =	7.750E-02 CM/DIV	XFRAT =	7.780E-02 CM/DIV
YFSET =	2.000E-01 MV/CM	XFSET =	5.000E-03 SEC/CM
VINC1 =	6.700E-01 IN.	VINC2 =	2.000E-01 IN.
VSET =	1.000E-01 SEC/CM	VTIM =	6.400E+01 DIV

INPUT DATA POINTS

0.	11.00	8.25	9.30	10.60
12.50	13.60	13.50	13.75	14.50
15.90	17.90	18.60	19.50	19.00
19.40	19.25	19.10	18.90	19.00
18.60	18.25	18.00	17.25	16.60
15.75	12.50	3.00	-1.10	

DROP HEIGHT = 4.67700E+01 INCHES
IMPACT VELOCITY = 1.56216E+01 FPS

TIME SEC	FORCE LBS	VELOCITY FPS	PENETRATION INCHES
0.	0.	1.5622E+01	0.
7.780E-04	9.59062E+01	1.5399E+01	1.4480E-01
1.556E-03	7.19297E+01	1.5009E+01	2.8675E-01
2.334E-03	8.10844E+01	1.4653E+01	4.2521E-01
3.112E-03	9.24187E+01	1.4250E+01	5.6013E-01
3.890E-03	1.08984E+02	1.3782E+01	6.9098E-01
4.668E-03	1.18575E+02	1.3253E+01	8.1718E-01
5.446E-03	1.17703E+02	1.2704E+01	9.3836E-01
6.224E-03	1.19883E+02	1.2152E+01	1.0544E+00
7.002E-03	1.26422E+02	1.1580E+01	1.1652E+00
7.780E-03	1.38628E+02	1.0964E+01	1.2704E+00
8.558E-03	1.56066E+02	1.0279E+01	1.3696E+00
9.336E-03	1.62169E+02	9.5399E+00	1.4621E+00
1.011E-02	1.70016E+02	8.7680E+00	1.5475E+00
1.089E-02	1.65656E+02	7.9881E+00	1.6258E+00
1.167E-02	1.69144E+02	7.2101E+00	1.6967E+00
1.245E-02	1.67836E+02	6.4271E+00	1.7604E+00
1.323E-02	1.66528E+02	5.6502E+00	1.8167E+00
1.400E-02	1.64784E+02	4.8804E+00	1.8659E+00
1.478E-02	1.65656E+02	4.1126E+00	1.9079E+00
1.556E-02	1.62169E+02	3.3508E+00	1.9427E+00
1.634E-02	1.59117E+02	2.6043E+00	1.9705E+00
1.712E-02	1.56937E+02	1.8699E+00	1.9914E+00

1.789E-02	1.50398E+02	1.1558E+00	2.0055E+00
1.867E-02	1.44731E+02	4.7002E-01	2.0131E+00
1.945E-02	1.37320E+02	-1.8535E-01	2.0144E+00
2.023E-02	1.08984E+02	-7.5766E-01	2.0100E+00
2.101E-02	2.61562E+01	-1.0717E+00	2.0015E+00
2.178E-02	-9.59062E+00	-1.1102E+00	1.9913E+00

APPENDIX C

ADDITIONAL DATA

IMPACT TEST DATA

Table No. 2 lists the pertinent soil data and static and dynamic force-penetration data for each test. The force-time and force-penetration curves for these tests are shown in Figures 33 to 45.

TABLE NO. 2

TEST DATA

TEST NO.	SOIL DATA					DYNAMIC				STATIC	
	TYPE					MAX. FORCE		PENETRATION		FORCE	PENETRATION
		γ_w	s_v	a_v	w_v	F_c	F_s	Calculated	Measured	P	Measured
		(pcf)	(%)	(%)	(%)	(lbs)	(lbs)	(in)	(in)	(lbs)	(in)
11-15-2	SP-(OS)	104.0	63.0	37.0	0.0	251.0	61.1	3.85	3.5	59	3.5
11-15-1	SP-(OS)	105.8	64.0	36.0	0.0	255.4	72.0	3.61	4.3	50	4.3
11-9-4	SP-(OS)	111.7	60.7	21.1	18.2	247.3	124.9	2.02	2.0	84	2.0
11-10-2	SP-(OS)	116.7	60.1	11.8	28.1	58.3	126.4	2.51	2.7	58	2.7
10-9-4	SP-(OS)	118.0	60.8	10.6	28.6	125.1	177.4	1.79	1.8	51	1.8
10-9-5	SP-(OS)	117.0	59.6	11.2	29.2	174.4	175.8	1.68	1.9	52	1.9
11-11-1	SP-(OS)	118.0	59.5	8.7	31.8	165.7	95.9	3.49	3.5	22	3.5
11-11-2	SP-(OS)	126.2	64.0	3.7	32.3	183.6	105.8	2.66	2.1	15	2.1
11-11-3	SP-(OS)	127.0	64.4	3.0	32.6	207.3	118.9	2.15	2.0	19	2.0
11-15-7	SP-(CRS)	97.5	59.0	41.0	0.0	221.4	65.4	5.11	5.0	90*	5.0
11-16-3	SP-(CRS)	100.8	61.0	39.0	0.0	517.1	54.8	3.02	2.8	66	2.8
11-15-9	SP-(CRS)	101.8	61.6	38.4	0.0	488.0	72.6	2.84	3.1	66	3.1
11-16-6	SP-(CRS)	95.2	53.1	34.8	12.1	275.7	70.4	3.55	3.5	98	3.5
11-18-3	SP-(CRS)	125.2	63.1	3.1	33.8	95.9	170.0	2.01	1.9	71	1.9

* Extrapolated values

TABLE NO. 2 (CONT.)

TEST DATA

TEST NO.	SOIL DATA					DYNAMIC				STATIC	
	TYPE					MAX. FORCE		PENETRATION		FORCE	PENETRATION
		γ_w	s_v	a_v	w_v	F_c	F_s	Calcu-lated	Meas-ured	P	Measured
		(pcf)	(%)	(%)	(%)	(lbs)	(lbs)	(in)	(in)	(lbs)	(in)
12-2-4	SW-(CA)	113.2	68.5	31.5	0.0	337.6	72.9	3.50	3.3	110*	3.3
12-2-1	SW-(CA)	114.7	69.5	30.5	0.0	468.7	68.4	3.66	2.8	93	2.8
10-10-2	SW-(CA)	99.2	58.7	37.2	4.1	419.9	87.9	1.99	2.0	100	2.0
10-10-3	SW-(CA)	101.4	60.0	35.9	4.1	533.4	82.4	1.43	1.7	110*	1.7
12-2-10	SW-(CA)	125.0	66.4	9.1	24.5	245.5	213.9	1.41	1.0	44	1.0
12-2-9	SW-(CA)	131.0	69.7	4.5	25.8	265.1	211.3	1.34	1.3	25	1.3
10-10-10	CH-(BS)	117.0	53.5	2.1	44.4	--	286.7	1.06	0.9	200*	0.9

*Extrapolated values

FIGURE 33

FORCE-TIME AND FORCE-PENETRATION CURVES FROM TESTS IN OTTAWA SAND, SP-(OS)

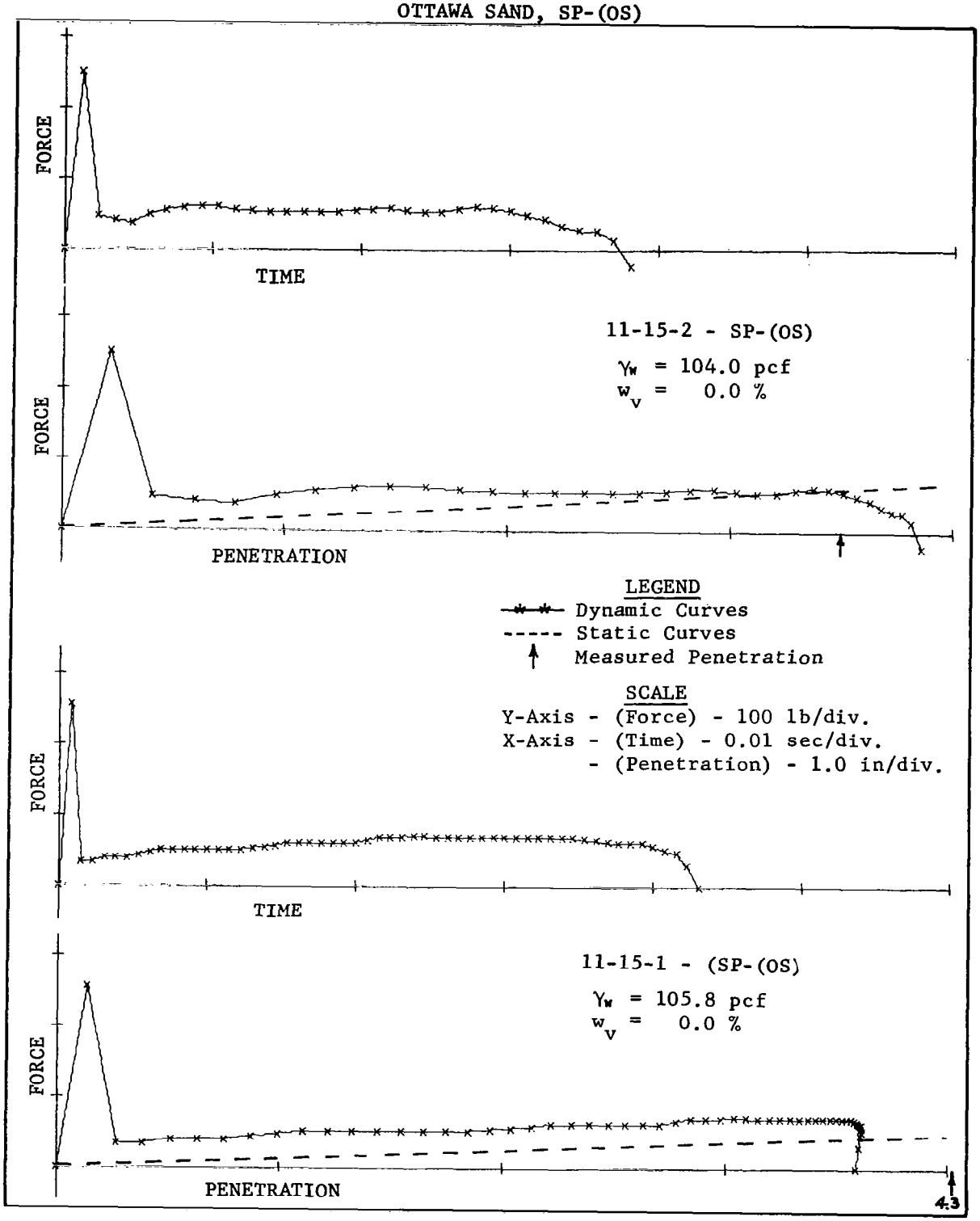

FIGURE 34

FORCE-TIME AND FORCE-PENETRATION CURVES FROM TESTS IN OTTAWA SAND, SP-(OS)

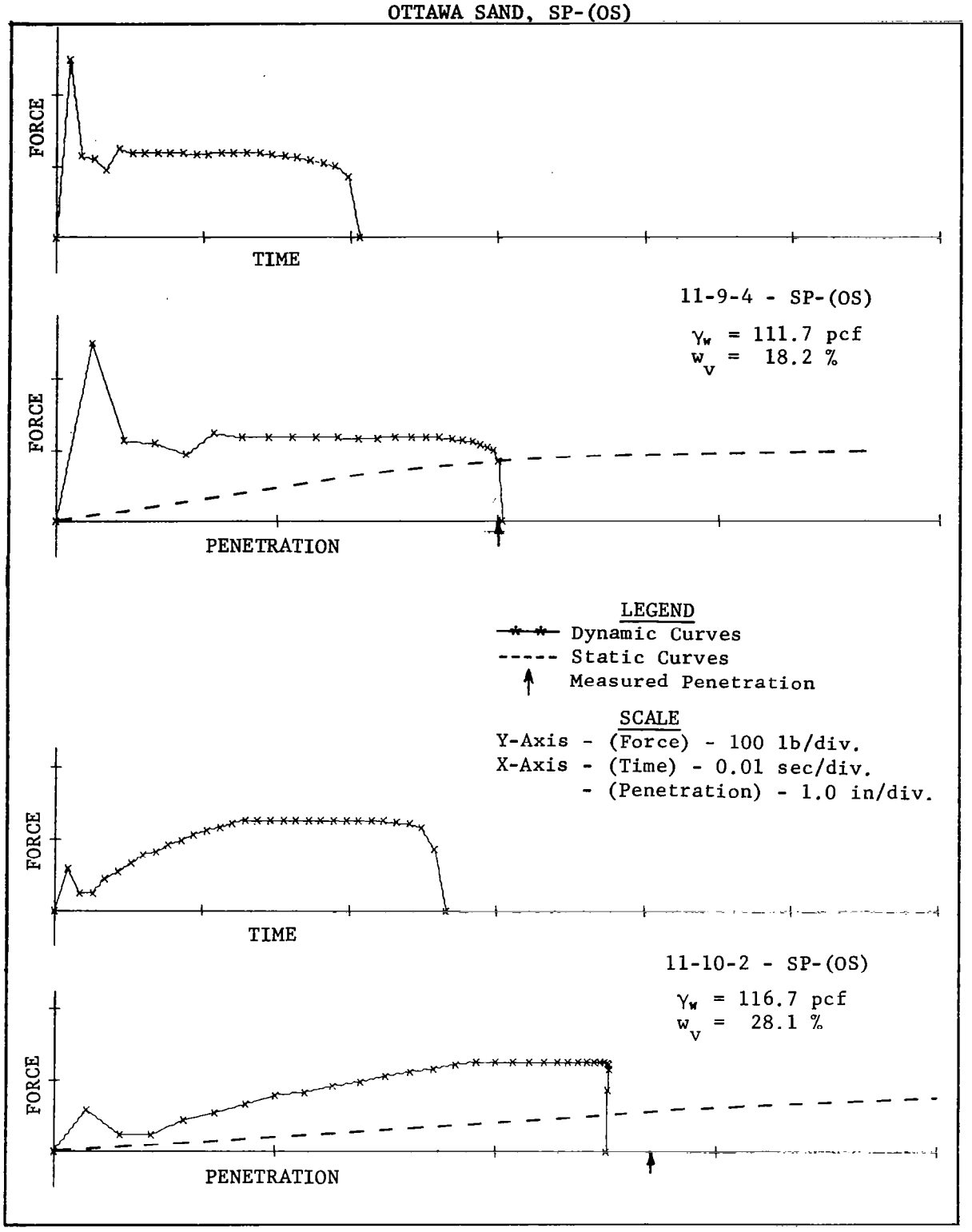

FIGURE 35

FORCE-TIME AND FORCE-PENETRATION CURVES FROM TESTS IN OTTAWA SAND, SP-(OS)

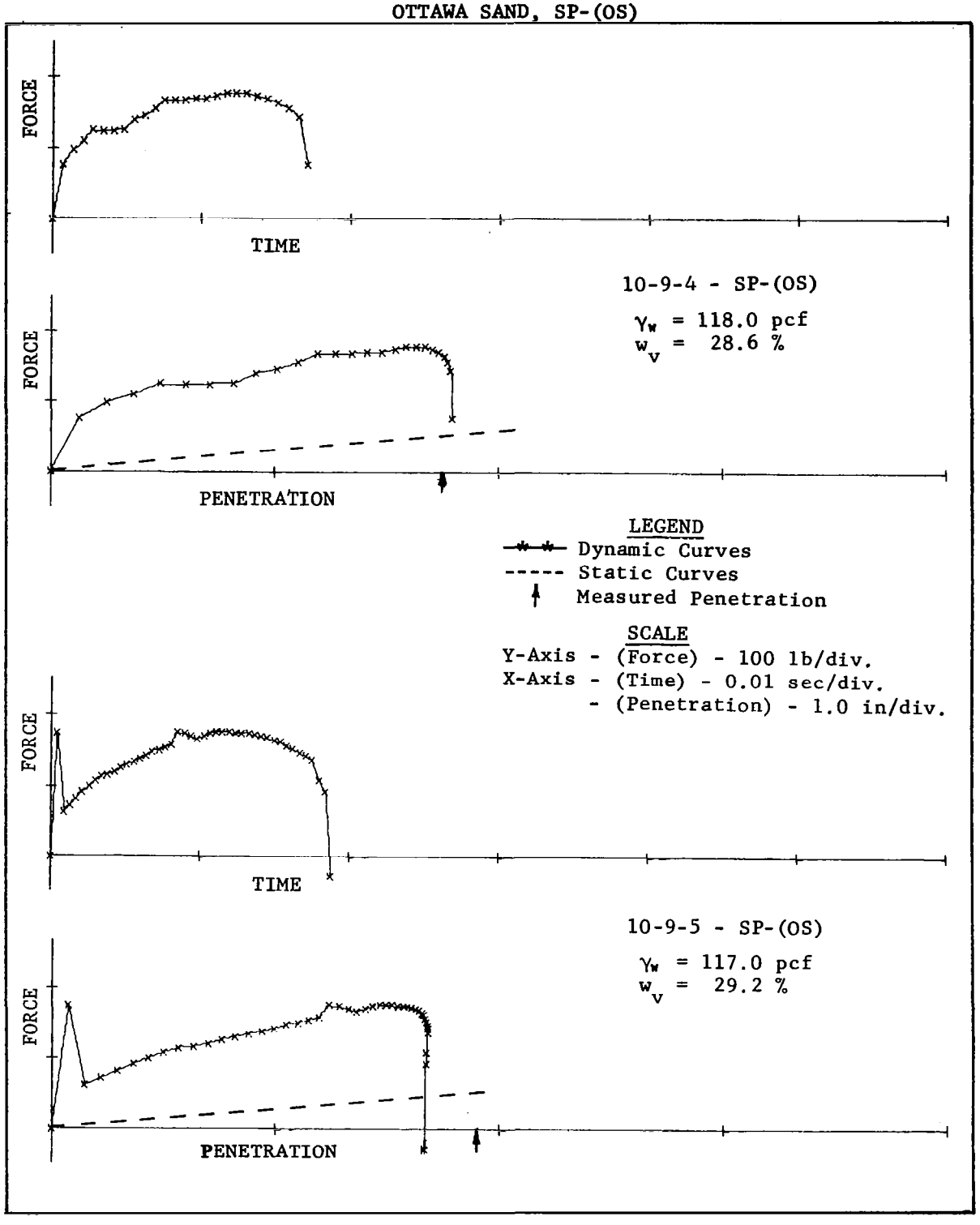

FIGURE 36

FORCE-TIME AND FORCE-PENETRATION CURVES FROM TESTS IN OTTAWA SAND, SP-(OS)

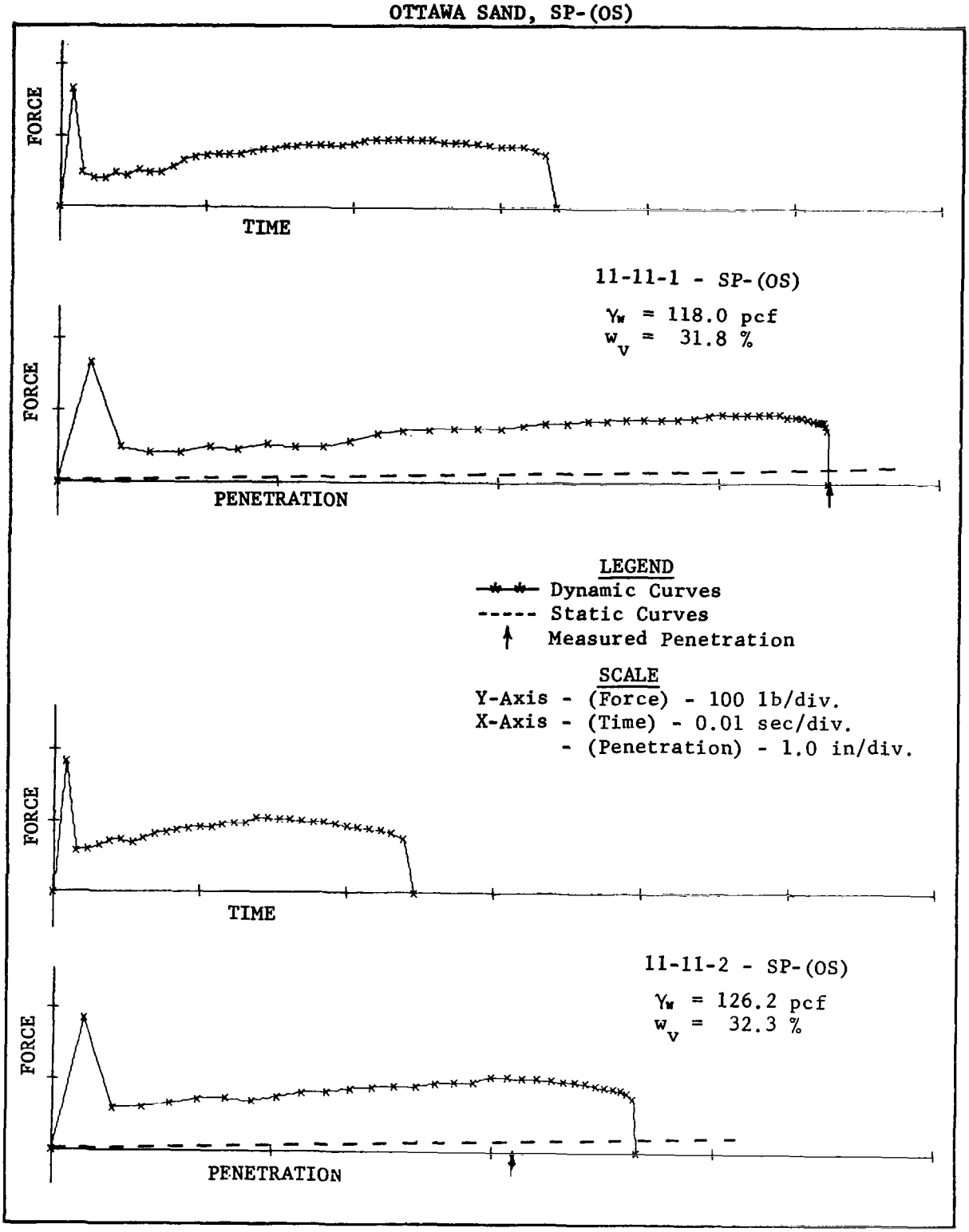

FIGURE 37

FORCE-TIME AND FORCE-PENETRATION CURVES FROM TESTS IN OTTAWA SAND, SP-(OS), AND COLORADO RIVER SAND, SP-(CRS)

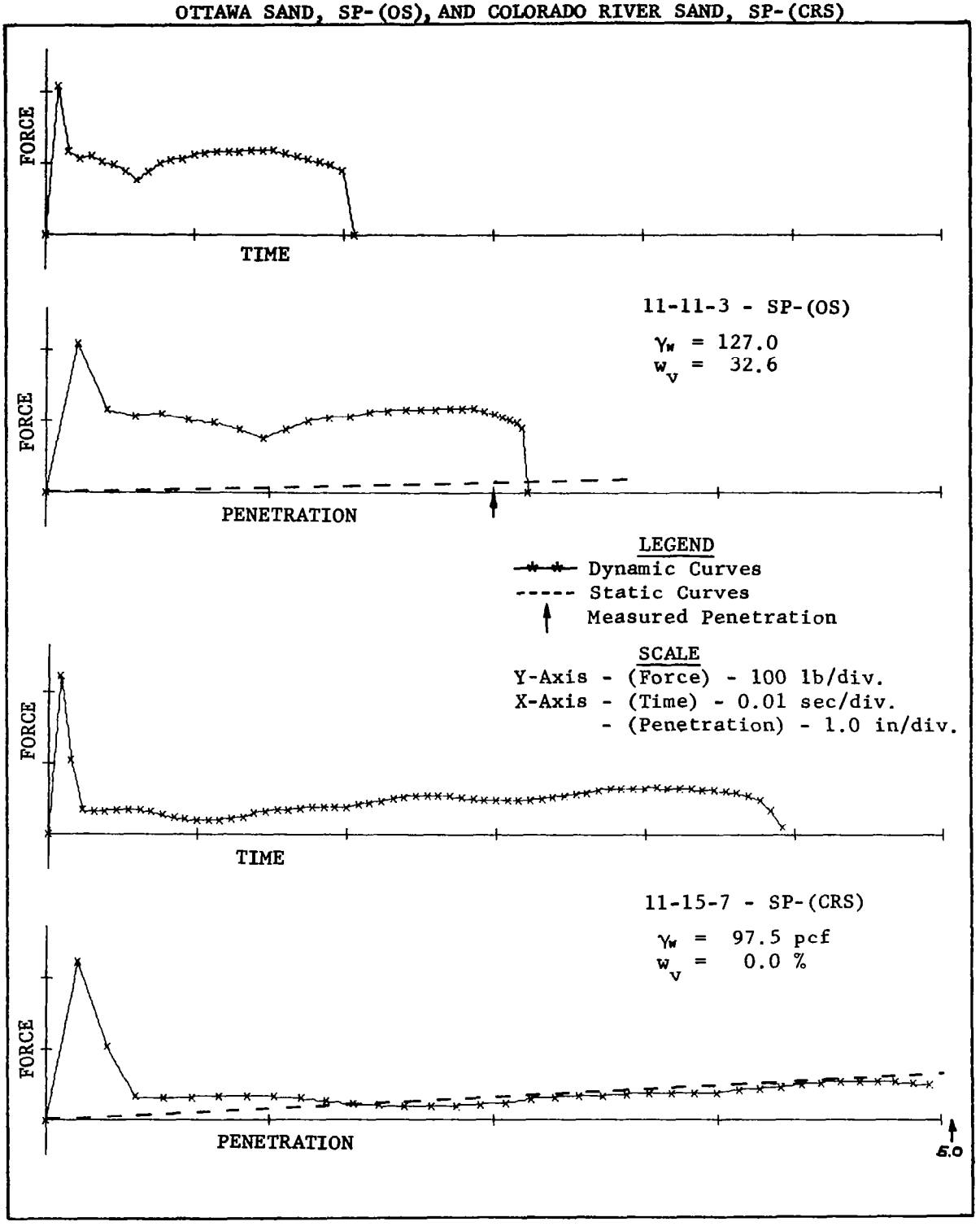

FIGURE 38

FORCE-TIME AND FORCE-PENETRATION CURVES FROM TESTS IN COLORADO RIVER SAND, SP-(CRS)

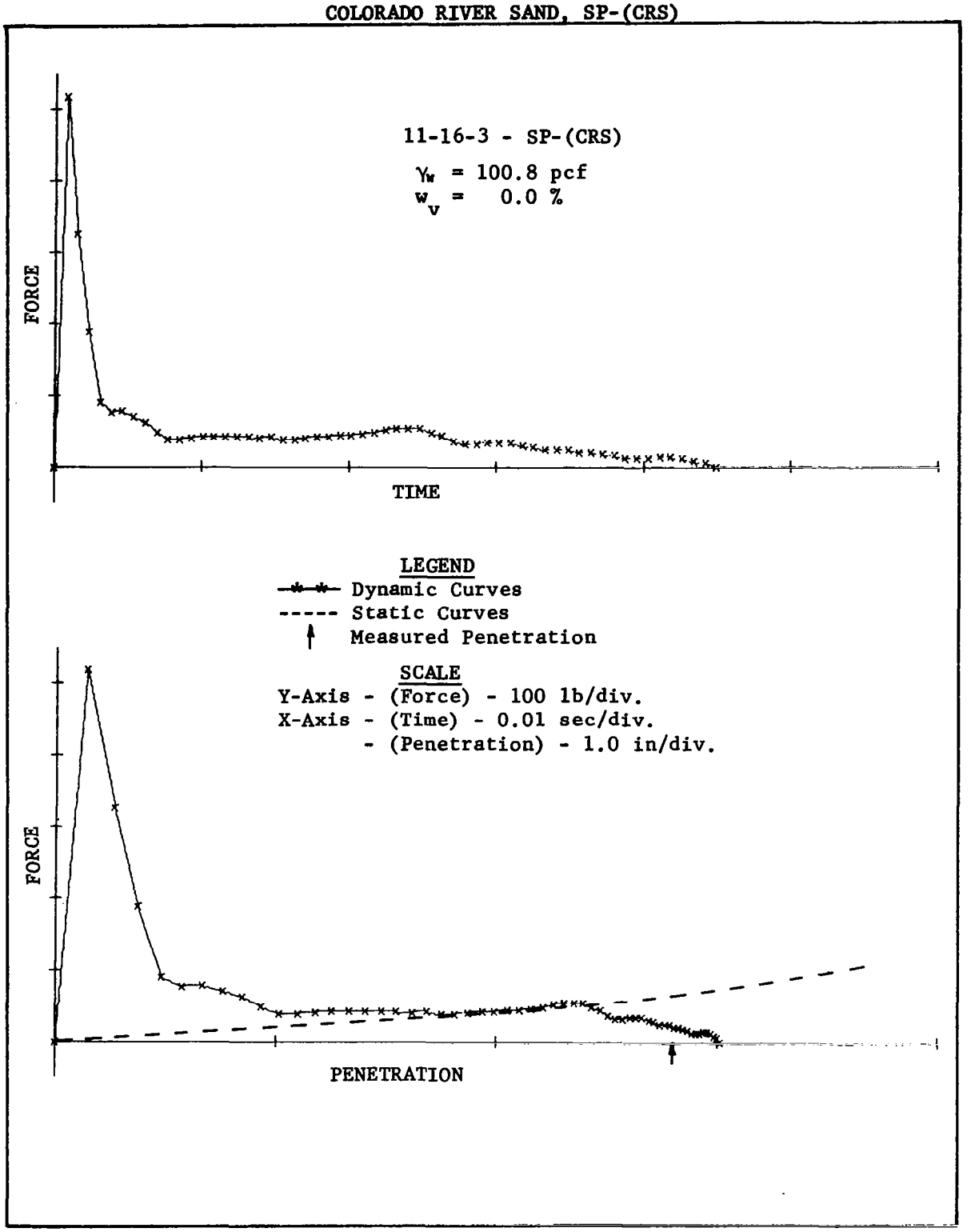

FIGURE 39

FORCE-TIME AND FORCE-PENETRATION CURVES FROM TESTS IN COLORADO RIVER SAND, SP-(CRS)

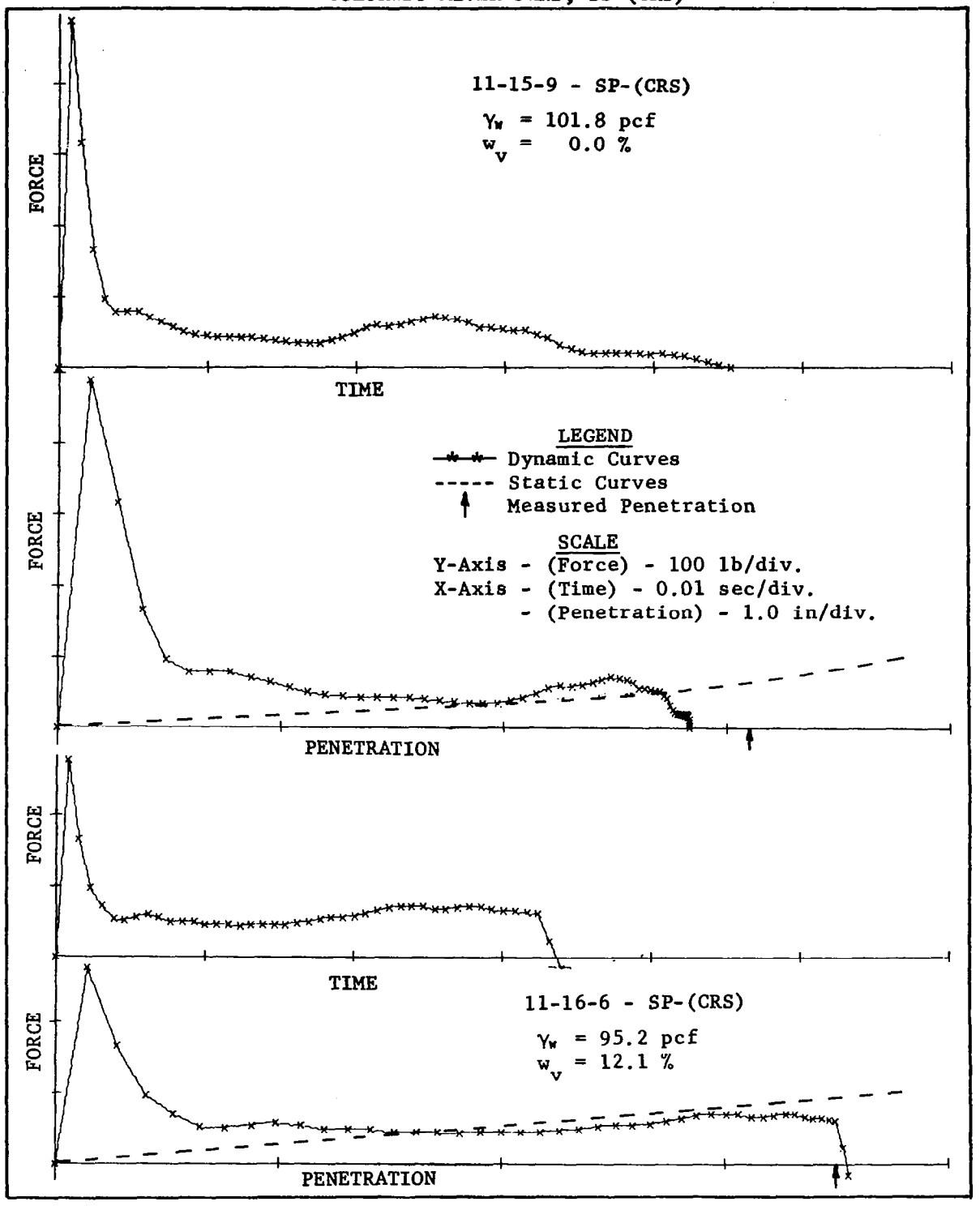

FIGURE 40

FORCE-TIME AND FORCE-PENETRATION CURVES FROM TESTS IN COLORADO RIVER SAND, SP-(CRS), AND CAPITOL AGGREGATES SAND, SW-(CA)

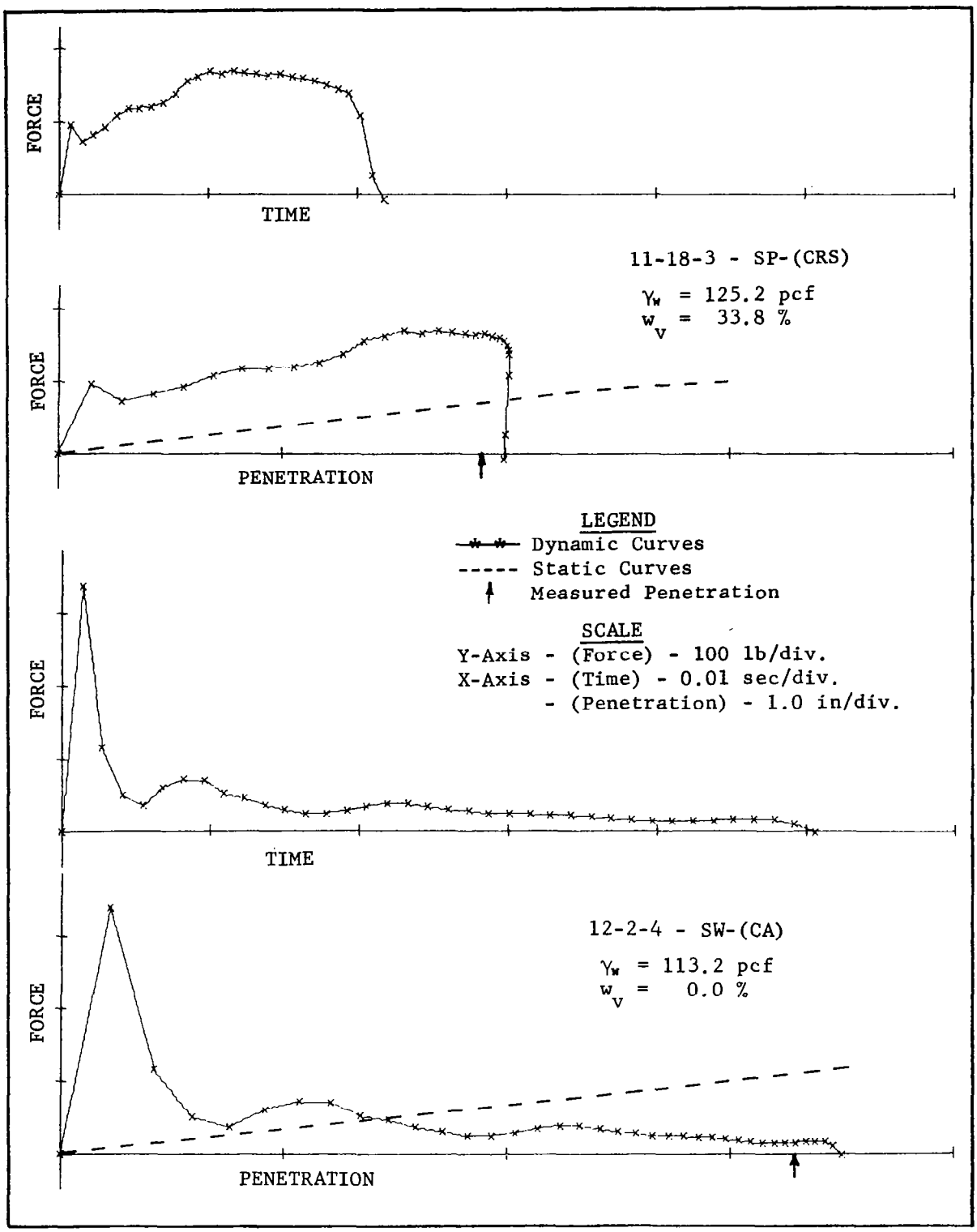

FIGURE 41

FORCE-TIME AND FORCE-PENETRATION CURVES FROM TESTS IN CAPITOL AGGREGATES SAND, SW-(CA)

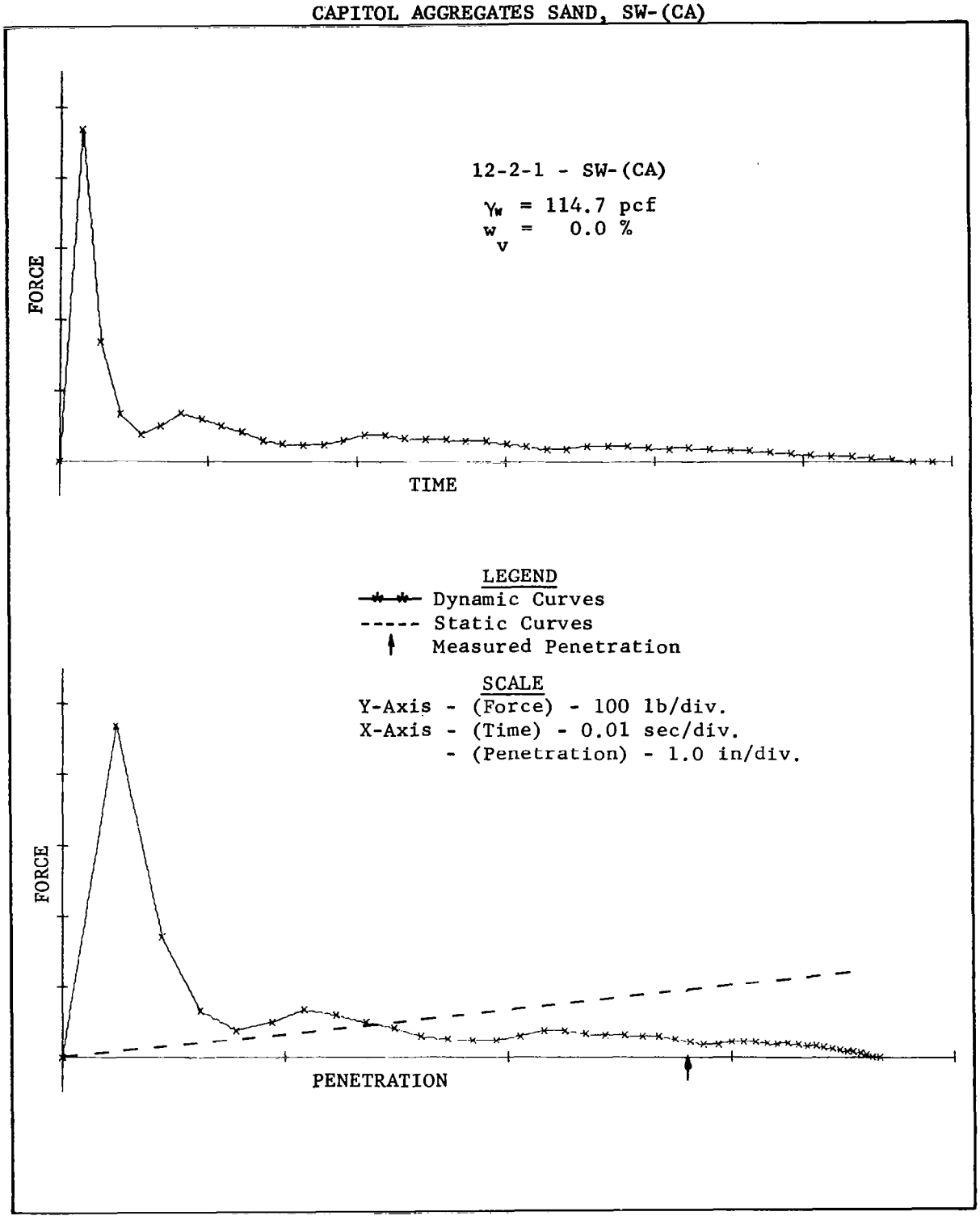

FIGURE 42

FORCE-TIME AND FORCE-PENETRATION CURVES FROM TESTS IN CAPITOL AGGREGATES SAND, SW-(CA)

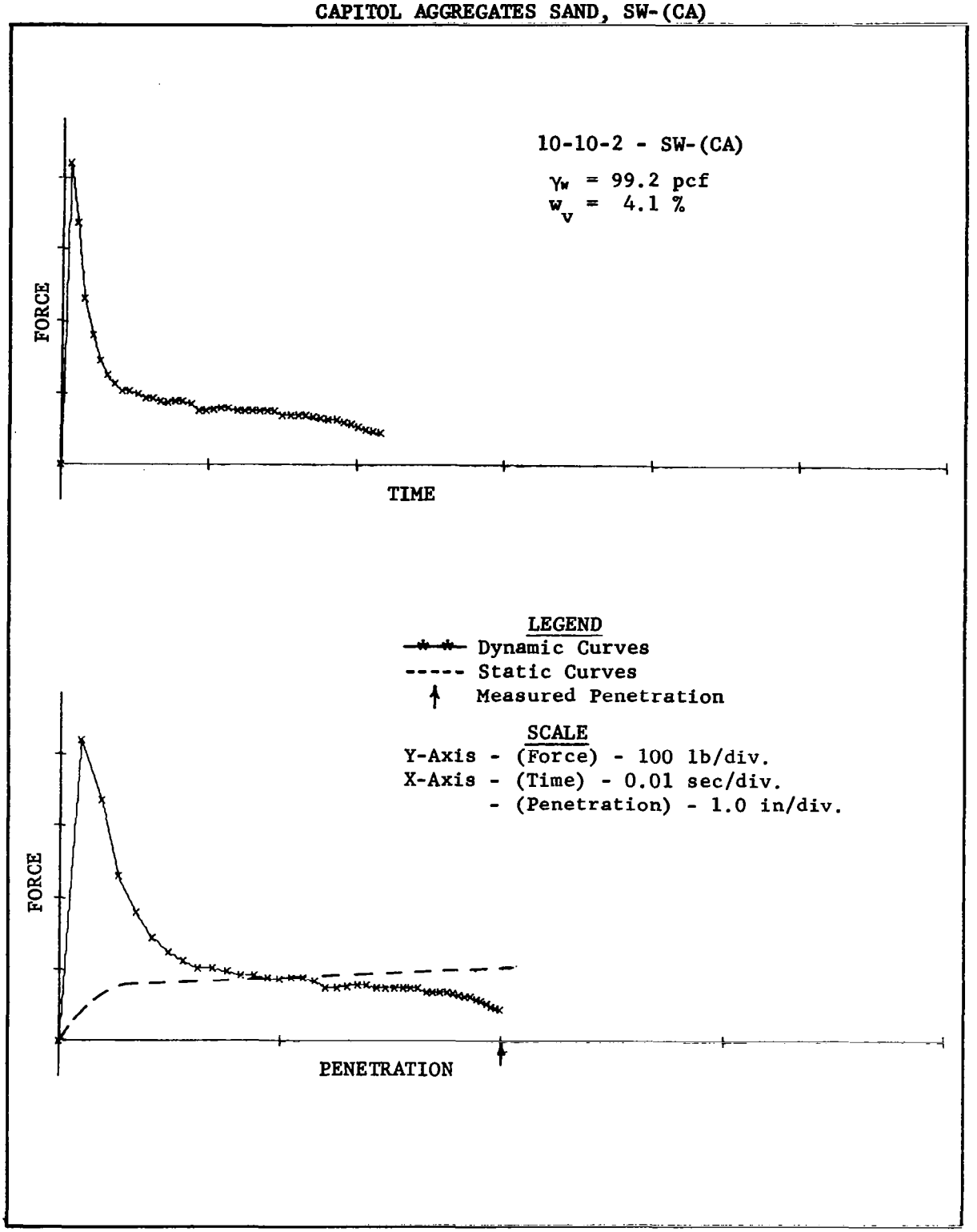

FIGURE 43

FORCE-TIME AND FORCE-PENETRATION CURVES FROM TESTS IN CAPITOL AGGREGATES SAND, SW-(CA)

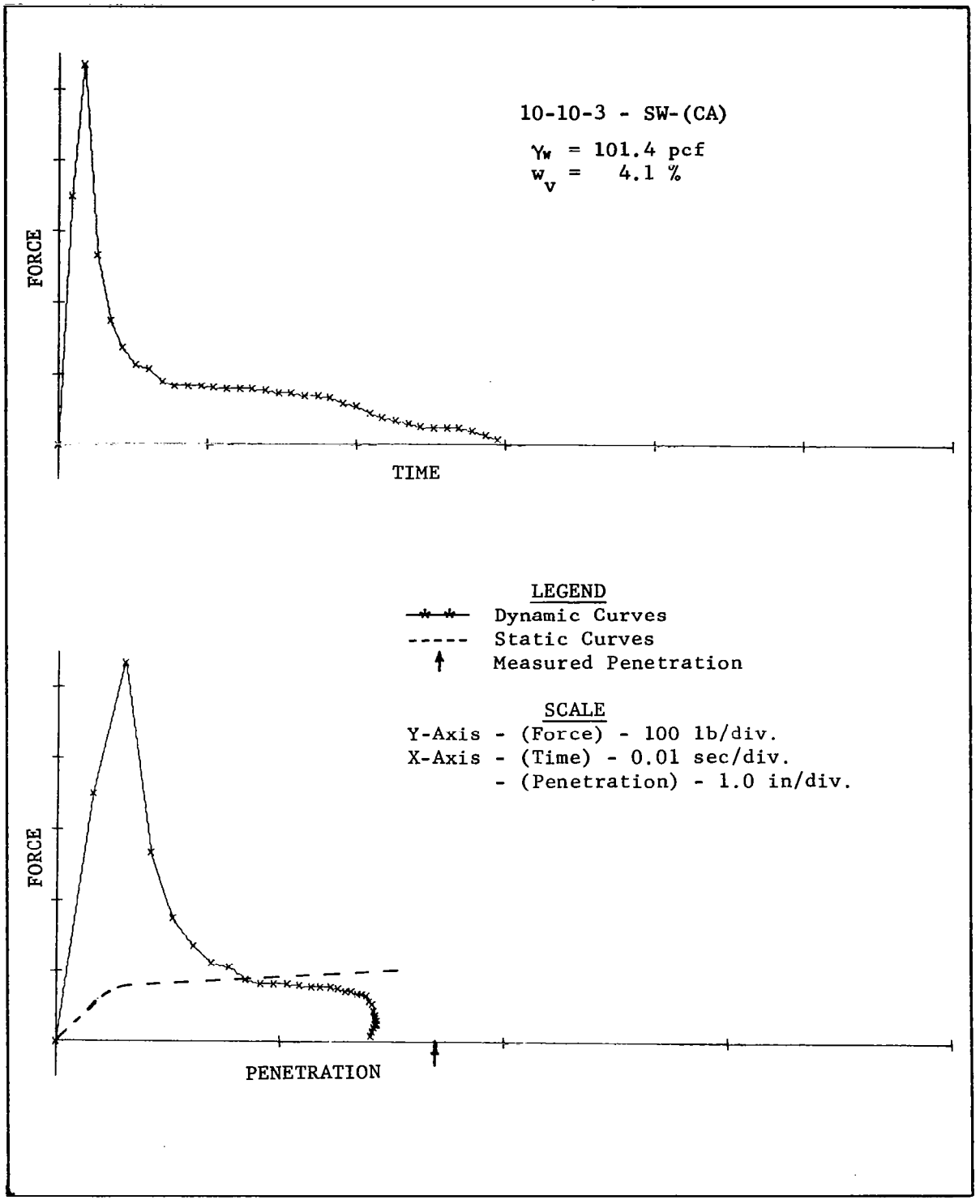

FIGURE 44

FORCE-TIME AND FORCE-PENETRATION CURVES FROM TESTS IN CAPITOL AGGREGATES SAND, SW-(CA)

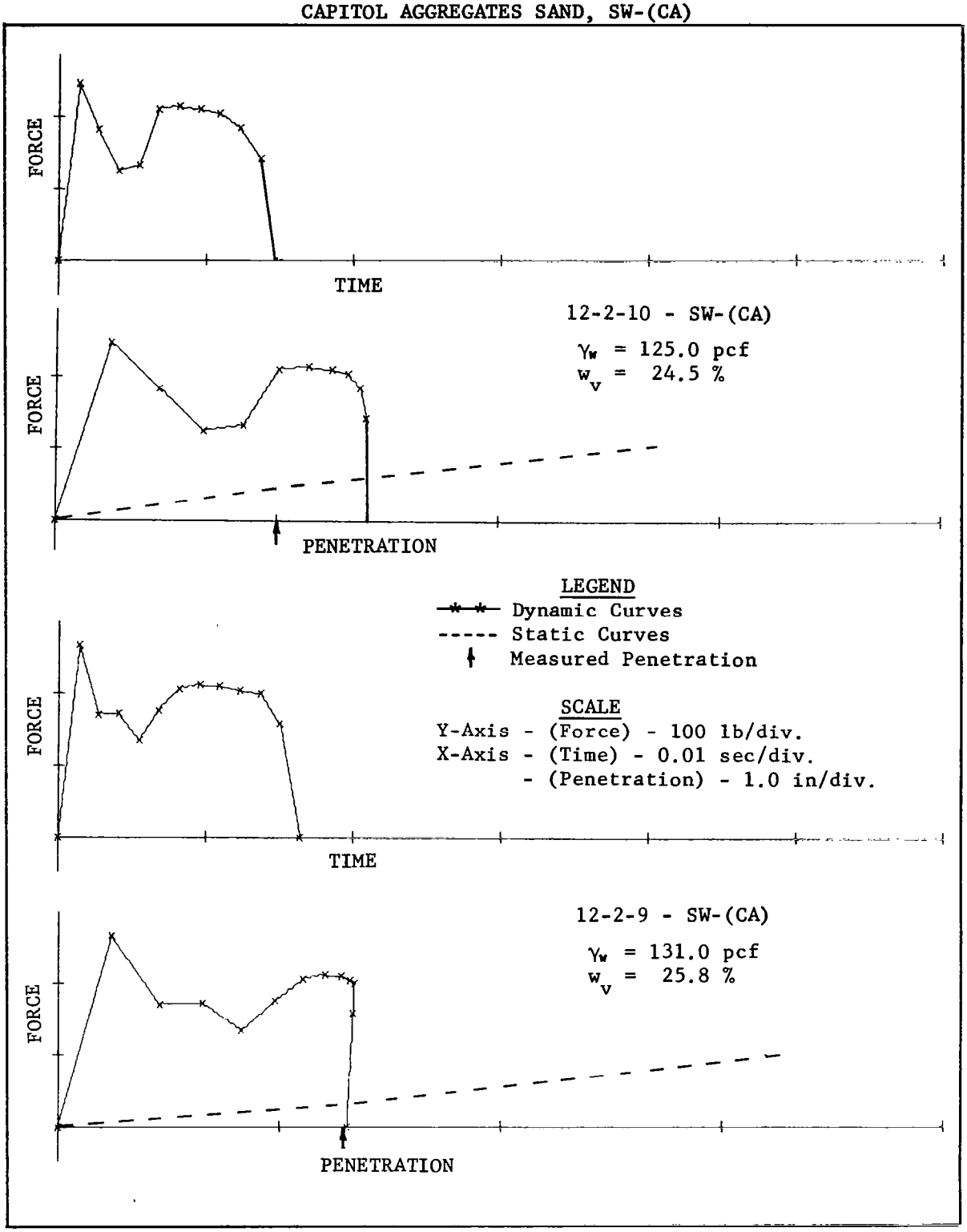

FIGURE 45

FORCE-TIME AND FORCE-PENETRATION CURVES FROM TESTS IN DEL RIO CLAY, CH-(BS)

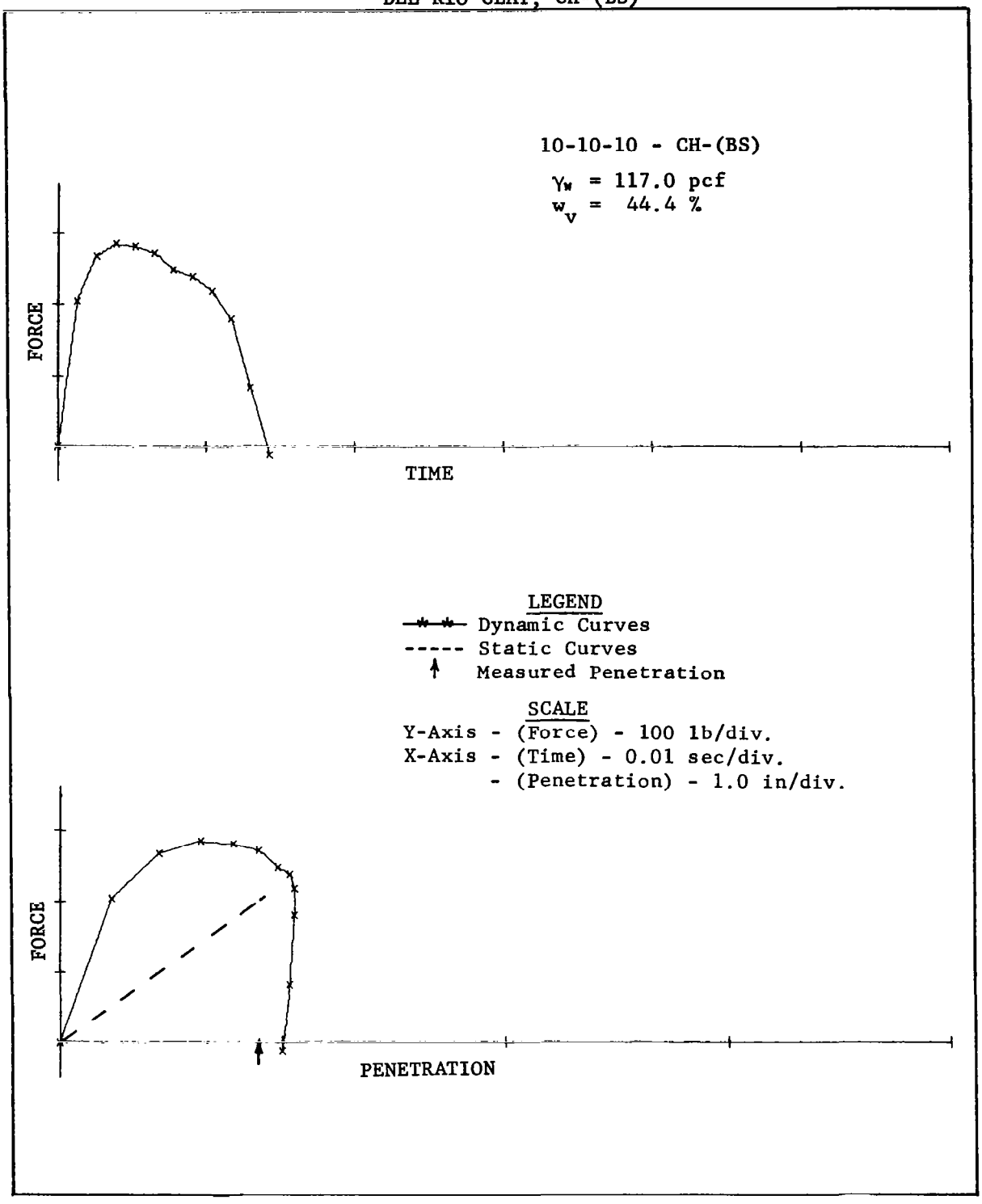

SOIL DATA

Table No. 3 is a chronological listing of the soil data of this investigation. The information includes the dry unit weight, (γ_d), and the natural water content, (w), as well as the wet unit weight and constituent volume percentages listed previously.

TABLE NO. 3

CHRONOLOGICAL LISTING OF SOIL DATA

TEST NO.	TYPE	γ_w	γ_d	w	s_v	a_v	w_v
		(pcf)	(pcf)	(%)	(%)	(%)	(%)
10-9-4	SP-(OS)	118.0	100.3	17.9	60.8	10.6	28.6
10-9-5	SP-(OS)	117.0	98.7	18.4	59.6	11.2	29.2
10-10-2	SW-(CA)	99.2	96.8	2.6	58.7	37.2	4.1
10-10-3	SW-(CA)	101.4	98.8	2.6	60.0	35.9	4.1
10-10-7	SW-(CA)	101.2	98.5	2.8	59.6	36.0	4.4
10-10-9	CH-(BS)	112.0	84.5	32.0	50.8	5.8	43.4
10-10-10	CH-(BS)	117.0	89.2	31.0	53.5	2.1	44.4
11-9-3	SP-(OS)	107.0	95.7	11.4	57.8	24.7	17.5
11-9-4	SP-(OS)	111.7	100.3	11.3	60.7	21.1	18.2
11-10-1	SP-(OS)	118.8	100.1	18.4	60.4	10.2	29.4
11-10-2	SP-(OS)	116.7	99.3	17.6	60.1	11.8	28.1
11-11-1	SP-(OS)	118.0	98.3	19.8	59.5	8.7	31.8
11-11-2	SP-(OS)	126.2	105.8	19.1	64.0	3.7	32.3
11-11-3	SP-(OS)	127.0	106.5	19.1	64.4	3.0	32.6
11-11-4	SP-(OS)	130.0	109.4	18.8	66.2	2.7	31.1
11-15-1	SP-(OS)	105.8	105.8	0.0	64.0	36.0	0.0
11-15-2	SP-(OS)	104.0	104.0	0.0	63.0	37.0	0.0
11-15-3	SP-(OS)	108.0	108.0	0.0	65.4	34.6	0.0
11-15-7	SP-(CRS)	97.5	97.5	0.0	59.0	41.0	0.0
11-15-9	SP-(CRS)	101.8	101.8	0.0	61.6	38.4	0.0
11-16-2	SP-(CRS)	100.4	100.4	0.0	60.7	39.3	0.0
11-16-3	SP-(CRS)	100.8	100.8	0.0	61.0	39.0	0.0
11-16-5	SP-(CRS)	99.8	92.2	8.5	55.8	31.7	12.5
11-16-6	SP-(CRS)	95.2	87.7	8.6	53.1	34.8	12.1
11-18-2	SP-(CRS)	111.6	92.7	20.3	56.1	13.7	30.2
11-18-3	SP-(CRS)	125.2	104.1	20.3	63.1	3.1	33.8
11-18-4	SP-(CRS)	121.0	100.0	20.6	60.6	6.4	33.0
11-22-1	Water	62.4	---	---	---	---	100.0

TABLE NO. 3 (CONT.)

CHRONOLOGICAL LISTING OF SOIL DATA

TEST NO.	TYPE	γ_w	γ_d	w	s_v	a_v	w_v
		(pcf)	(pcf)	(%)	(%)	(%)	(%)
11-22-7	SP-(TCS)	86.9	86.9	0.0	52.6	47.4	0.0
12-2-1	SW-(CA)	114.7	114.7	0.0	69.5	30.5	0.0
12-2-3	SW-(CA)	111.0	111.0	0.0	67.2	32.8	0.0
12-2-4	SW-(CA)	113.2	113.2	0.0	68.5	31.5	0.0
12-2-5	SW-(CA)	101.3	96.8	4.9	58.6	33.8	7.6
12-2-8	SW-(CA)	131.5	115.5	13.9	70.0	4.2	25.8
12-2-9	SW-(CA)	131.0	115.0	14.0	69.7	4.5	25.8
12-2-10	SW-(CA)	125.0	109.6	13.9	66.4	9.1	24.5

SUMMARY OF DYNAMIC TEST CHARACTERISTICS

Table No. 4 lists the characteristics of the dynamic tests with soil and penetration data added to supplement the information.

TABLE NO. 4

SUMMARY OF DYNAMIC TEST CHARACTERISTICS

TEST NO.	SOIL		DROP HEIGHT	IMPACT VELOCITY	TIME OF PULSE	CALCULATED PENETRATION
	TYPE	γ_w		V_i		
		(pcf)	(in)	(fps)	(msec)	(in)
11-22-1	Water	62.4	46.71	15.67	17.23	3.21
11-22-7	SP-(TCS)	86.9	46.97	15.53	47.77	2.64
11-15-2	SP-(OS)	104.0	46.67	15.66	38.16	3.85
11-15-1	SP-(OS)	105.8	46.63	14.90	43.12	3.61
11-15-3	SP-(OS)	108.0	46.76	15.40	36.19	3.55
11-9-3	SP-(OS)	107.0	46.94	15.63	33.15	3.22
11-9-4	SP-(OS)	111.7	46.96	15.58	20.64	2.02
11-10-2	SP-(OS)	116.7	46.77	14.56	26.63	2.51
10-9-4	SP-(OS)	118.0	46.83	15.47	17.14	1.79
10-9-5	SP-(OS)	117.0	46.75	14.80	18.81	1.68
11-10-1	SP-(OS)	118.8	46.54	14.34	26.72	2.35
11-11-1	SP-(OS)	118.0	46.87	15.86	33.79	3.49
11-11-2	SP-(OS)	126.2	46.87	15.38	24.58	2.66
11-11-3	SP-(OS)	127.0	46.77	15.34	20.68	2.15
11-11-4	SP-(OS)	130.0	46.73	14.99	19.16	1.84

TABLE NO. 4 (CONT.)

SUMMARY OF DYNAMIC TEST CHARACTERISTICS

TEST NO.	SOIL		DROP HEIGHT	IMPACT VELOCITY	TIME OF PULSE	CALCULATED PENETRATION
	TYPE	γ_w		V_i		
		(pcf)	(in)	(fps)	(msec)	(in)
11-15-7	SP-(CRS)	97.5	46.61	15.34	49.22	5.11
11-16-2	SP-(CRS)	100.4	46.92	15.04	45.90	2.81
11-16-3	SP-(CRS)	100.8	46.90	15.65	44.95	3.02
11-15-9	SP-(CRS)	101.8	46.95	15.80	45.19	2.84
11-16-6	SP-(CRS)	95.2	46.97	15.66	33.97	3.55
11-16-5	SP-(CRS)	99.8	46.76	15.68	34.87	3.35
11-18-2	SP-(CRS)	111.6	46.90	15.91	19.45	1.73
11-18-3	SP-(CRS)	125.2	46.77	15.62	21.78	2.01
11-18-4	SP-(CRS)	121.0	46.92	15.40	19.40	1.83
12-2-3	SW-(CA)	111.0	46.89	14.76	54.35	3.41
12-2-4	SW-(CA)	113.2	46.97	14.20	50.62	3.50
12-2-1	SW-(CA)	114.7	46.88	15.64	58.74	3.66
10-10-2	SW-(CA)	99.2	46.87	15.65	30.00	1.99
10-10-3	SW-(CA)	101.4	46.87	15.61	29.55	1.43
10-10-7	SW-(CA)	101.2	46.87	15.69	29.70	1.71
12-2-5	SW-(CA)	101.3	46.82	15.30	38.42	2.55
12-2-10	SW-(CA)	125.0	46.84	15.48	15.03	1.41
12-2-9	SW-(CA)	131.0	46.87	15.32	16.42	1.34
12-2-8	SW-(CA)	131.5	46.82	15.34	15.71	1.16

TABLE NO. 4 (CONT.)

SUMMARY OF DYNAMIC TEST CHARACTERISTICS

TEST NO.	SOIL		DROP HEIGHT	IMPACT VELOCITY	TIME OF PULSE	CALCULATED PENETRATION
	TYPE	γ_w		V_i		
		(pcf)	(in)	(fps)	(msec)	(in)
10-10-9	CH-(BS)	112.0	46.87	15.69	12.92	0.96
10-10-10	CH-(BS)	117.0	46.97	15.46	14.26	1.06

APPENDIX D

DEFINITION OF SYMBOLS AND NOTATIONS

The notations used in this report are defined in the following table.

TABLE NO. 5

LIST OF NOTATIONS

a_v	percent by volume of air in target (%)
c	cohesion of a soil (psi or tsf)
e	void ratio of soil (volume of voids/volume of solids)
F_c	initial, or contact force peak occurring in impacts on granular media (lbs)
F_s	later, or secondary maximum force occurring in impacts on granular media, or maximum force encountered for impacts on cohesive media (lbs)
P	force level obtained from static tests (lbs)
s_v	percent by volume of solid in target (%)
t_t	total time length of a force-time signature (msec)
v	penetrating velocity of projectile during impact (fps)
V_i	projectile velocity at impact (fps)
w	natural water content in percent of dry weight (%)
w_v	percent by volume of water in target (%)
y	penetrometer displacement into target media (in.)
γ_d	unit weight of oven-dried soil (pcf)
γ_w	unit weight of <u>in situ</u> soil (pcf)
ϕ	angle of internal friction of a soil (degrees)

REFERENCES

1. Colp, J. L., "An Experimental Investigation of the Continuous Penetration of a Blunt Body into a Simulated Cohesionless Soil," Sandia Corporation, Albuquerque, New Mexico, SC-RR-65-260, p. 46.

2. General American Transportation Corporation, "Lunar Survey Probe Sensor Study," (MR 1272-1), Final Report to NASA, Contract NAS 9-3731, June 1965, Section 4.

3. McCarty, J. L. and Carden, H. D., "Impact Characteristics of Various Materials Obtained by an Acceleration-Time-History Technique Applicable to Evaluating Remote Targets," NASA Technical Note, D-1269, June, 1962, p. 34.

4. Peck, R. B., Hanson, W. E., and Thornburn, T. H., Foundation Engineering, John Wiley & Sons, New York, 1953, p. 48.

5. Proctor, R. R., "Soil Compaction," Four-Article Series in "Engineering News-Record", Vol. III, Nos. 9, 10, 12, 13, 1933.

6. Reichmuth, D. R., Stagg, R. P., Womack, D. P., and Cox, W. R., "A Study of Soil-Spacecraft Interaction During Impact," Report to NASA, Contract NAS 9-3559, December, 1966, pp. 44, 78, 67.

7. Scott, R. F., "Problem of the Penetration of a Projectile into Soil, a Soil-Like Medium, or Compressible Rock (Pumice)," Report No. 4 (obtained from NASA, Houston, Texas), November 20, 1962, p. 1.

8. Stephenson, B. R., "Measurement of Dynamic Force-Penetration Characteristics in Indiana Limestone," University of Minnesota M. S. Thesis, September, 1963, p. A1.

9. Terzaghi, K. and Peck, R. B., Soil Mechanics In Engineering Practice, John Wiley & Sons, New York, 1948, p. 168.

10. Thompson, L. J., "Dynamic Penetration of Selected Projectiles into Particulate Media," Sandia Corporation, Albuquerque, New Mexico, SC-RR-66-376, p. 174.

11. Thompson, L. J. and Colp, J. L., "Preliminary Evaluation of Earth Targets for use in Impact Effects Studies," Sandia Corporation, Albuquerque, New Mexico, SC-DR 316-63, p. 10.

NASA-Langley, 1967 — 13 CR-849

"The aeronautical and space activities of the United States shall be conducted so as to contribute . . . to the expansion of human knowledge of phenomena in the atmosphere and space. The Administration shall provide for the widest practicable and appropriate dissemination of information concerning its activities and the results thereof."

—NATIONAL AERONAUTICS AND SPACE ACT OF 1958

NASA SCIENTIFIC AND TECHNICAL PUBLICATIONS

TECHNICAL REPORTS: Scientific and technical information considered important, complete, and a lasting contribution to existing knowledge.

TECHNICAL NOTES: Information less broad in scope but nevertheless of importance as a contribution to existing knowledge.

TECHNICAL MEMORANDUMS: Information receiving limited distribution because of preliminary data, security classification, or other reasons.

CONTRACTOR REPORTS: Scientific and technical information generated under a NASA contract or grant and considered an important contribution to existing knowledge.

TECHNICAL TRANSLATIONS: Information published in a foreign language considered to merit NASA distribution in English.

SPECIAL PUBLICATIONS: Information derived from or of value to NASA activities. Publications include conference proceedings, monographs, data compilations, handbooks, sourcebooks, and special bibliographies.

TECHNOLOGY UTILIZATION PUBLICATIONS: Information on technology used by NASA that may be of particular interest in commercial and other non-aerospace applications. Publications include Tech Briefs, Technology Utilization Reports and Notes, and Technology Surveys.

Details on the availability of these publications may be obtained from:

SCIENTIFIC AND TECHNICAL INFORMATION DIVISION

NATIONAL AERONAUTICS AND SPACE ADMINISTRATION

Washington, D.C. 20546